Shu, Qihai (2015) Ore-forming mechanisms and spatio-temporal framework for intrusion-related deposits in NE China. PhD thesis, James Cook University.

http://dx.doi.org/10.4225/28/5a94aded02e66

Ore-forming Mechanisms and Spatio-temporal Framework for Intrusion-related Deposits in NE China

Thesis submitted by

Qihai Shu

December 2015

For the Degree of Doctor of Philosophy in the

Department of Earth and Oceans, College of Science, Technology & Engineering

James Cook University

Statement of Access

I, the undersigned author of this thesis, understand that James Cook University will make this thesis available for use within the university library and allow access in other approved libraries after its submission. All users consulting this thesis will have to sign the following statement:

> *In consulting this thesis I agree not to copy or closely paraphrase it in whole or in part without the written consent of the author; and to make proper public written acknowledgement for any assistance which I have obtained from it.*

Beyond this, I do not wish to place any restrictions on access to this thesis.

Qihai Shu
December 2015

Statement of Contributions

Financial contributions towards this study have included:

- Geological Survey Project of China (No. 1212010981009)
- National Nature Science Foundation of China (No. 41390443)
- Chinese Scholarship Council award (No. 201306010045)
- Student research grant from the Society of Economic Geologists (SEG-Hugh McKinstry Fund)
- Postgraduate funding from EGRU and GRS of JCU.

Statement of Contribution by Others

Title of thesis: Ore-forming mechanisms and spatio-temporal framework for intrusion-related deposits in NE China

Name of candidate: Qihai Shu

Chapter #	Details of publication(s) on which chapter is based	Nature and extent of the intellectual input of each author
4	Shu, Q., Chang, Z., Lai, Y., and Zhou, Y., Regional metallogeny of Mo-bearing deposits in NE China, with new Re-Os dates of porphyry Mo deposits in the northern Xilamulun district (submitted to Gondwana Research)	I contributed to development of concepts and writing
6	Shu, Q., Chang, Z., Hammerli, J., Lai, Y., and Huizenga, J-M., Composition and evolution of fluids forming the Baiyinnuo’er skarn Zn-Pb deposit, NE China: insights from laser ablation ICP-MS study of fluid inclusions (in preparation for Economic Geology)	I contributed to development of concepts and writing

I confirm the candidate’s contribution to this paper and consent to the inclusion of the paper in this thesis.

Name (print): Zhaoshan Chang

Signature: Zhaoshan Chang [redacted]

Date: 31 October 2015

Statement of Contribution by Others

Title of thesis: Ore-forming mechanisms and spatio-temporal framework for intrusion-related deposits in NE China

Name of candidate: Qihai Shu

Chapter #	Details of publication(s) on which chapter is based	Nature and extent of the intellectual input of each author
2	Shu, Q., Lai, Y., Wang, C., Xu, J., and Sun, Y., 2014, Geochronology, geochemistry and Sr-Nd-Hf isotopes of the Haisugou porphyry Mo deposit, northeast China, and their geological significance: Journal of Asian Earth Sciences, v. 79, p. 777–791.	I contributed to part of the field investigation, sample collection and development of concepts
3	Shu, Q., Lai, Y., Zhou, Y., Xu, J., and Wu, H., 2015, Zircon U-Pb geochronology and Sr-Nd-Pb-Hf isotopic constraints on the timing and origin of Mesozoic granitoids hosting the Mo deposits in northern Xilamulun district, NE China: Lithos, v. 238, p. 64–75.	I contributed to part of the field investigation and primary idea discussion
4	Shu, Q., Chang, Z., Lai, Y., and Zhou, Y., Regional metallogeny of Mo-bearing deposits in NE China, with new Re-Os dates of porphyry Mo deposits in the northern Xilamulun district (submitted to Gondwana Research)	I contributed to part of the field investigation and primary idea discussion
5	Shu, Q., Lai, Y., Sun, Y., Wang, C., and Meng, S., 2013, Ore genesis and hydrothermal evolution of the Baiyinnuo'er zinc-lead skarn deposit, northeast China: evidence from isotopes (S, Pb) and fluid inclusions: Economic Geology, v. 108, p. 835–860.	I contributed to part of the field investigation and primary idea discussion
6	Shu, Q., Chang, Z., Hammerli, J., Lai, Y., and Huizenga, J-M., Composition and evolution of fluids forming the Baiyinnuo'er skarn Zn-Pb deposit, NE China: insights from laser ablation ICP-MS study of fluid inclusions (in preparation for Economic Geology)	I contributed to part of the field investigation and primary idea discussion

I confirm the candidate's contribution to this paper and consent to the inclusion of the paper in this thesis.

Name (print): Yong Lai

Signature: [redacted]

Date: 2015.10.12.

Statement of Contribution by Others

Title of thesis: Ore-forming mechanisms and spatio-temporal framework for intrusion-related deposits in NE China

Name of candidate: Qihai Shu

Chapter #	Details of publication(s) on which chapter is based	Nature and extent of the intellectual input of each author
6	Shu, Q., Chang, Z., Hammerli, J., Lai, Y., Huizenga, J-M., Composition and evolution of fluids forming the Baiyinnuo'er skarn Zn-Pb deposit, NE China: insights from laser ablation ICP-MS study of fluid inclusions (in preparation for Economic Geology)	I contributed to part of the analyses and primary idea discussion

I confirm the candidate's contribution to this paper and consent to the inclusion of the paper in this thesis.

Name (print): Jan-Marten Huizenga

Signature: [redacted]

Date: 30/10/15

Statement of Contribution by Others

Title of thesis: Ore-forming mechanisms and spatio-temporal framework for intrusion-related deposits in NE China

Name of candidate: Qihai Shu

Chapter #	Details of publication(s) on which chapter is based	Nature and extent of the intellectual input of each author
6	Shu, Q., Chang, Z., Hammerli, J., Lai, Y., Huizenga, J-M., Composition and evolution of fluids forming the Baiyinnuo'er skarn Zn-Pb deposit, NE China: insights from laser ablation ICP-MS study of fluid inclusions (in preparation for Economic Geology)	I contributed to part of the analyses, data reduction and interpretation

I confirm the candidate's contribution to this paper and consent to the inclusion of the paper in this thesis.

Name (print): Johannes Hammerli

Signature: [redacted]

Date: 30.10.2015

Statement of Contribution by Others

Title of thesis: Ore-forming mechanisms and spatio-temporal framework for intrusion-related deposits in NE China

Name of candidate: Qihai Shu

Chapter #	Details of publication(s) on which chapter is based	Nature and extent of the intellectual input of each author
2	Shu, Q., Lai, Y., Wang, C., Xu, J., and Sun, Y., 2014, Geochronology, geochemistry and Sr-Nd-Hf isotopes of the Haisugou porphyry Mo deposit, northeast China, and their geological significance: Journal of Asian Earth Sciences, v. 79, p. 777–791.	I contributed to part of the field investigation, sample collection and writing
5	Shu, Q., Lai, Y., Sun, Y., Wang, C., and Meng, S., 2013, Ore genesis and hydrothermal evolution of the Baiyinnuo'er zinc-lead skarn deposit, northeast China: evidence from isotopes (S, Pb) and fluid inclusions: Economic Geology, v. 108, p. 835–860.	I contributed to part of the field investigation, sample collection and writing

I confirm the candidate's contribution to this paper and consent to the inclusion of the paper in this thesis.

Name (print): Chao Wang

Signature: [redacted]

Date: Oct 16, 2015

Statement of Contribution by Others

Title of thesis: Ore-forming mechanisms and spatio-temporal framework for intrusion-related deposits in NE China

Name of candidate: Qihai Shu

Chapter #	Details of publication(s) on which chapter is based	Nature and extent of the intellectual input of each author
3	Shu, Q., Lai, Y., Zhou, Y., Xu, J., and Wu, H., 2015, Zircon U-Pb geochronology and Sr-Nd-Pb-Hf isotopic constraints on the timing and origin of Mesozoic granitoids hosting the Mo deposits in northern Xilamulun district, NE China: Lithos, v. 238, p. 64–75.	I contributed to primary idea discussion

I confirm the candidate's contribution to this paper and consent to the inclusion of the paper in this thesis.

Name (print): Huaying Wu

Signature: [redacted]

Date: 14 October, 2015

Statement of Contribution by Others

Title of thesis: Ore-forming mechanisms and spatio-temporal framework for intrusion-related deposits in NE China

Name of candidate: Qihai Shu

Chapter #	Details of publication(s) on which chapter is based	Nature and extent of the intellectual input of each author
2	Shu, Q., Lai, Y., Wang, C., Xu, J., and Sun, Y., 2014, Geochronology, geochemistry and Sr-Nd-Hf isotopes of the Haisugou porphyry Mo deposit, northeast China, and their geological significance: Journal of Asian Earth Sciences, v. 79, p. 777–791.	I contributed to part of the analyses and primary idea discussion
3	Shu, Q., Lai, Y., Zhou, Y., Xu, J., and Wu, H., 2015, Zircon U-Pb geochronology and Sr-Nd-Pb-Hf isotopic constraints on the timing and origin of Mesozoic granitoids hosting the Mo deposits in northern Xilamulun district, NE China: Lithos, v. 238, p. 64–75.	I contributed to part of the analyses and writing

I confirm the candidate's contribution to this paper and consent to the inclusion of the paper in this thesis.

Name (print): Jiajia Xu

Signature: [redacted]

Date: Oct. 14, 2015

Statement of Contribution by Others

Title of thesis: Ore-forming mechanisms and spatio-temporal framework for intrusion-related deposits in NE China

Name of candidate: Qihai Shu

Chapter #	Details of publication(s) on which chapter is based	Nature and extent of the intellectual input of each author
5	Shu, Q., Lai, Y., Sun, Y., Wang, C., and Meng, S., 2013, Ore genesis and hydrothermal evolution of the Baiyinnuo'er zinc-lead skarn deposit, northeast China: evidence from isotopes (S, Pb) and fluid inclusions: Economic Geology, v. 108, p. 835–860.	I contributed to part of the field investigation, sample collection, and analyses

I confirm the candidate's contribution to this paper and consent to the inclusion of the paper in this thesis.

Name (print): Shu Meng

Signature: [redacted]

Date: Oct. 5/ 2015

Statement of Contribution by Others

Title of thesis: Ore-forming mechanisms and spatio-temporal framework for intrusion-related deposits in NE China

Name of candidate: Qihai Shu

Chapter #	Details of publication(s) on which chapter is based	Nature and extent of the intellectual input of each author
2	Shu, Q., Lai, Y., Wang, C., Xu, J., and Sun, Y., 2014, Geochronology, geochemistry and Sr-Nd-Hf isotopes of the Haisugou porphyry Mo deposit, northeast China, and their geological significance: Journal of Asian Earth Sciences, v. 79, p. 777–791.	I contributed to part of the field investigation, sample collection and analyses
5	Shu, Q., Lai, Y., Sun, Y., Wang, C., and Meng, S., 2013, Ore genesis and hydrothermal evolution of the Baiyinnuo'er zinc-lead skarn deposit, northeast China: evidence from isotopes (S, Pb) and fluid inclusions: Economic Geology, v. 108, p. 835–860.	I contributed to part of the field investigation, sample collection, and primary idea discussion

I confirm the candidate's contribution to this paper and consent to the inclusion of the paper in this thesis.

Name (print): Yi Sun

Signature: [redacted]

Date: 15-OCT-2015

Statement of Contribution by Others

Title of thesis: Ore-forming mechanisms and spatio-temporal framework for intrusion-related deposits in NE China

Name of candidate: Qihai Shu

Chapter #	Details of publication(s) on which chapter is based	Nature and extent of the intellectual input of each author
3	Shu, Q., Lai, Y., Zhou, Y., Xu, J., and Wu, H., 2015, Zircon U-Pb geochronology and Sr-Nd-Pb-Hf isotopic constraints on the timing and origin of Mesozoic granitoids hosting the Mo deposits in northern Xilamulun district, NE China: Lithos, v. 238, p. 64–75.	I contributed to part of the field investigation, sample collection, and primary idea discussion
4	Shu, Q., Chang, Z., Lai, Y., and Zhou, Y., Regional metallogeny of Mo-bearing deposits in NE China, with new Re-Os dates of porphyry Mo deposits in the northern Xilamulun district (submitted to Gondwana Research)	I contributed to part of the field investigation and sample collection

I confirm the candidate’s contribution to this paper and consent to the inclusion of the paper in this thesis.

Name (print): Yitao Zhou

Signature: [redacted]

Date: 2015. 10. 14

Acknowledgements

First and foremost, I would like to express my sincere thanks to my supervisors Drs. Zhaoshan Chang and Jan-Marten Huizenga from James Cook University, Australia, and Professor Yong Lai from Peking University, China, without whom this thesis could not have been completed. I thank Zhaoshan for providing me the opportunity to study at JCU, training me to understand skarn and porphyry deposits, guidance, supervision and discussions during data analysis and interpretation, and tireless editing my written English. I thank Jan-Marten for training me about the basic theories of fluid inclusions, patiently teaching me on thick section preparation and subsequent microthermometric analysis, as well as time, effort and input during thesis writing. I am also grateful to Yong for guiding and supporting my fieldwork in NE China, and invaluable suggestions and discussions on my thesis and papers throughout this project.

I would like to thank Professor Paul Dirks, Drs Carl Spandler, Jahn Carranza, Gavin Clarke, Ioan Sanislav, Rob Holm and Christa Placzek at Economic Geology Research Centre (EGRU) of JCU, and many support staff from College of Science, Technology and Engineering, especially Rebecca Steele and Judy Botting, for all of their time and help. I would also like to thank many of my fellow PhD students, Johannes, George, Stephanie, Fredrik, Michael and many others, who made my 2-year life at JCU an enjoyable and worthwhile experience. I am also fortunate to have made a lot of Chinese friends who are studying or living in Townsville, including Zhiming, Baoshun, Yanbo, Hongrui, Lin, Huijuan, Qian, Hongzheng, and the Xie’s family, all of who have helped me a lot from my first day in Townsville.

I also benefited from many professors in China, including Yanjing Chen, Wenbo Li, Cheng Xu, and Bin Chen from Peking University, Hongrui Fan from Institute of Geology and Geophysics, Chinese Academy of Sciences, Jun Deng and Jiajun Liu from China University of Geosciences, Beijing, all of who have read and provided suggestions on the early draft potentially forming one/several chapter(s) of this thesis, and helped improved the quality of the thesis. I also thank many master or PhD students from Peking University including Yi Sun, Chao Wang, Jiajia Xu, Lin Jiang, Shu Meng and Yitao Zhou for their help during field investigations and sample processing.

I would also like to express my gratitude to those who have helped with analyses, including Yi Hu from the Advanced Analytical Centre, James Cook University (JCU), Qiuyue Jia, Fang Ma, Wenping Zhu and Guiming Shu from Peking University, Li Su from China University of Geosciences, Beijing, Mengning Dai from Northwest University, Xi’an, and Xianghui Li from the Institute of Geology and Geophysics, Chinese Academy of Science.

This thesis has benefited a lot from the critical reviews and constructive comments by Lawrence Meinert (U.S. Geological Survey) and David Huston (Geoscience Australia), who have helped improve the quality of the thesis significantly.

Lastly I would like to thank my parents, my sister and parents-in-law for their encouragement and support during my entire PhD study. I am also thankful, in the truest sense of the word, to my dear wife and soulmate, Yang Song, for her patience and endless love, and I shall be forever in her debt.

Abstract

Northeastern China is composed of the eastern part of the Central Asian Orogenic Belt and the northeastern margin of the North China Craton. It underwent two major sets of orogenic events, including the pre-Mesozoic amalgamation of several micro-continents and the Mesozoic subduction of the Paleo-Pacific plate. It hosts numerous ore deposits of dominantly porphyry and skarn types, most of which have Mesozoic ages. In this study, both mineralization types were studied, aiming to improve the understanding of ore genesis, hydrothermal evolution, mineralization mechanism, regional metallogeny as well as the geodynamic setting.

Systematic zircon U-Pb and/or molybdenite Re-Os dating on five porphyry deposits (i.e., Aolunhua, Haisugou, Shabutai, Banlashan, and Yangchang) in the northern Xilamulun district indicates that the timing of the magmatism and the Mo mineralization is broadly coeval, mainly at 130-140 Ma. Major and trace element geochemistry reveals the intrusions hosting Mo-only deposits (e.g., Haisugou) have stronger crystal fractionation than intrusions hosting porphyry Cu and Cu-Mo deposits (e.g., Aolunhua), indicating that such a process may have played a role in selective enrichment of Mo. A comparison of zircon Ce/Nd ratios as a proxy for the oxidation state of magmas between mineralized and barren intrusions shows that the mineralized intrusions are associated with more oxidized magmas than the cospatial barren granites, and therefore it is proposed that higher oxygen fugacity may also be important to produce economic Mo mineralization. Whole rock Sr-Nd-Pb and zircon Hf isotopes show that these mineralized granites in Xilamulun are associated with magmas generated from three different source regions (i.e., remelting of old crust material, mixing of old crust material with depleted mantle component, and juvenile mantle-derived magmas). The variation in the origin of the magmas from which the porphyry Mo systems were generated suggests that the composition of magma sources is unlikely to have played a major role in the formation of Mo deposits.

The compilation of existing geochronological data on Mo deposits in NE China, including the newly obtained data from this study, shows that Mesozoic Mo deposits (~250 to 90 Ma) widely occur in this region and are linked to three tectonic-magmatic events: (1) Triassic Mo deposits (250–220 Ma) are mainly distributed along the east-west Xilamulun fault and are related to post-collisional crustal extension following the final closure of the Paleo-Asian ocean; (2) Jurassic to Early Cretaceous Mo mineralization (200–130 Ma) displays a clear younging trend from southeast to northwest and is interpreted to be related to the northwestward flat-slab subduction of the Paleo-Pacific plate beneath the Eurasian continent that started from Early Jurassic (ca. 200 Ma); (3) Cretaceous Mo mineralization (130–90 Ma) shows a distinctly reversed migration trend from northwest to southeast, and can be explained by the coastward migration of slab rollback related lower crust delamination, asthenospheric upwelling and lithospheric thinning.

For skarns, the Baiyinnuo’er Zn-Pb deposit was selected as a representative example for detailed

study in this study. It is one of the largest Zn-Pb deposits in China, with 32.74 Mt resources averaging 5.44% Zn, 2.02% Pb and 31.36 g/t Ag. Several phases of igneous rocks, including Permian, Triassic and Early Cretaceous intrusions, are exposed in the mining areas, and among them the Early Cretaceous granites, which intruded into limestone of the early Permian Huanggangliang Formation, are interpreted to be the source of ore, since their Pb isotope compositions ($^{206}Pb/^{204}Pb$ = 18.25–18.35, $^{207}Pb/^{204}Pb$ = 15.50–15.56 and $^{208}Pb/^{204}Pb$ = 38.14–38.32) are highly consistent with the sulfides including sphalerite, galena and chalcopyrite ($^{206}Pb/^{204}Pb$ = 18.23–18.37, $^{207}Pb/^{204}Pb$ = 15.47–15.62 and $^{208}Pb/^{204}Pb$ = 37.93–38.44). Sulfur isotope values of the sulfides fall in a narrow $\delta^{34}S$ interval of -6.1 to -4.6‰ (mean = -5.4‰, n = 15), suggesting the ore-forming fluid is of magmatic origin.

The deposit formed in three stages: the pre-ore stage (prograde skarn minerals with minor magnetite), the syn-ore stage (sulfides and retrograde skarn minerals including calcite and minor quartz), and the post-ore stage (late veins composed of calcite, quartz, fluorite and chlorite; cutting the above mineral assemblages).The pre-ore stage fluids trapped in pyroxene have higher temperatures (471 ± 31 °C), higher salinity (43.0 ± 3.1 wt. % NaCl eq.), and higher concentrations of Zn (~1.1 wt. %), Pb (~1.7 wt. %), and other elements (e.g., Na, K, Li, As, Rb, Sr, Cs, Ba, Cl and Br) than syn-ore mineralizing fluids (<400 °C, <12 wt. % NaCl eq., ~0.05 wt. % Zn and ~0.03 wt. % Pb). The post-ore fluids are much cooler (<270 °C; averaging ~210°C), with much lower salinity (<5.1 wt. % NaCl eq.), Zn (~38 ppm) and Pb (~19 ppm). Geochemically, the fluids of all paragenetic stages in Baiyinnuo'er are characterized by magmatic signatures based on the element ratios, which are distinctively different from basin brines. The inclusion fluids in pre-ore stage show little variation in composition between ~520 °C and ~420 °C, indicative of a closed cooling system. In contrast, the major components of the syn- and post-ore stage fluids including Cl, Na and K decrease with the temperature dropping from ~350 to <200 °C, indicating a dilution by mixing with groundwater. The metal contents in pre-ore fluid are significantly higher than in syn-ore fluid, but no mineralization occurred. This confirms that the early fluid was, although enriched in metal elements, not responsible for ore precipitation, likely due to its high temperature high salinity nature. The metal deposition was mostly due to mixing with groundwater, which caused temperature decrease and dilution that significantly reduced the metal solubility, thereby promoting metal deposition. The deposition was probably accompanied and facilitated by carbonate dissolution that buffered the acidity generated during the breakdown of Zn (Pb)-Cl complexes and the formation of sulfides. Boiling occurred in both pre-ore and early part of the syn-ore stages, but no evidence indicates that it was related to metal deposition. The current Baiyinnuo'er massive skarns contain both prograde and retrograde minerals (including ore minerals). Paragenetically, they were not formed at the same time, but could be attributed to two (or more) successive pluses of hydrothermal fluids released episodically from residual melts of a progressively downward crystallizing magma. The prograde alteration increased the permeability and porosity, and created sufficient spaces, which was essential for later metal deposition.

Table of Contents

List of Tables

List of Figures

Contents of Appendix Supplementary Materials

Chapter 1

Introduction

Thesis structure

The present thesis is structured so that each individual chapter (Chapters 2-6) is an independent paper of various publication states in international journals in the field of Earth Sciences. At the time of submission, Chapters 2, 3 and 5 have been published in *Journal of Asian Earth Sciences*, *Lithos* and *Economic Geology*, respectively; Chapter 4 has been submitted to *Gondwana Research* and is under review; and Chapter 6 is ready for submission to *Geochimica et Cosmochimica Acta*. During the whole project, I benefited significantly from many others for assistance with field work, sample processing, analyses, data interpretation and manuscript writing, and some of them are co-authors in one/several of the papers, whereas the others have been acknowledged in the relevant chapter(s), depending on their contribution to each of the papers. I, as the undersigned author of this thesis, contributed the most to this project and therefore am the first author for all of these manuscripts listed in this thesis. During my PhD I have also contributed to other publications. I have not included such papers in the thesis but listed the publication information at the end of this chapter (Appendix 1-1).

It should be noted that since each chapter (Chapters 2-6) forms an independent paper published in or prepared for different journals, they are presented slightly differently in their journal formats. For Chapters 2, 3 and 5, the direct journal paper reprints are used. For Chapters 4 and 6, they are presented in a manuscript submission manner, with figures and tables incorporated in the text to make it easy to read. Nevertheless, all the chapters have followed the similar written style such as the consistent use of terminology, geological unit names and mineral abbreviations. Because the thesis is structured in such a manner, some minor repetition in the descriptive text is inevitable, especially in the sections including the geological background, deposit geology, and analytical methods. There are also repeated uses of a few geological maps (they may be slightly different reflecting the evolved understanding over the period of my PhD study), photographs and references.

An Electronic Appendix has been attached to include the supplementary materials for each chapter, following which an Addendum is given to indicate the corrigendum to the publications (Chapters 2, 3 and 5) generated from the reviews by the two examiners. We emphasize that these corrections are only restricted to some description related to deposit geology, methodology, results, as well as few sections in discussion, and that they don’t affect the overall discussion and conclusions presented in each chapter.

Study background, aims and subject of this thesis

Northeastern China hosts numerous ore deposits and prospects of dominantly porphyry and skarn types (Shao et al., 2007; Chen et al., 2007; Zeng et al., 2011), and is considered to be one of the most important nonferrous belts in China (Chen et al., 2009), where more than 100 deposits have been discovered, many of which are large to super-large in size (Fig. 1-1). Most of the porphyry deposits are Mo-dominated, and are generally characterized by Mesozoic ages (Chen et al., 2012; Ouyang et al., 2013), with a few being Paleozoic (e.g., Duobaoshan, Liu et al., 2012). In the past decade, many new Mo deposits have been discovered in NE China, including the giant Chalukou (discovered in 2005; 1.78 Mt Mo metal averaging 0.09% Mo; Liu et al., 2014) and Caosiyao (discovered in 2011; 1.33 Mt Mo metal averaging 0.102% Mo; Hao et al., 2014) porphyry Mo deposits. These new discoveries have made NE China the largest Mo ore region in China, with an estimated total metal resource of >9.2 Mt Mo metal. However, until recently the genesis of the magmatism causing the Mo mineralization, the controlling factors of Mo enrichment, and the geodynamic setting for the Mo deposits in the NE China region have not been fully understood. Skarn deposits are also an important mineralization type in NE China; to date they are poorly investigated.

Two issues will be addressed in this thesis, respectively focusing on porphyry and skarn deposits in NE China. For porphyry deposits, the ore-forming ages are constrained by zircon U-Pb and molybdenite Re-Os methods. The origin and evolution of Mo mineralization-related intrusions are deciphered based on detailed whole rock geochemical and Sr-Nd-Pb-Hf isotope studies. A geodynamic model for the regional magmatism and Mo mineralization is developed by incorporating geochronological data with local geological features, while geochemical data were used to understand the mechanisms controlling the formation of Mo deposits. For skarn deposits, the Baiyinnuo'er Zn-Pb-Ag deposit, the largest Zn-Pb deposit in this region, was selected as an example for detailed study of mineralogy, isotopes, and fluid inclusion microthermometric and LA-ICP-MS compositional analyses, to discuss the ore genesis and hydrothermal evolution of the skarn deposit.

Due to the limitation of time, logistics and financial support, not all the porphyry and skarn deposits in NE China could be studied. This project has chosen the Xilamulun district in the southern part of the Great Xing'an Range for detailed study, and field work and sampling were carried out in 11 representative deposits (Fig. 1-1). During the data interpretation, existing data on Mo deposits in NE China have also been compiled and taken into consideration. Following this introductory chapter, the next three chapters (Chapters 2, 3 and 4) are based on the study of five porphyry Mo deposits, and the two chapters afterwards (Chapters 5 and 6) report the research results on the Baiyinnuo’er skarn Zn-Pb deposit, the largest skarn deposit in NE China. At the end, a chapter (Chapter 7) summarizes the findings of this thesis. A general summary of the five major chapters (Chapters 2-6) is as below.

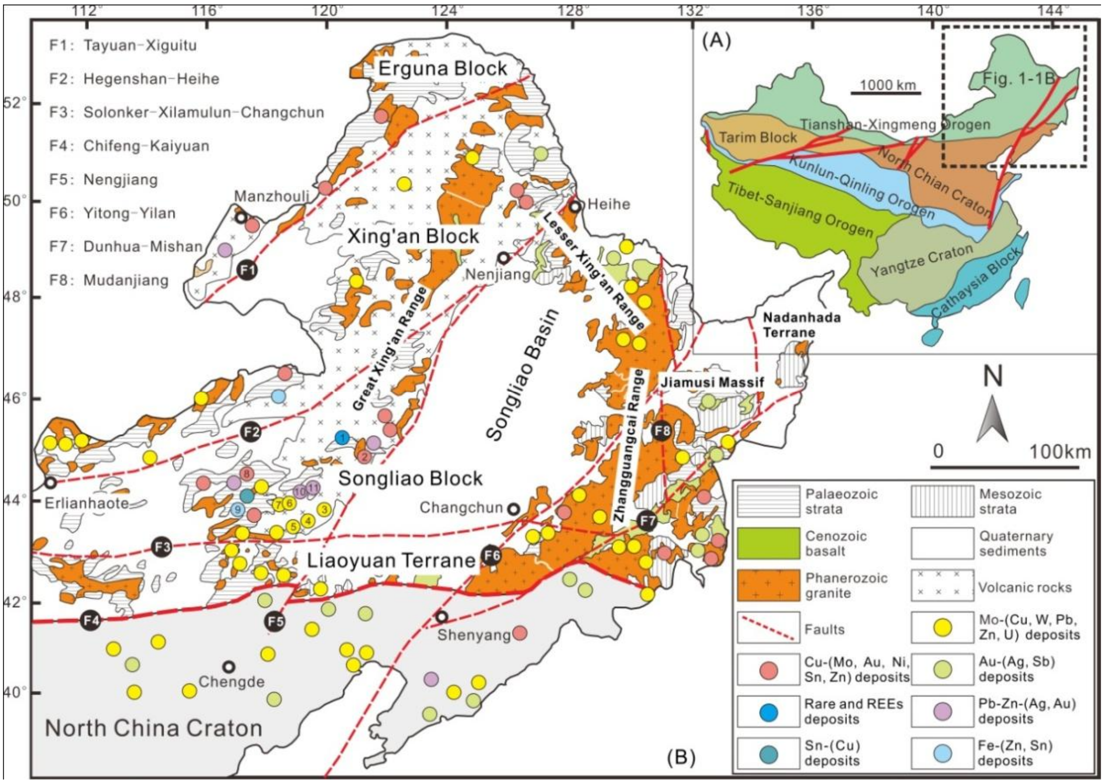

Figure 1-1.(A) Geotectonic division of China; and (B) Geological map of NE China and surrounding regions, showing the distribution of different types of major Mesozoic ore deposits (after Ouyang et al., 2013). Note the deposits numbered have been investigated in this project, though not all included in this thesis: 1-Baerzhe, 2-Budunhua, 3-Aolunhua, 4-Banlashan, 5-Yangchang, 6-Haisugou, 7-Shabutai, 8-Daolundaba, 9-Huanggang, 10-Haobugao, and 11-Baiyinnuo’er.

Chapter 2: Geochronology, geochemistry and Sr-Nd-Hf isotopes of the Haisugou porphyry Mo deposit, northeast China, and their geological significance

Chapter 2 presents zircon U-Pb dating and Hf isotope, and whole rock geochemistry and Sr-Nd isotopes of a typical porphyry Mo deposit, Haisugou, in the Xilamulun district, NE China, to constrain the timing of intrusion emplacement and its source, and to explore the relationship between magma fractional crystallization and Mo enrichment.

Chapter 3: Zircon U-Pb geochronology and Sr-Nd-Pb-Hf isotopic constraints on the timing and origin of Mesozoic granitoids hosting the Mo deposits in northern Xilamulun district, NE China

Chapter 3 presents zircon U-Pb dating, trace elements and Hf isotope, and/or whole rock Sr-Nd-Pb isotopic data for the host granitoids from three Mo deposits (Yangchang, Haisugou and Shabutai) in northern Xilamulun district, NE China, to characterize the age and petrogenesis of these intrusions and their implications for Mo mineralization.

Chapter 4: Regional metallogeny of Mo-bearing deposits in NE China, with new Re-Os dates of porphyry Mo deposits in the northern Xilamulun district

Chapter 4 proposes a hypothesis on the geodynamic setting of the whole NE China region based on the new dating results on Mo deposits in northern Xilamulun district and the compilation of Mo-bearing deposits in the whole NE China. The model also explains the seemingly random ages of mineralization in individual areas in NE China.

Chapter 5: Ore genesis and hydrothermal evolution of the Baiyinnuo'er zinc-lead skarn deposit, northeast China: evidence from isotopes (S, Pb) and fluid inclusions

Chapter 5 presents a detailed study of mineralogy, fluid inclusions and S-Pb isotopes from the Baiyinnuo'er skarn Zn-Pb deposit, to constrain the origin and evolution of this magmatic-hydrothermal deposit.

Chapter 6: Composition and evolution of fluids forming the Baiyinnuo'er skarn Zn-Pb deposit, NE China: insights from laser ablation ICP-MS study of fluid inclusions

Chapter 6 reports new results from the Baiyinnuo'er skarn Zn-Pb deposit, combining fluid inclusion petrography, microthermometry and LA-ICP-MS microanalysis of individual fluid inclusions, to trace the fluid sources, reconstruct the fluid evolution of the hydrothermal system, and contribute to the understanding of ore precipitation mechanisms.

References

Chen, Y.J., Chen, H.Y., Zaw, K., Pirajno, F., and Zhang, Z.J., 2007, Geodynamic settings and tectonic model of skarn gold deposits in China: An overview: Ore Geology Reviews, v. 31, p. 139–169.

Chen, Y.J., Zhang, C., Li, N., Yang, Y.F., and Deng, K., 2012, Geology of the Mo deposits in northeast China: Journal of Jilin University (Earth Science Edition), v. 42, p. 1223–1268 (in English with Chinese abstract).

Hao, Z., Fei, H., Liu, L., Hao, Q., and Turner, S., 2014, World's Third–Largest Molybdenum Deposit Discovered in Caosiyao Area, Xinghe County, Inner Mongolia: Acta Geologica Sinica (English Edition), v. 88, p. 1615–1616.

Liu, J., Wu, G., Li, Y., Zhu, M., and Zhong, W., 2012, Re-Os sulfide (chalcopyrite, pyrite and molybdenite) systematics and fluid inclusion study of the Duobaoshan porphyry Cu (Mo) deposit, Heilongjiang Province, China: Journal of Asian Earth Sciences, v. 49, p. 300–312.

Liu, J., Mao, J., Wu, G., Wang, F., Luo, D., and Hu, Y., 2014, Zircon U-Pb and molybdenite Re-Os dating of the Chalukou porphyry Mo deposit in the northern Great Xing'an Range, China and its geological significance: Journal of Asian Earth Sciences, v. 79, p. 696–709.

Ouyang, H.G., Mao, J.W., Santosh, M., Zhou, J., Zhou, Z.H., Wu, Y., and Hou, L., 2013, Geodynamic setting of Mesozoic magmatism in NE China and surrounding regions: Perspectives from spatio-temporal distribution patterns of ore deposits: Journal of Asian Earth Sciences, v. 78, p. 222–236.

Shao, J.A., Zhang, L.Q., Mu, B.L., and Han, Q.J., 2007, Upwelling of Da Hinggan Mountains and its geodynamic background: Beijing, Geological Publishing House, 250 p. (in Chinese).

Zeng, Q.D., Liu, J.M., Zhang, Z.L., Chen, W.J., and Zhang, W.Q., 2011, Geology and geochronology of the Xilamulun molybdenum metallogenic belt in eastern Inner Mongolia, China: International Journal of Earth Sciences, v. 100, p. 1791–1809.

Chapter 2

Geochronology, geochemistry and Sr-Nd-Hf isotopes of the Haisugou porphyry Mo deposit, northeast China, and their geological significance

Journal of Asian Earth Sciences 79 (2014) 777–791

Contents lists available at SciVerse ScienceDirect

Journal of Asian Earth Sciences

journal homepage: www.elsevier.com/locate/jseaes

Geochronology, geochemistry and Sr–Nd–Hf isotopes of the Haisugou porphyry Mo deposit, northeast China, and their geological significance

Qihai Shu [a], Yong Lai [a,*], Chao Wang [a], Jiajia Xu [b], Yi Sun [a]

[a] Key Laboratory of Orogenic Belt and Crustal Evolution, School of Earth and Space Sciences, Peking University, Beijing 100871, PR China
[b] National Geological Library of China, Beijing 100083, PR China

This publication has been removed due to copyright restrictions

http://dx.doi.org/10.1016/j.jseaes.2013.05.015

This publication has been removed due to copyright restrictions

This publication has been removed due to copyright restrictions

This publication has been removed due to copyright restrictions

This publication has been removed due to copyright restrictions

This publication has been removed due to copyright restrictions

This publication has been removed due to copyright restrictions

This publication has been removed due to copyright restrictions

This publication has been removed due to copyright restrictions

This publication has been removed due to copyright restrictions

This publication has been removed due to copyright restrictions

This publication has been removed due to copyright restrictions

This publication has been removed due to copyright restrictions

Chapter 3

Zircon U-Pb geochronology and Sr-Nd-Pb-Hf isotopic constraints on the timing and origin of Mesozoic granitoids hosting the Mo deposits in northern Xilamulun district, NE China

Lithos 238 (2015) 64–75

Contents lists available at ScienceDirect

Lithos

journal homepage: www.elsevier.com/locate/lithos

Zircon U–Pb geochronology and Sr–Nd–Pb–Hf isotopic constraints on the timing and origin of Mesozoic granitoids hosting the Mo deposits in northern Xilamulun district, NE China

Qihai Shu [a,b,c], Yong Lai [b,*], Yitao Zhou [b], Jiajia Xu [d], Huaying Wu [a,e]

[a] State Key Laboratory of Geological Processes and Mineral Resources, School of Earth Sciences and Resources, China University of Geosciences, Beijing 100083, China
[b] Key Laboratory of Orogenic Belt and Crustal Evolution, School of Earth and Space Sciences, Peking University, Beijing 100871, China
[c] Economic Geology Research Centre (EGRU), College of Science, Technology and Engineering, James Cook University, Townsville, QLD 4811, Australia
[d] National Geological Library of China, Beijing 100083, China
[e] Institute of Mineral Resources Research, China Metallurgical Geology Bureau, Beijing 100025, China

http://dx.doi.org/10.1016/j.lithos.2015.09.014

This publication has been removed due to copyright restrictions

This publication has been removed due to copyright restrictions

This publication has been removed due to copyright restrictions

This publication has been removed due to copyright restrictions

This publication has been removed due to copyright restrictions

This publication has been removed due to copyright restrictions

This publication has been removed due to copyright restrictions

Chapter 4

Regional metallogeny of Mo-bearing deposits in NE China, with new Re-Os dates of porphyry Mo deposits in the northern Xilamulun district

Regional metallogeny of Mo-bearing deposits in NE China, with new Re-Os dates of porphyry Mo deposits in the northern Xilamulun district

Qihai Shu [a, b, *], Zhaoshan Chang [b], Yong Lai [a], Yitao Zhou [a]

[a] *Key Laboratory of Orogenic Belt and Crustal Evolution, School of Earth and Space Sciences, Peking University, Beijing 100871, China*

[b] *Economic Geology Research Centre (EGRU), College of Science, Technology and Engineering, James Cook University, Townsville, Queensland 4811, Australia*

[*] Corresponding author: Qihai Shu, E-mail: qihai.s@gmail.com

Abstract

Northeastern China has become the largest molybdenum mineralization center in China with many new discoveries of giant Mo deposits in the recent decade. The Xilamulun district is in the southern part of NE China and contains 18 Mo deposits of dominantly porphyry type. These deposits are mostly along the EW-striking Xilamulun fault. Re-Os dating of hydrothermal molybdenite from four deposits in the northern Xilamulun district revealed mineralization ages from 140 to 130 Ma (129.4 ± 3.4 Ma for Aolunhua, 135.3 ± 2.6 Ma for Shabutai, 136.4 ± 0.8 Ma for Haisugou and 136.1 ± 6.6 Ma for Banlashan), in general agreement with the crystallization ages of their host granitic rocks.

The compilation of existing data on Mo-bearing deposits in NE China, including the new data of this study, shows that Mesozoic Mo deposits with ages ranging from ~250 to 90 Ma widely occur in this region. We propose that they are linked to three tectonic-magmatic events: (1) Triassic Mo deposits (250–220 Ma) are mainly distributed along the east-west Xilamulun fault and are related to the post-collisional crustal extension following the final closure of the Paleo-Asian ocean; (2) Jurassic to Early Cretaceous Mo mineralization (200–130 Ma) displays a clear younging trend from southeast to northwest, coincides well with the regional magmatism, and is interpreted to be related to the northwestward flat-slab subduction of the Paleo-Pacific plate beneath the Eurasian continent that started from Early Jurassic (ca. 200 Ma); (3) Cretaceous Mo mineralization (130–90 Ma), however, shows a distinctly reversed migration trend from northwest to southeast, and can be explained by the coastward migration of slab rollback related lower crust delamination, asthenospheric upwelling and lithospheric thinning in eastern China. The spatial-temporal distribution of the Mesozoic Mo mineralization is important for regional metallogeny and exploration. Recently numerous epithermal Au (Cu, Mo) deposits have been recognized in the southeast margin of NE China. According to this study, we predict that beneath these epithermal deposits, there could exist hidden porphyry/skarn systems, on which particular attention should be paid in exploration.

1. Introduction

China has more than half of the world's molybdenum metal resources (Mao et al., 2011a), and has increased its annual production from 30,000 t in 1999 to 210,000 t in 2009 (Zeng et al., 2013). Previously, the East Qinling-Dabie orogenic belt was the largest Mo district in China, with ~8.5 Mt Mo metal (Mao et al., 2011a). In the past decade, many new Mo deposits have been discovered in northeastern China, including the giant Chalukou (discovered in 2005; 1.78 Mt Mo metal averaging 0.09% Mo; Liu et al., 2014) and Caosiyao (discovered in 2011; 1.33 Mt Mo metal averaging 0.102% Mo; Hao et al., 2014) porphyry Mo deposits. These new discoveries have made NE China the largest Mo ore region in China, with an estimated total metal resource of >9.2 Mt Mo metal (Appendix 4-1).

In the NE China region, 18 Mo deposits are along the EW-trending Xilamulun fault in a newly identified district referred to as the Xilamulun Mo-Cu metallogenic district (Fig. 4-1; Zeng et al., 2009a; Zhang et al., 2009a). This ~400-km-long, ~300-km-wide district is subdivided by the Xilamulun fault into southern and northern parts (Fig. 4-1). Many studies have been carried out on the Mo deposits in the southern part (e.g., Nie et al., 2007; Chen et al., 2008; Qin et al. 2008, 2009; Wu et al., 2008, 2011a, 2014; Wan et al., 2009; Zeng et al., 2009a, b, 2011; Zhang et al., 2009d, 2010a; Liu et al., 2010a; Meng et al., 2013; Sun et al., 2013a), but to date only a few papers have focused on the northern deposits (e.g., Shu et al., 2009, 2014, 2015; Zhang et al., 2010b; Wu et al., 2011b; Ma et al., 2013; Zeng et al., 2014). In this contribution we report the Mo deposits in the northern Xilamulun district.

Most of the Mo deposits in NE China are of porphyry type. They are generally characterized by Mesozoic ages (Chen et al., 2012; Ouyang et al., 2013a; Shu et al., 2015), with a few being Paleozoic (e.g., Duobaoshan, Liu et al., 2012a). The mineralizing ages range from ~250 Ma to ~90 Ma (e.g., Han et al., 2009; Zhang et al., 2009a; Zeng et al., 2012; this study). The spatial distribution of the Mo deposits seems to be random, with some relatively small districts in the region containing deposits of various ages. For example, the Xilamulun district contains Mo mineralization formed in several periods from ~250 Ma to <130 Ma (Fig. 4-1C; Zhang et al., 2009a, and this study), whereas the Yanshan-Liaoxi district contains deposits formed in two periods (190–165 Ma, and 150–130 Ma; Fig. 4-1C; Han et al., 2009). There has been no consistent geodynamic models to explain the spatial-temporal distribution of the deposits, despite that most of the individual deposits have been documented (e.g., Mao et al., 2005; Zhang et al., 2009a; Chen et al., 2012; and references in Appendices 4-1 and 4-2). At district level, there are proposals that the discrete mineralizing intervals were related to two distinct geodynamic events, but there has been little understanding on what exactly the events were, and the proposed events are not comparable. For example, Han et al (2009) proposed 190–165 Ma and 150–130 Ma events in the Yanshan-Liaoxi area, whereas Zhang et al (2009a) proposed 185–150 Ma and 140–110 Ma events in the Xilamulun district. These two proposals cannot explain many dates reported after 2009 (c.f., Fig. 4-1C and Appendix 4-1), either. In summary the geodynamic setting for the Mo-bearing deposits in the NE China region is not well understood. In this study we propose a hypothesis on the geodynamic setting of the whole NE China region based on the new dating results on deposits in northern Xilamulun district and the compilation of Mo-bearing deposits in the whole region. The hypothesis also explains the seemingly random ages of mineralization in individual areas.

2. Geological setting

Northeastern China is composed of the eastern part of the Central Asian Orogenic Belt (or the Xing'an-Mongolian Orogenic Belt) and the northeastern margin of the North China craton (Fig. 4-1). It has undergone two major sets of events: (1) The amalgamation of NE China in the Paleozoic in several steps, including the fusion of the Erguna massif and the Xing'an terrane along the Tayuan-Xiguitu suture (~490 Ma), of the Xing'an terrane and the Songliao terrane along the Hegenshan-Heihe suture (290–260 Ma), of the Liaoyuan terrane and the North China craton along the Chifeng-Kaiyuan fault (290–260 Ma), and eventually the closure of the Paleo-Asian Ocean marked by the collision of the Songliao terrane and the Liaoyuan terrane along the Solonker-Xilamulun-Changchun suture at ~250 Ma (Fig. 4-1B; Xiao et al., 2003; Wu et al., 2011c). (2) During the Mesozoic, the Jiamusi Massif and Nadanhada Terrane were accreted to the previously combined continent as a result of the Paleo-Pacific plate subduction in the southeast (Fig. 4-1B; Wu et al., 2011c; Zhou and Wilde, 2013). The subduction and some subsequent collisional processes related to the events have induced extensive magmatism, some with mineralization (Wu et al., 2011c; Ouyang et al., 2013a).

2.1. Regional context

In the northernmost part of NE China, the Erguna massif is considered to be the eastern extension of the Central Mongolian microcontinent, and contains Proterozoic to Paleozoic strata and Mesozoic granitoids (Fig. 4-1C), with a few Precambrian granitic intrusions (Wu et al., 2011c). The Mesozoic magmatism was interpreted to be generated in an active continental margin related to the southward subduction of the Mongol-Okhotsk oceanic plate beneath the Erguna massif (e.g., Tang et al., 2014, 2015; Zhang et al., 2014; Wang et al., 2015).

The Xing'an terrane (Fig. 4-1C) has Paleozoic strata including Early Paleozoic limestone and Late Paleozoic clastic sediments (Wu et al., 2011c). The igneous rocks can be grouped into two sets: metamorphosed and deformed granites and pegmatites of Cambrian-Ordovician ages (500-460 Ma), and younger undeformed Mesozoic granitoids and volcanic rocks that are widely distributed throughout the region (Zhou and Wilde, 2013).

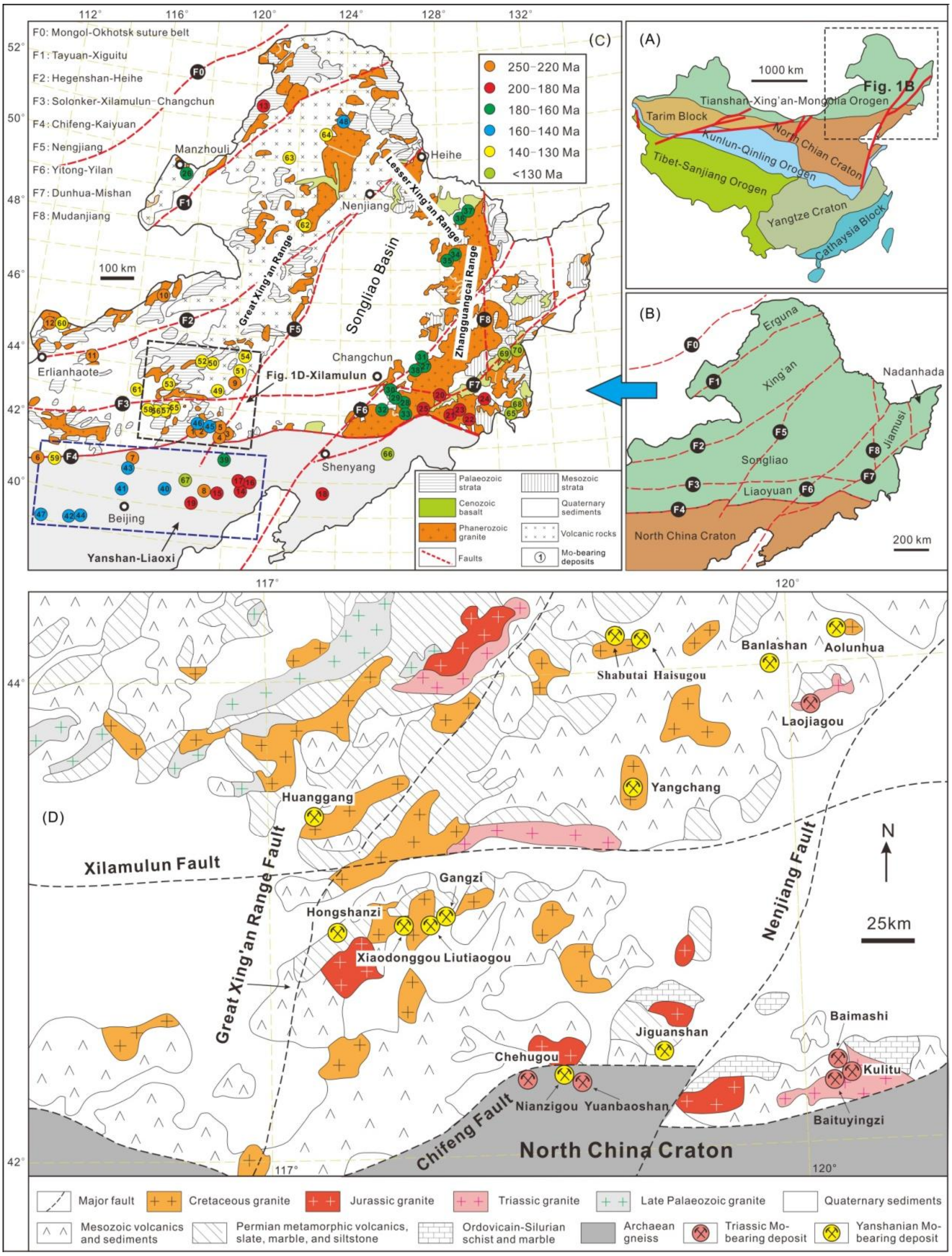

Figure 4-1. (A) Geotectonic division of China (from Mao et al., 2011a). (B) Tectonic subdivisions of NE China (from Wu et al., 2011c). (C) Geological map of NE China and surrounding regions (modified after Zeng et al., 2012, and Ouyang et al., 2013a), showing the distribution of Mesozoic Mo-bearing deposits (the details of the numbered deposits can be found in Appendix 4-1). (D) Geological map of the Xilamulun district and the location of major Mo deposits (modified after Zeng et al., 2012).

The Songliao terrane is situated in central NE China. It includes the Zhangguangcai Range in the east, the southern Great Xing'an Range in the west, the Lesser Xing'an Range in the northeast, and the Songliao Basin in the middle (Fig. 4-1C). The Songliao Basin is filled by dominantly Early Cretaceous volcanic rocks (140–106 Ma), commonly interlayered with sedimentary sequences, based on boreholes and outcrop observations (Wang et al., 2002; Ding et al., 2007; Shu et al., 2007; Zhang et al., 2007b, 2010a). Its basement is composed of Paleozoic to Mesozoic granitoids, as well as some Precambrian components (Xu et al., 2013). The southern Great Xing'an Range is characterized by the occurrence of Mesozoic igneous rocks, of which most are intermediate-felsic in composition, covering~75% area of the region (Shao et al., 2007). The Lesser Xing'an Range and Zhangguangcai Range are dominated by Mesozoic granitoids and minor volcanic rocks, with smaller amounts of Paleozoic strata and granitoids, as well as Mesozoic mafic-ultramafic intrusive rocks (Wu et al., 2011c; Xu et al., 2013).

The Liaoyuan terrane is located along the northern margin of the North China craton. Traditionally it was considered to be the "Northern Marginal Terrane" of the North China craton. It is composed of Paleozoic sedimentary strata, volcanic rocks and granitoids. Some units were thought to be Precambrian, but recent geochronological data indicate that they are in fact deformed Paleozoic-Mesozoic strata (Wu et al., 2011c, and references therein). The Liaoyuan terrane is similar to the Songliao terrane in that the outcrops are dominated by Mesozoic granitoids with subordinate Late Paleozoic magmatic rocks and the basement rocks do not contain any older rocks, and therefore has been proposed to be a part of the Central Asian Orogenic Belt, rather than the North China craton (Wu et al., 2011c).

Apart from the above mentioned terranes, there are also two smaller blocks that are located in the easternmost part of the NE China, i.e., the Jiamusi massif and the Nadanhada terrane (Fig. 4-1C). They have been recognized as accretionary terranes related to the subduction of the Paleo-Pacific plate (Wu et al., 2011c; Zhou and Wilde, 2013). The Jiamusi massif consists of the Mashan Complex (metamorphosed to granulite facies in the Early Paleozoic at ~500 Ma; Zhou and Wilde, 2013), Early-Late Paleozoic granitoids, Late Paleozoic sediments, and Late Paleozoic-Mesozoic volcanic rocks (Xu et al., 2013; Zhou and Wilde, 2013). The Nadanhada terrane contains Late Paleozoic limestone, Triassic-Jurassic radiolarian-bearing chert, mafic lava and gabbro referred to as the Raohe Complex (Wu et al., 2011c; Xu et al., 2013).

The northern margin of the North China craton (south of the Chifeng-Kaiyuan fault; Fig. 4-1C) is characterized by a Neoarchean to Paleoproterozoic basement of high-grade metamorphic rocks, which are overlain by Mesoproterozoic to Cenozoic thick marine clastic and carbonate platform sediments (Zhang et al., 2009b; Santosh, 2010; Zhai and Santosh, 2011). In the Paleozoic, with the southward subduction of the Paleo-Asian oceanic plate beneath the northern craton margin, abundant subduction-related plutons (from ~466 Ma; U-Pb zircon age of the Bainaimiao granodiorite; Tang and Yan, 1993; to ~260 Ma; Zhang et al., 2007c; 2009b, c; Yang et al., 2015) occurred in this region, forming a typical Andean-type continental margin (e.g., Zhang et al., 2009b, c; Yang et al., 2015). During the Triassic, a number of ultramafic-syenite complexes, lamprophyres, and A-type granites of similar ages emplaced in this region and its neighboring areas in NE China (e.g., Mu et al., 2001; Shao et al., 2003; Han et al., 2004; Zhang et al., 2009b; Yang et al., 2015), forming an East-West trending ultramafic/alkaline magmatic belt, implying that the region entered into a post-collisional intraplate evolution stage after the final closure of the Paleo-Asian Ocean.

2.2. Mesozoic magmatism in NE China and its geodynamic settings

Although pre-Mesozoic magmatism has been reported (e.g., Tang and Yan, 1993; Zhang et al., 2007c; Yang et al., 2015), it has been demonstrated by recent geochronological data that most of the igneous rocks in NE China were emplaced during the Mesozoic, with the majority having Jurassic to Cretaceous ages (e.g., Zhang et al., 2008b, 2010c; Wu et al., 2011c; Xu et al., 2013). Several hypotheses have been raised to explain the tectonic background for the Jurassic to Cretaceous magmatism in NE China. Some authors proposed a mantle plume model or other intraplate processes (e.g., Shao et al., 1995, 2001), or post-orogenic lithospheric extension models related to the closure of the Mongol-Okhotsk ocean (Fan et al., 2003; Meng, 2003), while others insist on the subduction model of Paleo-Pacific plate beneath the eastern China (Zhang et al., 2010a, and reference therein). Extensive zircon U-Pb dating in recent years have shed new light on the geodynamic settings. It has been noticed that the intrusive rocks, mainly granitoids, display a northwestward younging trend. In East Jihei and Jiamusi terrane on the most SE part of the continent (Zone I; Fig. 4-2), the ages of the granitoids are mostly in the range of 210–180 Ma. In Songliao Basin-Lesser Xing'an and Zhangguangcai Ranges towards northwest (Zone II; Fig. 4-2), the ages are mostly in the 180–150 Ma range. At the northwestern end, the intrusive ages in the Great Xing'an Range (Zone III; Fig. 4-2) are even younger, mostly 140–130 Ma (Fig. 4-2). In contrast, the volcanic rocks in NE China have an opposite younging direction, from NW to SE. Their ages have a strong mode at ~130–120 Ma in Zone III, the most NW part, slightly younger than the intrusive rocks in the same region. Towards SE in Zone II (Songliao Basin-Lesser Xing'an and Zhangguangcai Ranges), the volcanic ages are mostly 130–110 Ma (Fig. 4-2). At the SE end in Zone I (East Jihei and Jiamusi terranes), the volcanic rocks are even younger, mostly in the 120–80 Ma range (Fig. 4-2). The above space-time distribution pattern, summarized in Zhang et al. (2010a), is strong evidence for the Paleo-Pacific plate subduction model. It was proposed that the subduction was from SE towards NW and along with the progress of the subduction and the migration of the magma-generating front towards NW, the granitoids formed subsequently from SE to NW. Eventually the subducted slab rolled back from NW to SE, generating a new series of magma from NW to SE (Zhang et al., 2010a; Sun et al., 2013b; Dash et al., 2015).

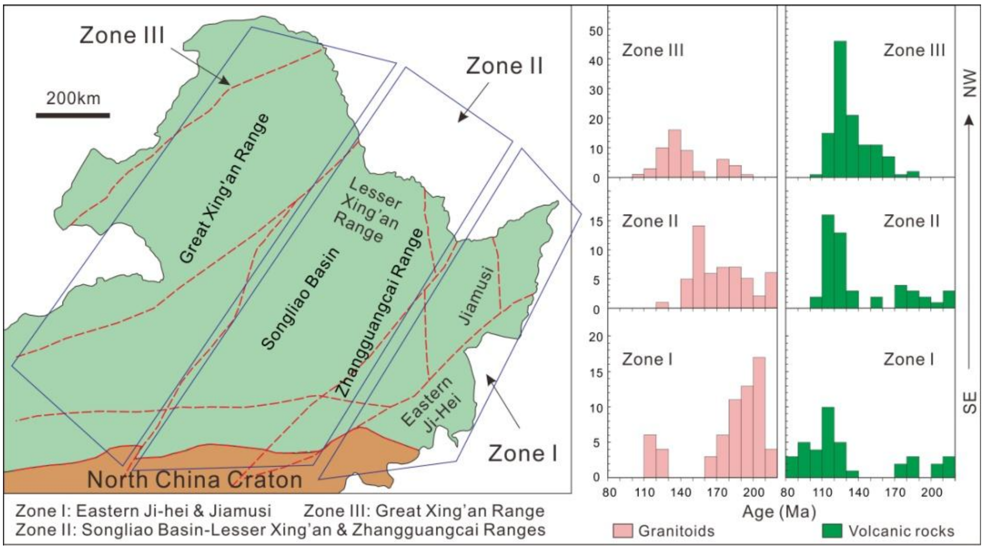

Figure 4-2. Jurassic-Cretaceous granitoids and volcanic rocks in NE China and their spatial-temporal distribution. Note most of the granitoids are characterized by Jurassic ages (mainly from 200 to 130 Ma) and getting younger from southeast to northwest, while volcanic rocks are of mainly Cretaceous ages (between 130 and 80 Ma) and younging coastward. Age data are from Zhang et al. (2010a), Xu et al. (2013), and references therein.

2.3. Geology of the Xilamulun district

The Xilamulun Mo-Cu district is between the eastern part of the Central Asian Orogenic Belt and the North China craton (Fig. 4-1). The northern part of this belt (north of the Xilamulun fault) lies within the Songliao terrane, and the southern section (south of the Xilamulun fault) is part of the Liaoyuan terrane and the northern margin of the North China craton (Fig. 4-1C, D). The NNE-striking faults in this region, including the Great Xing'an Range fault and the Nenjiang fault (Fig. 4-1D), are much younger than the E-W trending Xilamulun fault (middle segment of the Solonker-Xilamulun-Changchun suture), and have been considered to have resulted from the northwestward subduction of the Paleo-Pacific plate (Liu et al., 2010a). This region contains Archaean gneiss, Paleozoic schist and marble in the south, and Mesozoic sedimentary, intrusive, and volcanic rocks in the north (Fig. 4-1D). The Xilamulun district contains 18 Mo-bearing deposits, most of which were discovered in the past decade. Six of these deposits have Triassic ages, while the rest 12 were formed in Late Jurassic to Early Cretaceous (Fig. 4-1D; Table 4-1).

3. Geological characteristics of the four Mo deposits in the northern Xilamulun district dated in this study

In the northern Xilamulun district there are seven Mo-bearing deposits (Fig. 4-1D), namely the

Table 4-1 Geological and mineralogical features of the Mesozoic Mo-bearing deposits in the Xilamulun district.

Deposit	Mineralization Style	Country rocks	Intrusive units and ages (Ma)	Mol Re-Os age (Ma)	Grade and tonnage	Alteration	Ore minerals	Ore-forming fluid(s)	References
Southern Xilamulun									
Chehugou	Mo-Cu porphyry type; mainly disseminations or veins in porphyry intrusions	Precambrian basement with migmatitic granites	Syenogranite (U-Pb, 376 ± 3), monzogranite, and granitic porphyry (U-Pb, 251.6 ± 3.2)	250.2 ± 7.2	50 Kt Mo @ 0.12%; 111 Kt Cu @ 0.5%	K-feldspar, quartz, sericite, epidote, chlorite, and clay	Mol, Ccp, Py, Sp, Mag	T: 210 to 423 °C; S: 1.7 to 43.8 wt.% NaCl eqv.	Wan et al., 2009; Liu et al., 2010a; Meng et al., 2013
Yuanbaoshan	Mo porphyry type; disseminations or thin coatings within the fractures of the host granitic cataclasite	Late Jurassic-Early Cretaceous volcanic rocks and Oligocene basalt	Quartz monzonite (U-Pb, 269 ± 3)	248.0 ± 2.7	N.d.	N.d.	Mol, Oy	N.d.	Liu et al., 2010a; Zeng et al., 2012
Kulitu	Mo-Cu porphyry type; veins, veinlets and disseminated blocks within the porphyritic monzogranitic stock	Early Permian sedimentary sequences and Early Cretaceous volcanic rocks	Monzogranite (U-Pb, 249.1 ± 1.6)	245.1 ± 1.3	7.4 Kt Mo @ 0.05%	Sericite, quartz, K-feldspar, chlorite, epidote, and carbonate	Mol, Ccp, Py	N.d.	Zhang et al., 2009a; Zeng et al., 2012
Baimashi	Cu-Mo porphyry type; veins and veinlets within the porphyritic granite stock	Early Permian sedimentary sequences and Early Cretaceous volcanic rocks	Porphyritic granite (U-Pb, 249.4 ± 2.2)	248.6 ± 6.7	22 Kt Mo @ 0.08%; 143 Kt Cu @ 0.49%	K-feldspar, biotite, quartz, sericite, carbonate, chlorite, and epidote	Ccp, Bn, Py, Mol	N.d.	Zeng et al., 2012; Sun et al., 2013a
Baituyingzi	Porphyry Mo-Cu; veinlets and stockworks within the monzogranitic stock	Early Permian sedimentary sequences and Early Cretaceous volcanic rocks	Monzogranite porphyry	248.0 ± 10	Mo @ 0.08-0.18%	K-feldspar, quartz, sericite, chlorite, and epidote	Mol, Py, Ccp	N.d.	Sun et al., 2013a
Jiguanshan	Mo porphyry type; disseminations and flakes in the granite porphyry; stockworks in the lithic tuff and rhyolitic rocks	Permian volcanic and sedimentary rocks, Mesozoic felsic volcanic and pyroclastic rocks	Granite porphyry (Ar-Ar, 155.1 ± 1.9), post-ore diabase (Ar-Ar, 149.4 ± 0.9) and quartz porphyry	155.3 ± 0.9	> 100 Mt @ 0.08-0.11% Mo	K-feldspar, quartz, sericite, fluorite, carbonate, chlorite, and epidote	Mol, Py, Ccp, Sp, Mag	T: 250 to >550 °C; S: 0.9 to >66 wt.% NaCl eqv.	Wu et al., 2011a, 2014
Nianzigou	Porphyry Mo; disseminations and veinlets in monzonitic granite	Precambrian basement and Early Cretaceous volcanic rocks	Monzonitic granite (U-Pb, 152.4 ± 1.6)	154.3 ± 3.6	15 Kt Mo @ 0.39%	K-feldspar, quartz, sericite, chlorite, and kaolinite	Mol, Py, Ccp	T: 134 to 459 °C; S: 0.5 to 19.9 wt.% NaCl eqv.	Chen et al., 2008; Zhang et al., 2010d; Zeng et al., 2011a
Gangzi	Mo porphyry type; disseminated and massive ores hosted by greisen at the top of the granite stock	Jurassic volcanic rocks	porphyritic granite (U-Pb, 139.1 ± 2.3)	N.d.	Mo: 0.01-0.06%	Quartz, muscovite, and sericite	Py, Mol, Sp, Gn	N.d.	Zeng et al., 2011a
Xiaodonggou	Mo porphyry type; disseminations and quartz-sulfide veinlets in the inner contact zone at the top of the granitoid stock	Precambrian basement and Permian volcano-sedimentary rocks	Porphyritic granite (U-Pb, 142.2 ± 2)	138.1 ± 2.8	32 Kt Mo @ 0.11%	K-feldspar, quartz, sericite, fluorite, and calcite	Mol, Py, Ccp, Sp, Mag, Gn	T: 260 to 480 °C; S: 15 to 40 wt.% NaCl eqv.	Qin et al., 2008, 2009; Zeng et al., 2011a

(*Cont.*) Table 4-1 Geological and mineralogical features of the Mesozoic Mo-bearing deposits in the Xilamulun district.

Liutiaogou	Mo-U volcanic hydrothermal vein type	Permian slate, Cretaceous tuff and rhyolite	Tuff (Rb-Sr, 137 ± 12)	N.d.	1.9 Kt Mo @ 0.29%	N.d.	Py, Mol	N.d.	Zeng et al., 2012
Hongshanzi	Mo-U volcanic hydrothermal vein type; veinlets and disseminations within the rhyolite porphyry	Early Permian metamorphic tuff and andesite and Cretaceous volcanic rocks	Rhyolite porphyry (U-Pb, 130 ± 8)	N.d.	4.5 Kt Mo @ 0.65%	Quartz, albite, biotite, chloride, fluorite, and calcite	Mol, Py	N.d.	Nie et al., 2007; Zeng et al., 2011a, 2012
Northern Xilamulun									
Yangchang	Mo-Cu porphyry type; veins and disseminations within the altered granite	Permian slate and Late Jurassic volcanic rocks	Monzogranite (U-Pb, 137.4 ± 2.1) and granite porphyry (U-Pb, 132 ± 2)	138.5 ± 4.5	Mo: 0.07%	K-feldspar, quartz, sericite, chlorite, fluorite and kaolinite	Py, Mol, Ccp, Sp, Gn	T: 180 to 467 °C; S: 2.1 to 10.4 wt.% NaCl eqv.	Zeng et al., 2010, 2014; Zhang et al., 2012; Shu et al., 2015
Haisugou	Mo porphyry type; veins, disseminations and hydrothermal breccias within the granite	Permian limestone and Mesozoic granites	Granodiorite and granite (U-Pb, 137.6 ± 0.9)	136.4 ± 0.8	N.d.	Quartz, sericite, chlorite, fluorite, calcite and skarn	Mol, Ccp, Py	T: 225 to 510 °C; S: 1.7 to 58.2 wt.% NaCl eqv.	Shu et al., 2014, 2015; This study
Banlashan	Mo porphyry type; hydrothermal breccias, vein, disseminations and stockworks infilling open spaces within rhyolitic clasts	Permian limestone and Late Jurassic volcanic rocks	Rhyolite porphyry (U-Pb, 157.5 ± 3.3), granodiorite porphyry (U-Pb, 133.5 ± 1.7), and granite porphyry	136.1 ± 6.6	11 Kt Mo @ 0.07%	Sericite, quartz, chlorite, epidote and calcite	Mol, Py, Ccp, Sp, Gn	T: 145 to >550 °C; S: 0.7 to >66 wt.% NaCl eqv.	Yan, 2009; Zhang et al., 2010b; This study
Shabutai	Mo porphyry type; veins and disseminations within the granite	Permian limestone and Mesozoic granites	Monzogranite (U-Pb, 138.4 ± 1.5)	135.3 ± 2.6	N.d.	Quartz, sericite, chlorite, kaolinite and calcite	Mol, Ccp, Py	T: 200 to 480 °C; S: 0.5 to 57.2 wt.% NaCl eqv.	Shu et al., 2015; This study
Huanggang	Mo-bearing Fe-Sn skarn type; massive skarn orebodies within the contact zone between granite and marble	Permian limestone and sandstone, and Jurassic volcanic rocks	K-feldspar granite and granite porphyry (U-Pb, 136.8 ± 0.6)	135.3 ± 0.9	N.d.	Skarn alteration (garnet, pyroxene, actinolite, epidote, chlorite, and quartz)	Mag, Cst, Sch, Mol, Ccp, Py, Sp, Gn	T: 270 to 470 °C; S: 3.4 to 55.8 wt.% NaCl eqv.	Zhou et al., 2010, 2012; This study
Aolunhua	Mo-Cu porphyry type; Mo-bearing quartz veins within grantic stock or crosscutting the Permian strata	Permian felsic volcanic rocks and Permian slate and sandstone	Monzogranite-porphyry (U-Pb, 131.9 ± 0.5) and post-ore quartz porphyry (U-Pb, 125.7 ± 0.6)	129.4 ± 3.4	32 Kt Mo @ 0.08%; 100 Kt Cu @ 0.25%	K-feldspar, quartz, sericite, kaolinite, chlorite, epidote, and calcite	Mol, Py, Ccp, Sp, Gn	T: 250 to >490 °C; S: 0.9 to 58.4 wt.% NaCl eqv.	Shu et al., 2009; Wu et al., 2011b; Ma et al., 2013; This study
Laojiagou	Porphyry Mo; veins and disseminations within the monzogranite porphyry	Precambrian basement and Jurassic volcanic rocks	Monzogranite porphyry (U-Pb, 238.6 ± 1.8)	234.9 ± 3.1	135 Kt Mo @ 0.07%	K-feldspar, quartz, sericite, chlorite, calcite, and epidote	Mol, Py, Ccp	T: 280 to >550 °C; S: 5.0 to >66.8 wt.% NaCl eqv.	Liu et al., 2012b; Zeng et al., 2012

N.d. = no data. T = homogenization temperature; S = salinity. Ore mineral abbreviations: Bn = bornite, Cst = cassiterite, Ccp = chalcopyrite, Gn = galena, Mol = molybdenite, Mag = magnetite, Py = pyrite, Sch = scheelite, Sp = sphalerite.

Aolunhua, Yangchang, Haisugou, Shabutai, Banlashan, Laojiagou and the Mo-bearing Huanggangliang Fe-Sn deposit. The general geological characteristics of these deposits are summarized in Table 4-1. These deposits are temporally and spatially associated with small granitic intrusions. Their mineralization style, alteration features and fluid characteristics indicate that they are all of porphyry type, except for Huanggang, a typical skarn type deposit. In this study we report the molybdenite Re-Os dates of four deposits, namely Aolunhua, Haisugou, Shabutai and Banlashan. Below we report their geological features based on our own observations and previously publications.

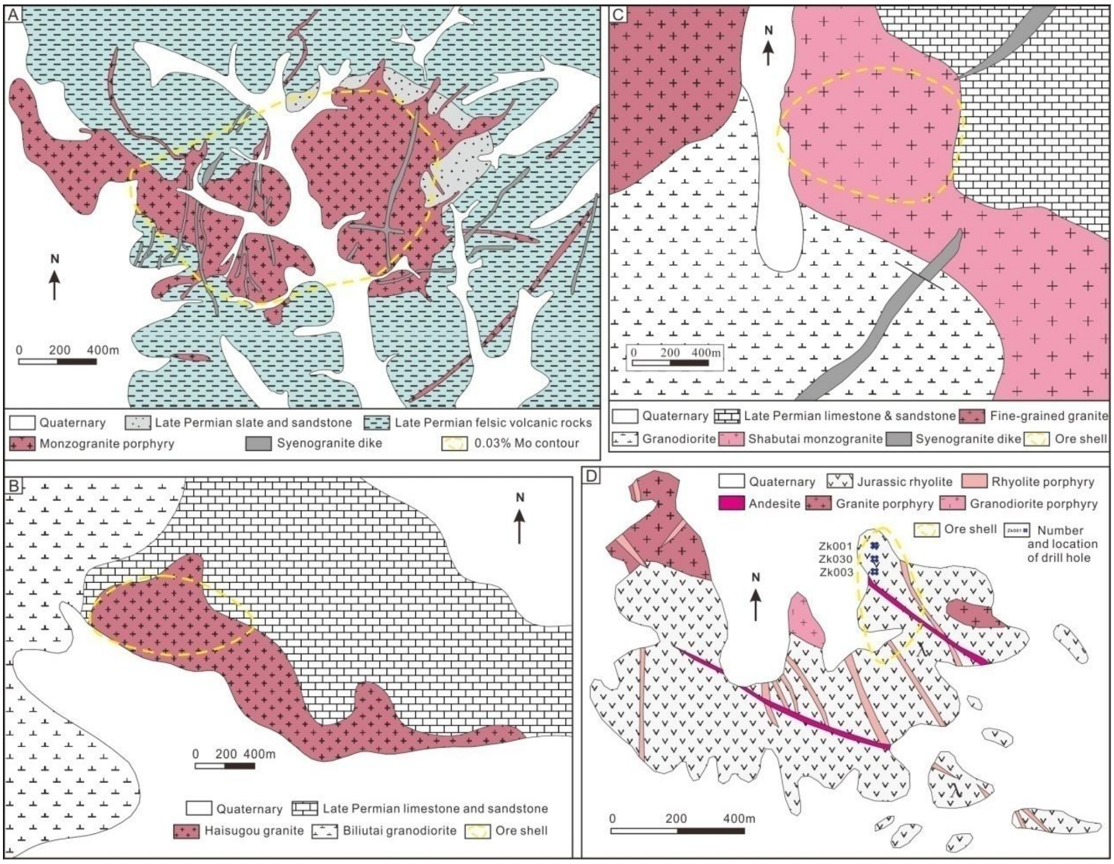

Figure 4-3. Geological sketch maps of the Mo deposits in the northern Xilamulun district. (A) Aolunhua (after Wu et al., 2011b); (B) Haisugou (after Shu et al., 2014); (C) Shabutai (after Shu et al., 2015); (D) Banlashan (after Yan, 2009).

3.1. Aolunhua Cu-Mo deposit

The Aolunhua deposit contains ~40 Mt ore resource averaging 0.08% Mo and 0.25% Cu (Wu et al., 2011b). Wall rocks are mostly Permian felsic volcanic rocks with subordinate Permian slate and sandstone (Fig. 4-3A). They were intruded by Early Cretaceous monzogranite porphyry (zircon U-Pb age of 131.9 ± 0.5 Ma; Ma et al., 2013) and subsequent syenogranite (zircon U-Pb age of 125.7 ± 0.6 Ma; Ma et al., 2013). Most orebodies occur in monzogranite porphyry, whereas syenogranite dikes cut through the wall rocks, monzogranite porphyry and the orebodies (Figs.

4-3A, 4A). The least altered monzogranite porphyry has medium-grained phenocrysts including plagioclase (~40%), K-feldspar (~30%), quartz (~20%) and minor biotite and amphibole (<10%). The groundmass is very fine-grained and consists mostly of quartz and plagioclase. Accessory minerals include titanite, apatite and zircon. The post-ore syenogranite is also porphyritic, consisting of K-feldspar (~50%), plagioclase (~20%), quartz (~25%) and minor biotite (~5%).

The orebody has a Mo-dominant core surrounded by Cu-Mo mineralization. The Mo-rich core occurs mainly in the center of the monzogranite porphyry (the lower part of the open pit in Fig. 4-4A). In this zone, there is intensive potassic alteration consisting of hydrothermal K-feldspar and biotite, with minor sericite overprint, and quartz-molybdenite ± pyrite veins. Microthermometric studies showed that the homogenization temperatures of fluid inclusions in these veins are up to 500 °C (Shu et al., 2009). In the surrounding Cu-Mo mineralization zone, quartz-chalcopyrite- molybdenite stockworks and sericite alteration are abundant (Fig. 4-4B). Boiling fluid inclusion assemblages occur in the sulfides-bearing quartz (Fig. 4-4C), with homogenization temperatures ranging from 240 to 400 °C (Shu et al., 2009). Hematite commonly occurs as daughter mineral in fluid inclusions, suggesting that the ore-forming fluids were highly oxidized (Fig. 4-4D). The $\delta^{18}O$ values of water in equilibrium with the mineralized quartz are between -0.2‰ to +2.6‰ (Ma and Chen, 2011), indicating the fluid was a mixture between magmatic fluid and meteoric fluid, with more magmatic component than meteoric component. Molybdenite samples for Re-Os isotopic analysis were collected from various locations in the open pit, including these quartz-molybdenite veinlets in the potassic zone, quartz-molybdenite-chalcopyrite veins with sericite alteration halo, and disseminated molybdenite (fine-grained flakes) in altered monzogranite porphyry.

3.2. Haisugou Mo deposit

Haisugou is ~100 km west of Aolunhua (Fig. 4-1D). Exploration is still on-going and its resources have not been defined. The mineralization is mostly hosted in the Haisugou granite. The granite is porphyritic with fine-grained groundmass and contains mafic microgranular enclaves (MMEs). The granite outcrop is <1 km^2. It intrudes into the Lower Permian Qingfengshan Formation limestone and sandstone (Fig. 4-3B). The zircon U-Pb age is 137.6 ± 0.9 Ma (Shu et al., 2014). The phenocrysts include ~20% plagioclase (3–6 mm) and ~5% biotite + amphibole (2–3 mm). Plagioclase phenocrysts are typically zoned and rimed by K-feldspar. The groundmass is composed of quartz (~20%), plagioclase (~35%), K-feldspar (~15%) and minor biotite; the grain size is ~0.2–0.5 mm. The granite shows various degrees of hydrothermal alteration. Hydrothermal K-feldspar veinlets are common in the mineralized granite (Fig. 4-4E). At the contact between the granite stock and the limestone, there are massive skarns composed of garnet, pyroxene, and minor wollastonite and chlorite (Fig. 4-4F); stratibound skarn zones also occur in hornfels. The skarn zone is typically less than 20 cm thick, with no obvious mineralization.

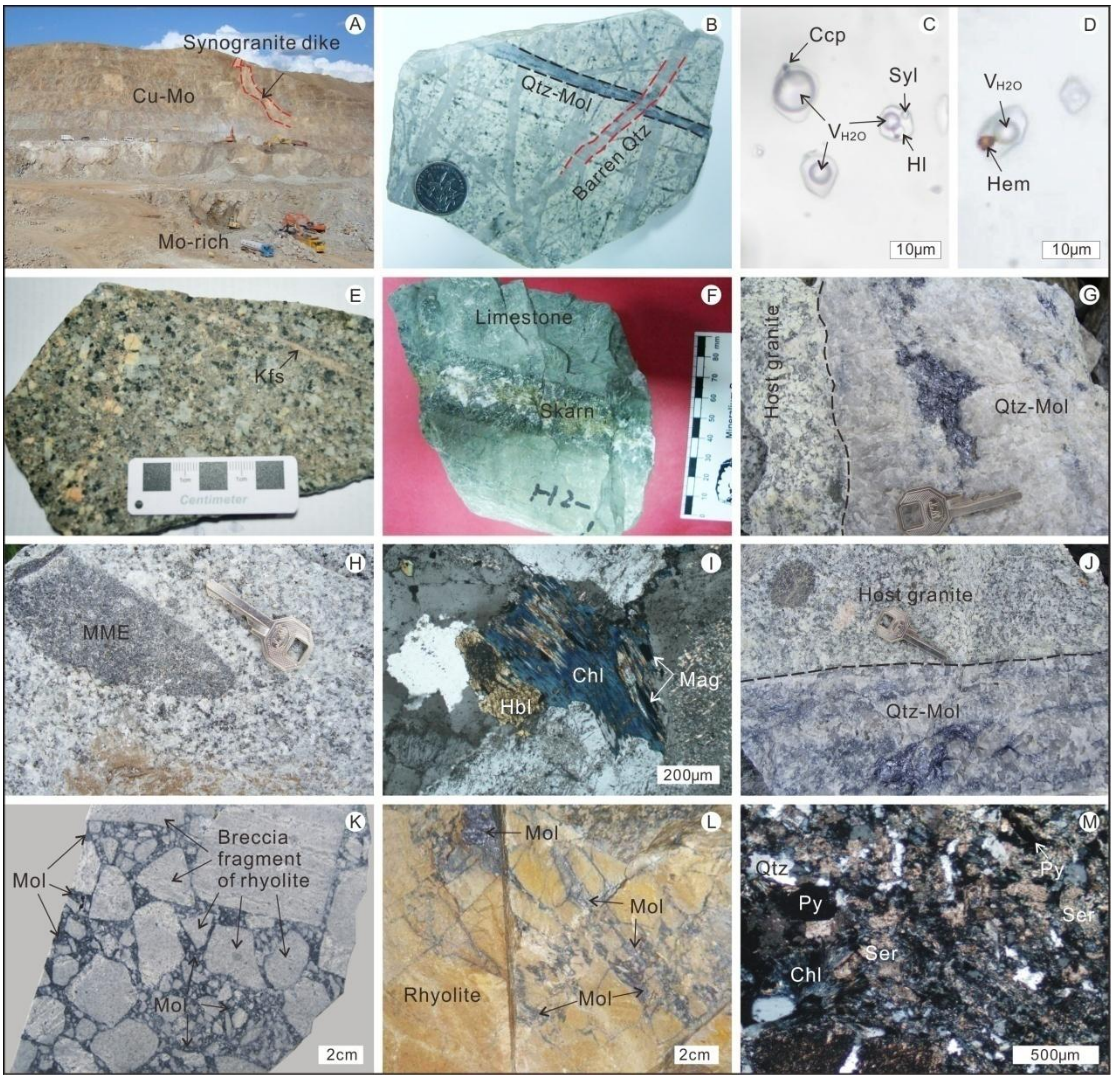

Figure 4-4. Photographs showing alteration and mineralization of the Mo deposits in the northern Xilamulun district. (A) Open pit of the Aolunhua mine, with Mo-rich mineralization in the lower level of the monzogranite porphyry stock (cut by syenogranite dike) and Cu-rich mineralization in the upper part. (B) Quartz-molybdenite vein cut by late barren quartz in altered monzogranite porphyry (Aolunhua). (C) Fluid inclusions of different types (high-salinity liquid, low-salinity vapor, and low-salinity liquid) present in sulfides-quartz vein (Aolunhua). (D) Hematite-bearing fluid inclusion in sulfides-quartz vein (Aolunhua). (E) Haisugou granite with potassic alteration. (F) Skarn vein in carbonate wallrock (Haisugou). (G) Foliated molybdenite in Mo-bearing quartz vein cutting the host granite (Haisugou). (H) Mafic microgranular enclaves within Shabutai monzogranite. (I) Pervasive chlorite-magnetite alteration replacing hornblende phenocrysts (Shabutai). (J) Quartz-molybdenite vein in host monzogranite (Shabutai). (K) Molybdenite infilling open spaces between rhyolitic breccia clasts (Banlashan). (L) Molybdenite-bearing veinlets crosscutting rhyolitic rocks (Banlashan). (M) Pervasive quartz-sericite-pyrite-chlorite alteration (Banlashan). Abbreviations: Ccp = chalcopyrite, Chl = chlorite, Cu = copper, Hl = halite, Hbl = hornblende, Hem = hematite, Kfs = K-feldspar, Mag = magnetite, MME = mafic microgranular enclave, Mo = molybdenum, Mol = molybdenite, Py = pyrite, Qtz = quartz, Ser = sericite, Syl = sylvite.

Sulfide minerals, mostly molybdenite with trace pyrite and chalcopyrite, mainly occur in quartz-sulfide veins (Fig. 4-4G) and to a lesser extend as disseminated grains in the granite. Breccia ores with centimeter-sized, angular to subrounded clasts of sulfide-quartz fragments cemented by late barren quartz have also been recognized (Shu et al., 2014). The quartz-sulfide veins are several millimeters to ~10 centimeters wide, and locally contain hydrothermal minerals including K-feldspar, biotite, epidote, and chlorite. Minor calcite and fluorite also occur. We collected four quartz-molybdenite veins cutting altered granites, three disseminated molybdenite samples, and one breccia ore for Re-Os dating.

3.3. Shabutai Mo deposit

Shabutai is ~10 kilometers west of Haisugou (Fig. 4-1D), and its geological characteristics are similar to that of Haisugou (Fig. 4-3C). Exploration in Shabutai is also on-going. Most of the ore is hosted in a monzogranite stock, which is medium to coarse grained, and composed of K-feldspar (~35%), plagioclase (~30%), quartz (~25%), biotite (5%) and hornblende (<3%), as well as minor zircon, titanite, and apatite. The zircon U-Pb age of the monzogranite is 138.4 ± 1.5 Ma (Shu et al., 2015). Compared with Haisugou, mafic microgranular enclaves (MMEs) in the Shabutai monzogranite are more abundant (Fig. 4-4H). The monzogranite is intensely altered. Plagioclase is commonly altered to sericite and most hornblende is replaced by magnetite and chlorite (Fig. 4-4I).

Potassic alteration is characterized by the formation of hydrothermal biotite in quartz veinlets. Sericite alternation is extensive, composed of quartz, sericite and sulfides. Mineralization occurs as quartz-sulfides veins (Fig. 4-4J), typically with sericite halos. The latest quartz-carbonate veins are barren and cut across all other veins. Ore minerals are mainly molybdenite (>95%), with minor pyrite and chalcopyrite. For Re-Os analysis, six molybdenite samples have been collected, of which two are from disseminated ores composed of molybdenite and minor chalcopyrite and pyrite in monzogranite, and four are from quartz-molybdenite ± pyrite veins with sericite alteration halo.

3.4. Banlashan Mo deposit

The Banlashan Mo deposit has an estimated resource of ~11,000 t of Mo metal averaging 0.07% Mo (Yan, 2009). The stratigraphic unit in the mining area is mainly the Upper Jurassic Baiyingaolao Formation rhyolite. The rhyolite has been intruded by several phases of intrusions including rhyolite porphyry, granodiorite porphyry, granite porphyry and andesite dikes (Fig. 4-3D), and the former three have zircon U-Pb ages of 157.5 ± 3.3 Ma, 133.5 ± 1.7 Ma and 126.3 ± 2.1 Ma, respectively (Yan, 2009; Zhang et al., 2010b).

The orebodies are mainly hosted in the Jurassic rhyolite and occur as wedge-shaped lenses, striking north-west and dipping about 30–40° to the northeast. There are 11 orebodies, mostly 10–20 m thick and with a maximum length of 620 m. The mineralization styles include hydrothermal breccias (Fig. 4-4K), stockworks/veins (Fig. 4-4L) and disseminations, among which hydrothermal breccias is the most common ore type. The breccias are monomictic, with angular-subangular rhyolite fragments cemented by hydrothermal minerals including molybdenite and minor quartz (Fig. 4-4K). The sulfides include molybdenite and minor pyrite, chalcopyrite, sphalerite and galena. The host rhyolitic rocks are commonly replaced by hydrothermal minerals including quartz, sericite, fluorite, calcite, kaolinite, chlorite, and epidote. Sericite and chlorite are the most abundant alteration minerals (Fig. 4-4M). Fluid inclusion study by Yan (2009) indicated that the ore-forming fluid system evolved from high temperature (up to 550 °C) and high salinity (66 wt% NaCl equiv) to low temperature (80 to 300 °C) and low salinity (1 to 5 wt% NaCl equiv). The decrease of temperature and salinity of the ore-forming fluid is speculated to be caused by mixing with meteoric water (Yan, 2009). The five molybdenite samples for Re-Os dating were all collected from breccia ores from drill holes.

4. Molybdenite Re-Os geochronology

4.1. Analytical method

Molybdenite samples from the Aolunhua, Haisugou, Shabutai and Banlashan deposits were handpicked under a binocular microscope after crushing, cleaning and sieving to 30–60 mesh. Osmium and rhenium were then separated by distillation and extraction according to the procedures described in Du et al. (2004). The Re and Os isotope ratios for each sample were determined using a TJA Plasmaquad ExCell inductively coupled plasma-mass spectrometry (ICP-MS) at the Re-Os Lab of the National Research Center of Geoanalysis, Chinese Academy of Geosciences.

Repeated analyses of molybdenite standard HLP from a carbonate vein-type Mo-Pb deposit in the Jinduicheng-Huanglongpu area of Shaanxi Province, China were performed in order to test the analytical reliability (Stein et al., 1997). The ^{187}Re decay constant of 1.666×10^{-11} y^{-1} obtained by Smoliar et al. (1996) was used for calculating molybdenite ages. The uncertainty in each individual age determination is about 1.4%, comprising the uncertainty of the decay constant of ^{187}Re, uncertainty in isotope measurement, spike calibration for ^{185}Re and ^{190}Os, as well as individual weighing and analytical random errors.

4.2. Molybdenite Re–Os dating results

The Re-Os dating results are listed in Table 4-2 and shown in Fig. 4-5. The uncertainties are at 95% confidence level. Analyses of six molybdenite samples from the Aolunhua Cu-Mo deposit yield

Table 4-2 Re-Os isotopic data for molybdenites from the Mo deposits in the northern Xilamulun district.

Deposit	Sample No.	Sample description	Weight (g)	Total Re ± 2σ (ng/g)	^{187}Re ± 2σ (ng/g)	^{187}Os ± 2σ (ng/g)	Model age ± 2σ (Ma)
Aolunhua							
	OLH-08(c)	Disseminated molybdenite grains	0.0503	25535 ± 214	16049 ± 135	35.30 ± 0.29	131.9 ± 1.9
	OLH-11(c)	Disseminated molybdenite grains	0.0505	31284 ± 328	19663 ± 206	43.07 ± 0.36	131.3 ± 2.1
	OLH-00	Disseminated molybdenite grains	0.0510	24486 ± 232	15390 ± 146	34.13 ± 0.30	133.0 ± 2.0
	OLH-04	Quartz-molybdenite-chalcopyrite veins	0.0502	19471 ± 156	12238 ± 98	27.32 ± 0.29	133.9 ± 2.1
	AQ-8	Quartz-molybdenite-chalcopyrite veins	0.0509	18834 ± 150	11837 ± 94	26.23 ± 0.23	132.8 ± 1.9
	OLH-G01	Quartz-molybdenite veins	0.0505	29728 ± 236	18684 ± 148	41.22 ± 0.35	132.3 ± 1.9
Haisugou							
	HSG27	Quartz-molybdenite veins	0.0505	14470 ± 150	9095 ± 96	20.53 ± 0.18	135.3 ± 2.2
	HSG12	Quartz-molybdenite veins	0.0500	12230 ± 120	7685 ± 77	17.54 ± 0.16	136.9 ± 2.2
	HSG18	Quartz-molybdenite veins	0.0502	28780 ± 250	18090 ± 150	41.29 ± 0.35	136.9 ± 2.0
	HSG30	Quartz-molybdenite veins	0.0500	22400 ± 250	14080 ± 160	32.24 ± 0.26	137.3 ± 2.2
	HSG33	Breccia ore	0.0527	15810 ± 120	9937 ± 77	22.83 ± 0.19	137.8 ± 1.9
	HSG50	Disseminated molybdenite grains	0.0504	21140 ± 180	13290 ± 110	30.06 ± 0.25	135.6 ± 2.0
	HSG61	Disseminated molybdenite grains	0.0508	7322 ± 67	4602 ± 42	10.44 ± 0.09	136.0 ± 2.0
	HSG62	Disseminated molybdenite grains	0.0504	2113 ± 21	1328 ± 13	3.06 ± 0.03	138.2 ± 2.1
Shabutai							
	SBT-2	Disseminated molybdenite grains	0.0500	22318 ± 170	14027 ± 107	31.90 ± 0.27	136.3 ± 1.9
	SBT-1	Quartz-molybdenite veins	0.0501	34719 ± 323	21822 ± 203	48.86 ± 0.41	134.3 ± 2.0
	SBT-3	Quartz-molybdenite veins	0.0503	37554 ± 280	23603 ± 176	53.62 ± 0.44	136.2 ± 1.9
	SBT-4	Quartz-molybdenite veins	0.0503	19560 ± 244	12294 ± 153	27.63 ± 0.25	134.8 ± 2.4
	SBT-5	Quartz-molybdenite-pyrite veins	0.0503	2321 ± 28	2321 ± 28	3.26 ± 0.03	134.0 ± 2.3
	SBT-6	Disseminated molybdenite grains	0.0502	27016 ± 247	27016 ± 247	37.95 ± 0.31	134.0 ± 2.0
Banlashan							
	ZK108A	Breccia ore	0.0245	2988 ± 27	1878 ± 17	4.38 ± 0.04	135.0 ± 3.0
	ZK001	Breccia ore	0.1007	117 ± 2	74 ± 1	0.19 ± 0.00	131.8 ± 7.6
	ZK003	Breccia ore	0.0512	971 ± 10	610 ± 1	1.61 ± 0.02	136.0 ± 8.2
	ZK108B	Breccia ore	0.1002	895 ± 10	562 ± 6	1.33 ± 0.01	135.4 ± 3.5
	ZK110	Breccia ore	0.0251	1226 ± 11	771 ± 7	1.91 ± 0.02	142.7 ± 3.5

model ages of 131.3–133.9 Ma, with a well-defined ^{187}Re-^{187}Os isochron age of 129.4 ± 3.4 Ma (MSWD = 0.55). Eight molybdenite samples from the Haisugou Mo deposit have model ages ranging from 135.3 to 138.2 Ma, and an isochron age is calculated to be 136.4 ± 0.8 Ma (MSWD = 1.2). In Shabutai, an isochron age of 135.3 ± 2.6 Ma (MSWD = 1.9) is obtained based on six molybdenite samples, which have a relatively narrow range of model ages from 134.0 to 136.3 Ma. Five samples from Banlashan Mo deposit have model ages of 131.8–142.7 Ma, and the isochron age is 136.1 ± 6.6 Ma (MSWD = 0.42). In Banlashan, the Re content is significantly lower (0.1–3.0 ppm) than the other three deposits (2.3–34.7 ppm), with one sample containing as low as 117 ppb Re, which is probably one of the reasons for the large uncertainty of the dating result.

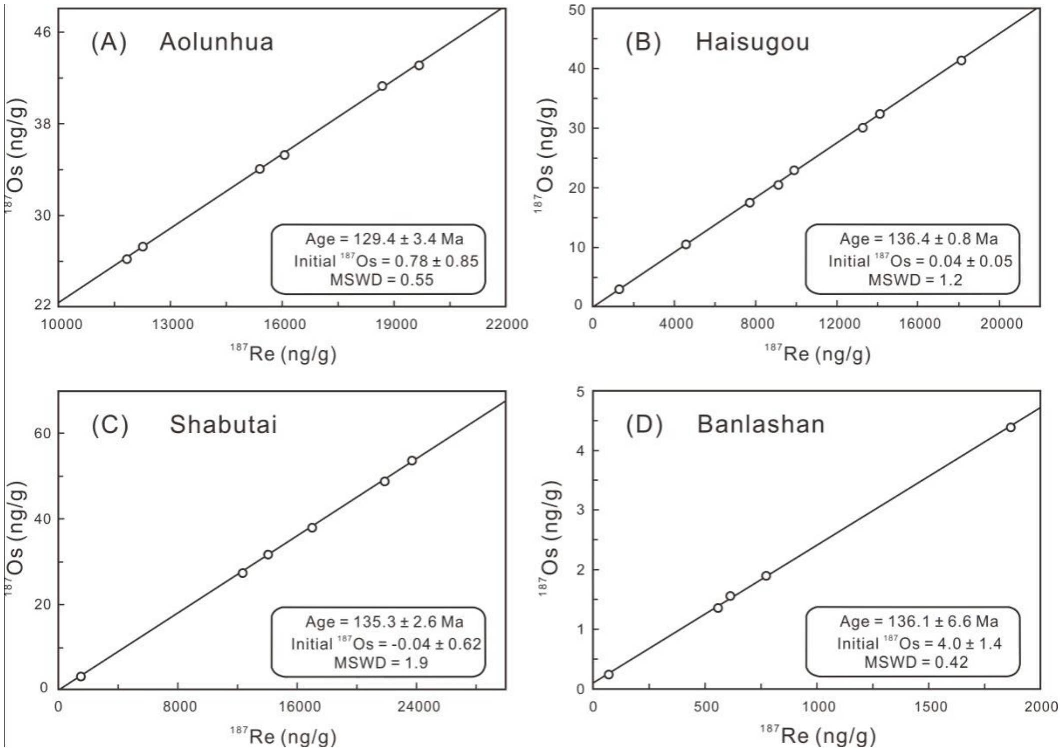

Figure 4-5. Molybdenite Re-Os isochrones for the Mo deposits in the northern Xilamulun district. The Isoplot of Ludwig (2003) was used for the isochron determinations. The data are listed in Table 4-2.

5. Compilation of the types and ages of Mesozoic Mo-bearing deposits and epithermal deposits in NE China

To understand the geodynamic background and tectonic setting of the deposits in the northern part of the Xilamulun district, and of the whole NE China, we have compiled the basic geological features, deposit type, and formation ages of Mo-bearing deposits and epithermal deposits in NE China, shown in Appendices 4-1 and 4-2, respectively, so as to investigate the space-time distribution pattern of the deposits. In total 70 Mo-bearing deposits and 11 epithermal deposits have been summarized. The deposit locations are shown in Figs. 4-1 and 6, with the deposits grouped by their ages. The data were mainly extracted from publications in international and Chinese academic journals, with a few from unpublished student dissertations; the references for Appendices 4-1 and 4-2 are listed in Appendix 4-3.

The Mo-bearing deposits in NE China are mostly porphyry Mo, Mo-Cu, Cu-Mo-(Au) or Mo-W deposits (n = 58). In addition to porphyry type deposits, there are seven skarn deposits with Mo being the dominant economic metal or as a by-product, two greisen type Mo deposits, and one porphyry-skarn type Mo deposit. The classification of the remaining two deposits (Liutiaogou and Hongshanzi Mo-U deposits) in the Chinese literature is Volcanic Hydrothermal Vein type (Zeng et al., 2011a), which is not compatible with international terminology. These two deposits are hosted by rhyolite, rhyolite porphyry, trachyte, and tuff, with alternation minerals including quartz, albite, biotite, chloride, fluorite, calcite and pyrite (Zeng et al., 2011a). Further investigation is needed to constrain their genetic type. Both magmatism and mineralization ages (when available) have been listed in Appendix 4-1. The mineralization ages are represented by molybdenite Re-Os isochron dates, and magma emplacement ages have been obtained with various methods including zircon U-Pb, whole rock K-Ar, Ar-Ar and Rb-Sr dating.

The epithermal deposits are mostly Au, Au-Ag, Ag-Au and Cu-Au deposits, as well as one Au-Te deposit (Sandaowanzi). Details on these epithermal deposits can be found in Han et al. (2013), Sun et al. (2013c) and Goldfarb et al. (2014). Some of them are Mo-bearing; such deposits have been dated using molybdenite Re-Os method (e.g., Sishanlinchang). Many ages have been obtained using Ar-Ar method either on alteration minerals like sericite (Dong'an and Naozhi) or on fluid inclusions in gold-bearing quartz (Wuxingshan and Duhuangling). Pyrite Rb-Sr dating has also been reported for three deposits (Sandaowanzi, Jinchang and Wulaga). For Sipingshan and Tuanjiegou deposits, hydrothermal zircon grains have been extracted from the sulfide-quartz veins and hence the zircon U-Pb ages can represent the mineralization ages. For the remaining one deposit (Jiusangou), only the zircon U-Pb age of the ore-hosting porphyritic diorite has been obtained, which could be older than the real mineralization age (Appendix 4-2).

6. Discussion

6.1. Timing of Mo mineralization in the northern Xilamulun district

Molybdenite samples from four Mo-bearing deposits (i.e., Aolunhua, Shabutai, Haisugou, and Banlashan) have been dated in this study using the Re-Os method. The Re-Os isochron age is 129.4 ± 3.4 Ma for Aolunhua, 135.3 ± 2.6 Ma for Shabutai, and 136.4 ± 0.8 Ma for Haisugou. The Re-Os isochrons have MSWD values close to 1 (0.42–1.9; Fig. 4-5), suggesting that these dates are reliable and can hence represent the molybdenite crystallization age, therefore the mineralization age. The molybdenite Re-Os date for the Banlashan deposit is 136.1 ± 6.6 Ma. It has unusually large uncertainty for the Re-Os method. The low Re content, 117 to 2988 ppb, is probably one of the reasons for the large uncertainties of the individual grain analysis, particularly the two with dates of 131.8 ± 7.6 Ma (117 ± 2 ppb Re) and 136.0 ± 8.2 Ma (971 ± 10 ppb Re; Table 4-2). In addition, there is a possibility that there was an older molybdenite-depositing event as indicated by a molybdenite sample dated at 142.7 ± 3.5 Ma, compared with other grains dated at ~131–136 Ma (131.8 ± 7.6 Ma, 135.0 ± 3.0 Ma, 135.4 ± 3.5 Ma, and 136.0 ± 8.2 Ma), mostly close to ~135 Ma. However for the purpose of this study covering a long period of time (~160 myrs from ~250 Ma to ~90 Ma; Appendix 4-1 and Fig. 4-1) this date is still useful.

At the Aolunhua, Haisugou and Shabutai porphyry deposits, the molybdenite ages (129.4 ± 3.4 Ma, 136.4 ± 0.8 Ma, and 135.3 ± 2.6 Ma) are respectively within the 2-sigma uncertainty range of the zircon U-Pb ages (131.9 ± 0.5 Ma; 137.6 ± 0.9 Ma; and 138.4 ± 1.5 Ma; Table 4-1) of their host granites. This is consistent with the porphyry deposit origin and the granitic rocks being the syn-mineralization intrusions. At Banlashan, the Re-Os age (136.1 ± 6.6 Ma) is similar to the zircon U-Pb age of the granodiorite porphyry (133.5 ± 1.7 Ma; Zhang et al., 2010b), and much younger than the rhyolite porphyry dike (157.5 ± 3.3 Ma; Yan, 2009) and older than the granite porphyry intrusion (126.3 ± 2.1 Ma; Yan, 2009), indicating that the mineralization may be related to magmatism of the same stage as the granodiorite. The granodiorite cropping out about 200m west of the mineralized rhyolite body (Fig. 4-3D) does not have significant alteration and mineralization, which makes it unlikely to be the direct source of Banlashan mineralization. The causative intrusion may be still undercover but have an age similar to the granodiorite.

6.2. Spatial-temporal distribution of Mo deposits in NE China and its geodynamic background

Molybdenum deposits in NE China formed in a long period of time, from ~250 Ma to ~90 Ma. The deposits are plotted in Figs. 4-1C and 4-6 in age groups. The distribution of all the individual deposits seems to be random without any spatial-temporal trends. However, if we examine the deposits in appropriate age groups separately, some space-time patterns do exist, as described in the following sections and shown in Fig. 4-6. The patterns are likely related to the geodynamic setting.

6.2.1. Triassic Mo mineralization (250–220 Ma)

It was previously believed that mineralization in NE China occurred mainly in Jurassic to Early Cretaceous (~200–120 Ma; Liu et al., 2004; Mao et al., 2005). However, recent studies have shown that 14 Triassic Mo deposits (250–220 Ma) are also present in this region (Fig. 4-6A; Appendix 4-1; Dai et al., 2009; Wan et al., 2009; Zhang et al., 2009a; Liu et al., 2010a; Meng et al., 2013; Zhang and Li, 2014). These deposits are mainly distributed in east-westerly direction, parallel to the Solonker-Xilamulun-Changchun suture (Fig. 4-6A) which has been considered to

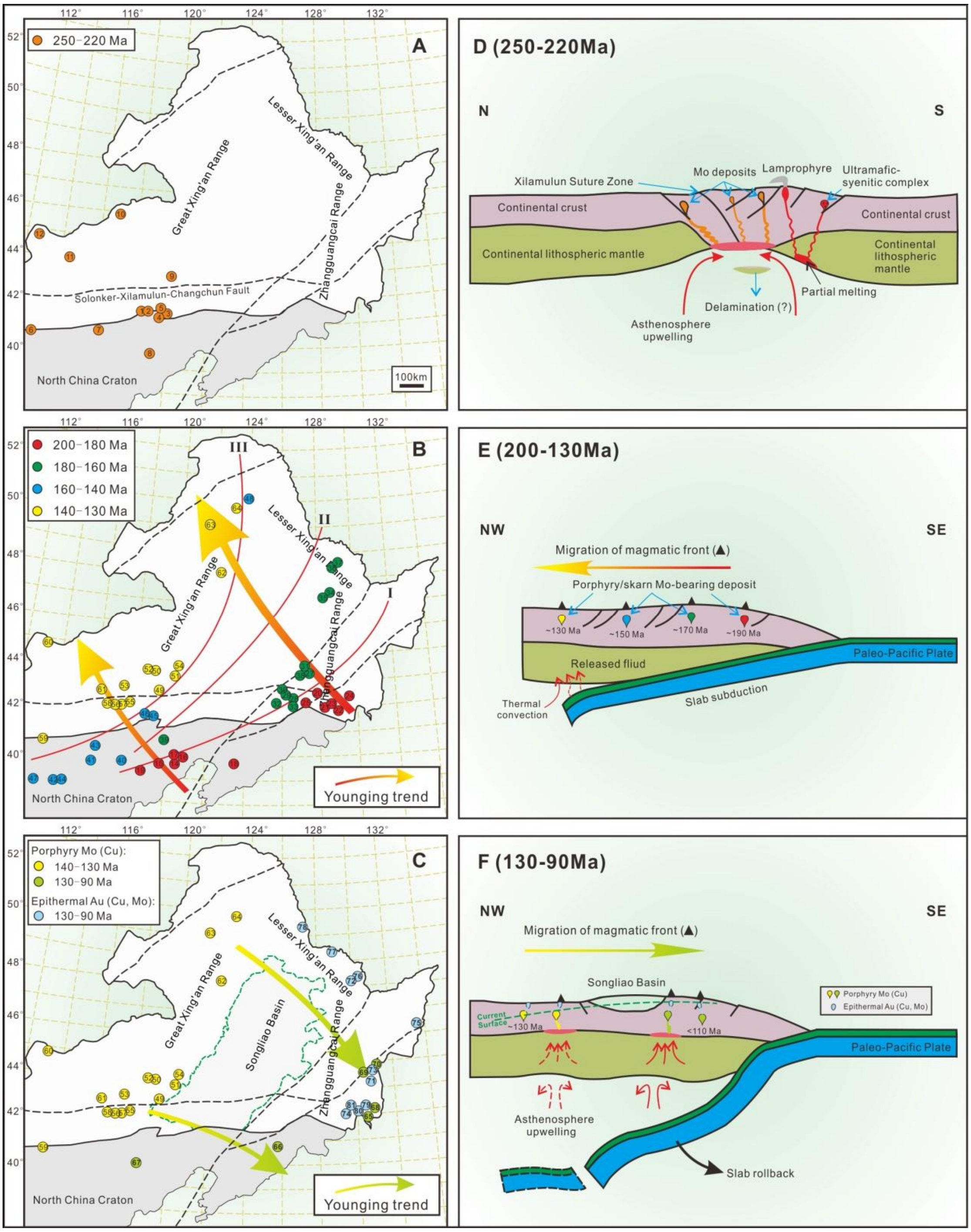

Figure 4-6. A three-stage model for Mesozoic Mo mineralization in NE China. The spatial-temporal distribution of these Mo deposits are shown in the left maps (A, B and C), while their corresponding geodynamic processes are illustrated in the right cartoons (D, E and F). The deposit numbers are the same as in Fig. 1C and detailed in Appendices 4-1 and 4-2. The Triassic (250 to 220 Ma) Mo deposits are related to post-collisional extension after the terminal closure of the Paleo-Asian Ocean (D). The Jurassic to Early Cretaceous (200 to 130 Ma) Mo mineralization shows a younging trend from 200 Ma in the southeast margin to 130 Ma in the northwesternmost NE China (B), suggesting their formation due to the flat-slab subduction of the Paleo-Pacific plate beneath the Eurasian continent (E; modified after Zhang et al. 2010a). Cretaceous (130 to 90 Ma) porphyry/skarn Mo deposits and epithermal Au (Cu, Mo) deposits display a distinctly reversed younging trend, namely, migrated southeastward from 130 Ma to 90 Ma (C), and can be caused by coastward asthenosphere upwelling induced by the rollback of the subducting oceanic slab (F).

be the position of the final closure of the Paleo-Asian ocean between the North China and Siberia cratons (Wu et al., 2011c).

After the closure of the Paleo-Asian ocean at ~260 Ma (e.g., Zhang et al., 2009b; Yang et al., 2015), there was post-collisional magmatism along the Solonker-Xilamulun-Changchun suture zone in the period of ~250–220 Ma (e.g., Han et al., 2004; Zhang et al., 2009b). For example, Zhang et al. (2009b) reported a series of intrusions (quartz monzonite, monzogranite and syenogranite) located in the northern margin of the North China craton with ages of 237–254 Ma. Detailed geological, geochemical and Sr-Nd-Hf isotopic study led Zhang et al. (2009b) to interpret these rocks as post-collisional granitoids linked to lithospheric extension and asthenosphere upwelling. Such an extensional tectonic setting can be further supported by the occurrence of the alkaline rocks along the Solonker-Xilamulun- Changchun suture zone, including the syenogranite porphyries at Bilihe (~253 Ma; Yang et al., 2015), the Fanshan alkaline ultramafic-syenite complex (240 Ma; Mu et al., 2001), the Datong lamprophyre (ca. 230 Ma; Shao et al., 2003), the Saima nepheline syenite complex (ca. 240–220 Ma; Mu and Yan, 1992), and the Guangtoushan A-type granite (ca. 220 Ma; Han et al., 2004). In addition, whole-rock geochemical study of the host granite (ca. 250 Ma) of the Chehugou Mo deposit also indicated that underplating of hot mantle-derived material may have occurred, facilitating crustal melting under a post-collisional condition (Wan et al., 2009). In summary, this period of the post-collisional magmatism coincides well with the time of the Triassic Mo mineralization, therefore the Triassic Mo mineralization is believed to be related to such magmas (Fig. 4-6D).

6.2.2. Jurassic to Early Cretaceous Mo mineralization (200–130 Ma)

In NE China, the Jurassic to Early Cretaceous Mo-bearing deposits (200–130 Ma) can be geographically divided into four groups as shown in Fig. 4-6B: Group I (east to Line I) contains 12 deposits with ages from 200 Ma to 180 Ma. To its northwest, Group II (between Line I and II) includes 13 deposits with ages between 180 and 160 Ma. Farther west, Group III (between Line II and III) have nine deposits dated at 160 to 140 Ma. At the northwest end, Group IV (west of Line III) contains 16 deposits formed during 140 to 130 Ma. The deposits show a clear northwest-ward younging trend, from 200-180 Ma at the SE to 140–130 Ma at the NW end. Two exceptions are the Taipingchuan and Wunugetu porphyry Cu-Mo deposits in the Erguna massif (Fig. 4-1C), which are located in the northernmost NE China; they have Early Jurassic ages (i.e., 200.1 ± 2.5 Ma and 179.0 ± 1.9 Ma, respectively). Their host granitic rocks were formed in a subduction setting based on the geochemical study by Zhang et al. (2014) and Wang et al. (2015), respectively. The granitic rocks are in a NE–SW zone defined by many subduction-related intrusive rocks, and the zone is roughly parallel to Mongol–Okhotsk suture belt (Tang et al., 2015). Therefore these two deposits were suggested to be likely related to the subduction of the Mongol-Okhotsk oceanic plate beneath the Erguna massif (Zhang et al., 2014; Wang et al., 2015). Excluding these two deposits, the remaining 50 Mo deposits with Jurassic to Early Cretaceous ages define a nice northwest-ward younging trend. This younging trend and time interval is very similar to that of the Jurassic-Early Cretaceous granitoids in NE China (starting from ~210–180 Ma in the southeast and ending at ~140–130 Ma in the northwest, Fig. 4-2; Zhang et al., 2010a) as described on Section 2.2. The younging trend of the granitoids was explained by northwestward flat-slab subduction of the Paleo-Pacific plate beneath the Eurasian continent (Zhang et al., 2010a, and reference therein). Similarly, we propose that the younging trend of the Jurassic to Early Cretaceous intrusion-related Mo deposits, mostly of porphyry type, were also caused by the flat-slab subduction of the Paleo-Pacific plate.

Flat-slab subduction has been identified in many regions worldwide, e.g., the western margin of the United States (Coney and Reynolds, 1977); central Chile (Kay and Mpodozis, 2002); Central Mexico (Manea et al., 2006); and south Alaska (Finzel et al., 2011), and has been suggested to occur along ~10% of the world's convergent margins, with subduction distance ranging from 250 to 1500 km inland from subduction sites (Gutscher et al., 2000). In eastern China and its surrounding areas including South Korea and Japan, flat-slab subduction of Paleo-Pacific plate has also been suggested to have occurred from Jurassic to Early Cretaceous, and is the reason of the westwards-younging magmatism from along the current continental margin to far inland (~1000 km; e.g., Li and Li, 2007; Zhang et al., 2010a; Kiminami and Imaoka, 2013). Considering that the NE-SW extending Songliao basin (~300–350 km wide; Fig. 4-1), parallel to the subduction front line of the Paleo Pacific plate, developed during extension after the subduction ceased (please see more discussion in the next section), the real subduction distance would be shorter than the current width of compression-related igneous belt (~1000 km). Molybdenum-bearing deposits in this region during this period of time are caused by the intrusions. The deposits also have a northwestward younging direction, therefore they are also related to the northwestward flat slab subduction of the Paleo Pacific plate (Fig. 4-6E).

6.2.3. Early to Middle Cretaceous Mo mineralization (130–90 Ma)

In the Early to Middle Cretaceous (130–90 Ma), Mo mineralization had a southeastward younging trend, distinctly opposite to the 200–130 Ma northwestward trend. The Mo deposits become younger from 140–130 Ma in the northwest to 130–90 Ma in the southeast (Fig. 4-6C). This trend coincides with the younging trend of the volcanic rocks from northwest (~130–120 Ma) to southeast (~120–80 Ma) in NE China (Fig. 4-2; Zhang et al., 2010a). This could be explained by slab rollback, which can lead to a transformation of the tectonic regime in the upper plate from compression to extension and result in coastward magmatism (Humphreys et al., 2003; Ramos and Folguera, 2009; Kiminami and Imaoka, 2013; Fig. 4-6F).

In eastern China the geodynamic setting switched from compressional to extensional in the Early Cretaceous (e.g., Zhang et al., 2010a; Lin et al., 2013). In NE China, this transformation is evidenced by the occurrence of the A-type granites emplaced at 130–120 Ma (Li and Yu, 1993; Jahn et al., 2001), the coeval bimodal mafic and felsic dykes (~100 Ma; Sun et al., 2013b), the Yiwulüshan and Louzidian-Dachengzi metamorphic core complexes (133–116 Ma) controlled by detachment faults (Zhang et al., 2002a, b), and the development of extensional basins (e.g., the Songliao Basin; Meng et al., 2003). The switch was proposed to have been caused by the rollback of the Paleo-Pacific plate (e.g., Wu et al., 2007; Zhang et al., 2010a; Kiminami and Imaoka, 2013; Sun et al., 2013b). As shown in Fig. 4-6F, the subducted slab rollback resulted in upwelling of the asthenosphere, which in turn caused extension and intraplate magmatism (including alkaline basalts, bimodal volcanic rocks, and A- and I-type granites; Sun et al., 2013b). The rolling back of the slab towards southeast caused the magmatism to migrate from northwest to southeast. Accompanying such magmatism, many porphyry Mo deposits as well as several epithermal Au polymetallic deposits formed (Fig. 4-6F).

6.3. Implications for regional metallogeny

Among the numerous Mo-bearing hydrothermal deposits in NE China, most of the older deposits (>130 Ma) are porphyry or skarn deposits, whereas the younger ones, 130–90 Ma in age, are mostly epithermal deposits and are mostly in the SE end of the region. In a porphyry system, there are typically epithermal deposits above porphyry (or skarn deposits if the wall rocks are carbonates), including high-sulfidation epithermal deposits directly above porphyry deposits, and intermediate-sulfidation epithermal deposits above porphyry deposits but also on the sides (e.g., Sillitoe, 2010; Chang et al., 2011). An intrusion may also set off convection of groundwater and cause low-sulfidation epithermal deposits at shallow levels (e.g., Hedenquist et al., 2000). In the northwestern part of the NE China region, the older deposits have experienced more exhumation, therefore the deeper deposits (porphyry and skarn type deposits) in the systems are now outcropping or sitting at shallow positions; the shallower epithermal deposits linked to them would have been eroded away. In the SE side of the region, the younger deposits (~130–90 Ma) have undergone less exhumation, therefore the epithermal deposits are exposed on the current surface or are located at shallow depth. Based on this understanding, we predict that there should be deeper deposits (porphyry or skarn types) linked to the known epithermal deposits beneath the current surface (Fig. 4-6F) in the SE part of the NE China region.

7. Conclusion

This study focuses on the geology and Re-Os geochronology of the Mo-bearing deposits in the northern Xilamulun district. Based on the alteration and mineralization nature, Aolunhua, Haisugou, Shabutai, and Yangchang can be classified as typical porphyry deposits. Molybdenite Re-Os dating shows a narrow mineralization age range of 140 to 130 Ma. The mineralization closely correlates in time and space with granite intrusions.

When taking all the Mesozoic Mo deposits in NE China into consideration, three pulses of Mo mineralization can be recognized; they reflect three stages of significant tectonic-magmatic events: (1) the Triassic Mo mineralization (250–220 Ma) occurred in an east-west zone after the final closure of the Paleo-Asian ocean in a regional extensional environment, postdating the collision; (2) the Jurassic to Early Cretaceous Mo deposits (200–130 Ma) show a northwestward younging trend towards the continental interior, and can be linked to the northwestward flat-slab subduction of Paleo-Pacific plate beneath the Eurasian continent that started at Early Jurassic (e.g., ca. 200 Ma); (3) the Early to Middle Cretaceous Mo mineralization (130–90 Ma), as well as its synchronous magmatism, displays a reversed trend of younging, towards the coast, and is believed to be a response to the eastward migration of lower crust delamination, asthenospheric upwelling and lithospheric thinning in eastern China related to slab rollback. Such a three-stage model can not only explain the spatio-temporal distribution of Mesozoic Mo deposits and igneous rocks in NE China, but also predict a significant potential for porphyry and skarn mineralization at lower elevations below the currently known epithermal deposit zone in the southeast part of the region with ages ranging from ~120 to ~90 Ma.

Acknowledgments

This study was financially supported by a National Nature Science Foundation of China grant (No. 41390443). Qihai Shu was also funded by a Chinese Scholarship Council award (No. 201306010045) and a student research grant from the Society of Economic Geologists (Hugh McKinstry Fund). We thank Chao Li for assistant with molybdenite Re-Os dating, Zhiming Yang, Carl Spandler and Robert Holm for helpful discussions, and Lawrence Meinert (U.S. Geological Survey) and David Huston (Geoscience Australia) for construction reviews on an early version of this paper.

References

Chang, Z., Hedenquist, J.W., White, N.C., Cooke, D.R., Roach, M., Deyell, C.L., Garcia, J. Jr., Gemmell, J.B., McKnight, S., Cuison, A.L., 2011. Exploration tools for linked porphyry and epithermal deposits: Example from the Mankayan intrusion-centered Cu-Au district, Luzon, Philippines. Economic Geology106, 1365–1398.

Chen, Y.J., Zhang, C., Li, N., Yang, Y.F., Deng, K., 2012. Geology of the Mo deposits in northeast

China. Journal of Jilin University (Earth Science Edition) 42, 1223–1268 (in English with Chinese abstract).

Chen, Z.G., Zhang, L.C., Wu, H.Y., Wan, B., Zeng, Q.D., 2008. Geochemistry study and tectonic background of A style host granite in Nianzigou molybdenum deposit in Xilamulun molybdenum metallogenic belt, Inner Mongolia. Acta Petrologica Sinica 24, 879–898 (in Chinese with English abstract).

Coney, O.J., Reynolds, S.J., 1977. Cordilleran Benioff zones. Nature 270, 403–406.

Dai, J.Z., Mao, J.W., Zhao, C.S., Xie, Q.Q., Yang, F.Q., Wang, Y.T., 2009. New U-Pb and Re-Os age data and the geodynamic setting of the Xiaojiayingzi Mo (Fe) deposit, western Liaoning province, Northeastern China. Ore Geology Reviews 35, 235–244.

Dash, B., Yin, A., Jiang, N., Tseveendorj, B., Han, B., 2015. Petrology, structural setting, timing, and geochemistry of Cretaceous volcanic rocks in eastern Mongolia: Constraints on their tectonic origin. Gondwana Research 27, 281–299.

Ding, R.X., Shu, P., Ji, X.Y., Qu, Y.M., Chen, R.H., Zhang, B., 2007. SHRIMP zircon U-Pb age and geological meaning of reservoir volcanic rocks in Qingshen gas field of the Songliao Basin, NE China. Journal of Jilin University (Earth Science Edition) 37, 525–530 (in Chinese with English abstract).

Du, A.D., Wu, S.Q., Sun, D.Z., Wang, S.X., Qü, W.J., Markey, R., Stein, H., Morgan, J.W., Malinovskiy, D., 2004. Preparation and certification of Re-Os dating reference materials: molybdenite HLP and JDC. Geostandards and Geoanalytical Research 28, 41–52.

Fan, W.M., Guo, F., Wang, Y.J., Lin, G., 2003. Late Mesozoic calc-alkaline volcanism of post-orogenic extension in the northern Da Hinggan Mountains, northeastern China. Journal of Volcanology and Geothermal Research 121, 115–135.

Finzel, E.S., Trop, J.M., Ridgway, K.D., Enkelmann, E., 2011. Upper plate proxies for flat-slab subduction processes in southern Alaska. Earth and Planetary Science Letters 303, 348–360.

Goldfarb, R.J., Taylor, R.D., Collins, G.S., Goryachev, N.A., Orlandini, O.F., 2014. Phanerozoic continental growth and gold metallogeny of Asia. Gondwana Research 25, 48–102.

Gutscher, M. A., Maury, R., Eissen, J.P., Bourdon, E., 2000. Can slab melting be caused by flat subduction. Geology 28, 535–538.

Han, B.F., Kagami, H., Li, H.M., 2004. Age and Nd-Sr isotopic geochemistry of the Guangtoushan alkaline granite, Hebei Province, China: Implications for early Mesozoic crust-mantle interaction in North China block. Acta Petrologica Sinica 20, 1375–1388 (in Chinese with English abstract).

Han, C.M., Xiao, W.J., Zhao, G.C., Sun, M., Qu, W.J., Du, A.D., 2009. A Re-Os study of molybdenites from the Lanjiagou Mo deposit of North China Craton and its geological significance. Gondwana Research 16, 264–271.

Han, S.J., Sun, J.G., Bai, L.A., Xing, S.W., Chai, P., Zhang, Y., Yang, F., Meng, L.J., Li, Y.X., 2013. Geology and ages of porphyry and medium-to high-sulphidation epithermal gold deposits of the continental margin of Northeast China. International Geology Review 55, 287–310.

Hao, Z., Fei, H., Liu, L., Hao, Q., Turner, S., 2014. World's Third–Largest Molybdenum Deposit Discovered in Caosiyao Area, Xinghe County, Inner Mongolia. Acta Geologica Sinica (English Edition) 88, 1615–1616.

Hedenquist, J.W., Arribas, A., Gonzalez-Urien, E., 2000. Exploration for epithermal gold deposits. Reviews in Economic Geology13, 245−277.

Humphreys, E., Hessler, E., Dueker, K., Farmer, G.L., Erslev, E., Atwater, T., 2003. How Laramide-age hydration of North American lithosphere by the Farallon slab controlled subsequent activity in the western United States. International Geology Review 45, 575–595.

Jahn, B. M., Wu, F., Capdevila, R., Martineau, F., Zhao, Z., Wang, Y., 2001. Highly evolved juvenile granites with tetrad REE patterns: the Woduhe and Baerzhe granites from the Great Xing'an Mountains in NE China. Lithos 59, 171–198.

Kay, S.M., Mpodozis, C., 2002. Magmatism as a probe to the Neogene shallowing of the Nazca plate beneath the modern Chilean flat-slab. Journal of South American Earth Sciences 15, 39–57.

Kiminami, K., Imaoka, T., 2013. Spatiotemporal variations of Jurassic-Cretaceous magmatism in eastern Asia (Tan-Lu Fault to SW Japan): evidence for flat-slab subduction and slab rollback. Terra Nova 25, 414–422.

Li, P.Z., Yu, J.S., 1993. Nianzishan miarolitic alkaline granite stock, Heilongjiang–its ages and geological implications. Geochimica 4, 389–398 (in Chinese with English abstract).

Li, Z.X., Li, X.H., 2007. Formation of the 1300-km-wide intracontinental orogen and postorogenic magmatic province in Mesozoic South China: a flat-slab subduction model. Geology 35, 179–182.

Lin, W., Faure, M., Chen, Y., Ji, W.B., Wang, F., Wu, L., Charles, N., Wang, J., Wang, Q.C., 2013. Late Mesozoic compressional to extensional tectonics in the Yiwulüshan massif, NE China and its bearing on the evolution of the Yinshan-Yanshan orogenic belt: Part I: Structural analyses and geochronological constraints. Gondwana Research 23, 54–77.

Liu, J.M., Zhang, R., Zhang, X.Z., 2004. The regional metallogeny of Da Hingganling, China. Earth Science Frontier 11, 269–277 (in Chinese with English abstract).

Liu, J.M., Zhao, Y., Sun, Y.L., Li, D.P., Liu, J., Chen, B.L., Zhang, S.H., Sun, W.D., 2010. Recognition of the latest Permian to Early Triassic Cu-Mo mineralization on the northern margin of the North China block and its geological significance. Gondwana Research 17, 125–134.

Liu, J., Mao, J., Wu, G., Wang, F., Luo, D., Hu, Y., 2014. Zircon U-Pb and molybdenite Re-Os dating of the Chalukou porphyry Mo deposit in the northern Great Xing'an Range, China and its geological significance. Journal of Asian Earth Sciences 79, 696–709.

Liu, J., Wu, G., Li, Y., Zhu, M., Zhong, W., 2012a. Re-Os sulfide (chalcopyrite, pyrite and molybdenite) systematics and fluid inclusion study of the Duobaoshan porphyry Cu (Mo) deposit, Heilongjiang Province, China. Journal of Asian Earth Sciences 49, 300–312.

Liu, L., Zeng, Q.D., Liu, J.M., Duan, X.X., Sun, S.K., Zhang, L.C., 2012b. Characteristics of fluid inclusions from the Laojiagou porphyry Mo deposit in the Xilamulun metallogenic belt, Inner Mongolia and their geological significance. Geology and Exploration 48, 663–676.

Ludwig, K.R., 2001. Users manual for Isoplot/Ex rev. 2.49. Berkeley Geochronology Centre Special, Publication. No. 1a, pp. 1–56.

Ma, X.H., Chen, B., 2011. The source of hydrothermal fluids and mineralization in the Aolunhua porphyry Mo-Cu deposit, southern Da Hinggan Mountains: constraints from stable (C, H, O and S) and radiogenic (Pb) isotopes. Journal of Jilin University (Earth Science Edition) 41, 1770–1783 (in Chinese with English abstract).

Ma, X., Chen, B., Yang, M., 2013. Magma mixing origin for the Aolunhua porphyry related to Mo-Cu mineralization, eastern Central Asian Orogenic Belt. Gondwana Research 24, 1152–1171.

Manea C., Manea, M., Kostoglodov, V., Sewell, G., 2006. Intraslab seismicity and thermal stress in the subducted Cocos plate beneath central Mexico. Tectonophysics 420, 389–408.

Mao, J.W., Xie, G.Q., Zhang, Z.H., Li, X.F., Wang, Y.T., Zhang, C.Q., Li, Y.F., 2005. Mesozoic large-scale metallogenic pulses in North China and corresponding geodynamic settings. Acta Petrologica Sinica 21, 169–188 (in Chinese with English abstract).

Mao, J.W., Pirajno, F., Xiang, J.F., Gao, J.J., Ye, H.S., Li, Y.F., Guo, B.J., 2011. Mesozoic molybdenum deposits in the east Qinling-Dabie orogenic belt: Characteristics and tectonic settings. Ore Geology Reviews 43, 264–293.

Meng, Q.R., 2003. What drove late Mesozoic extension of the northern China-Mongolia tract? Tectonophysics 369, 155–174.

Meng, S., Yan, C., Lai, Y., Shu, Q.H., Sun, Y., 2013. Study on the mineralization chronology and characteristics of mineralization fluid from the Chehugou porphyry Cu-Mo deposit, Inner Mongolia. Acta Petrologica Sinica 29, 255–269 (in Chinese with English abstract).

Mu, B.L., Yan, G.H., 1992. Geological features of Triassic alkaline and subalkaline igneous complexes in the Yan-Liao area. Acta Geologica Sinica 5, 339–355 (in Chinese with English abstract).

Mu, B.L., Shao, J.A., Chu, Z.Y., Yan, G.H., Qiao, G.S., 2001. Sm-Nd age and Sr-Nd isotopic characteristics of the Fanshan potassic alkaline ultramafic-syenite complex in Hebei Province. Acta Petrologica Sinica 17, 358–365 (in Chinese with English abstract).

Nie, F.J., Zhang, W. Y., Du, A. D., Jiang, S. H., Liu, Y., 2007. Re-Os isotopic dating on molybdenite separates from the Xiaodonggou porphyry Mo deposit, Hexigten Qi, Inner Mongolia. Acta Geologica Sinica 81, 898–905 (in Chinese with English abstract).

Ouyang, H.G., Mao, J.W., Santosh, M., Zhou, J., Zhou, Z.H., Wu, Y., Hou, L., 2013. Geodynamic setting of Mesozoic magmatism in NE China and surrounding regions: Perspectives from spatio-temporal distribution patterns of ore deposits. Journal of Asian Earth Sciences 78, 222–236.

Qin, F., Liu, J.M., Zeng, Q.D., Zhang, R.B., 2008. The metallogenic epoch and source of ore-forming materials of the Xiaodonggou porphyry molybdenum deposit, Inner Mongolia. Geoscience 22, 173–180 (in Chinese with English abstract).

Qin, F., Liu, J.M., Zeng, Q., Luo, Z., 2009. Petrogenetic and metallogenic mechanism of the Xiaodonggou porphyry molybdenum deposit in Hexigten Banner, Inner Mongolia. Acta Petrologica Sinica 25, 3357–3368 (in Chinese with English abstract).

Ramos, A., Folguera, A., 2009. Andean flat slab subduction through time. Geological Society, London, Special Publications 327, 31–54.

Santosh, M., 2010. Assembling North China Craton within the Columbia supercontinent: the role of double-sided subduction. Precambrian Research 178, 149–167.

Shao, J.A., Zang, S.X., Mu, B.L., 1995. Extensional tectonics and asthenospheric upwelling in the orogenic belt: a case study from Hinggan-Mongolia Orogenic belt. Chinese Science Bulletin 39, 533–537.

Shao, J.A., Liu, F.T., Chen, H., Han, Q.J., 2001. Relationship between Mesozoic magmatism and subduction in Da Hinggan-Yanshan area. Acta Geologica Sinica 75, 56–63.

Shao, J.A., Zhang, Y.B., Zhang, L.Q., Mu, B.L., Wang, P.Y., Guo, F., 2003. Early Mesozoic dike swarms of carbonatites and lamprophyres in Datong area. Acta Petrologica Sinica 19, 93–104 (in

Chinese with English abstract).

Shao, J.A., Zhang, L.Q., Mu, B.L., Han, Q.J., 2007. Upwelling of Da Hinggan Mountains and its geodynamic background: Beijing, Geological Publishing House, 250 p. (in Chinese).

Shu, P., Ding, R.X., Ji, X.Y., Qu, Y.M., 2007. SHRIMP zircon geochronology of reservoir volcanic rocks in the Qingshen gas field, Songliao Basin. Acta Petrologica et Mineralogica 26, 239–246 (in Chinese with English abstract).

Shu, Q.H., Jiang, L., Lai, Y., Lu, Y.H., 2009. Geochronology and fluid inclusion study of the Aolunhua porphyry Cu-Mo deposit in Arhorqin area, Inner Mongolia. Acta Petrologica Sinica 25, 2601–2614 (in Chinese with English abstract).

Shu, Q., Lai, Y., Wang, C., Xu, J., Sun, Y., 2014. Geochronology, geochemistry and Sr-Nd-Hf isotopes of the Haisugou porphyry Mo deposit, northeast China, and their geological significance. Journal of Asian Earth Sciences 79, 777–791.

Shu, Q., Lai, Y., Zhou, Y., Xu, J., Wu, H., 2015. Zircon U-Pb geochronology and Sr-Nd-Pb-Hf isotopic constraints on the timing and origin of Mesozoic granitoids hosting the Mo deposits in northern Xilamulun district, NE China. Lithos 238, 64–75.

Sillitoe, R.H.,2010. Porphyry copper systems. Economic Geology 105, 3–41.

Smoliar, M.I., Walker, R.J., Morgan, J.W., 1996. Re-Os ages of group IIA, IIIA, IVA and VIB iron meteorites. Science 271, 1099–1102.

Stein, H.J., Markey, R.J., Morgan, M.J., Du, A., Sun, Y., 1997. Highly precise and accurate Re-Os ages for molybdenite from the East Qinling-Dabie molybdenum belt, Shaanxi province, China. Economic Geology 92, 827–835.

Sun, Y., Liu, J.M., Zeng, Q.D., Chu, X.S., Zhou, L.L., Wu, G.B., Gao, Y.Y., Shen, W.J., 2013a. Geological characteristics and molybdenite Re-Os ages of the Baituyingzi Mo-Cu field, eastern Inner Mongolia and their geological implications. Acta Petrologica Sinica 29, 241–254.

Sun, M.D., Chen, H.L., Zhang, F.Q., Wilde, S.A., Dong, C.W., Yang, S.F., 2013b. A 100 Ma bimodal composite dyke complex in the Jiamusi Block, NE China: an indication for lithospheric extension driven by Paleo-Pacific roll-back. Lithos 162–163, 317–330.

Sun, J.G., Zhang, Y., Han, S.J., Men, L.J., Li, Y.X., Chai, P., Yang, F., 2013c. Timing of formation and geological setting of low-sulphidation epithermal gold deposits in the continental margin of NE China. International Geology Review 55, 608–632.

Tang, K., Yan, Z., 1993. Regional metamorphism and tectonic evolution of the Inner Mongolian suture zone. Journal of Metamorphic Geology 11, 511–522.

Tang, J., Xu, W.L., Wang, F., Wang, W., Xu, M.J., Zhang, Y.H., 2014. Geochronology and geochemistry of Early-Middle Triassic magmatism in the Erguna Massif, NE China: Constraints on the tectonic evolution of the Mongol-Okhotsk Ocean. Lithos 184, 1–16.

Tang, J., Xu, W.L., Wang, F., Zhao, S., Wang, W., 2015. Early Mesozoic southwards subduction history of the Mongol-Okhotsk oceanic plate: evidence from geochronology and geochemistry of Early Mesozoic intrusive rocks in the Erguna Massif, NE China. Gondwana Research, doi: 10.1016/j.gr.2014.12.010.

Wan, B., Hegner, E., Zhang, L., Rocholl, A., Chen, Z., Wu, H., Chen, F., 2009. Rb-Sr geochronology of chalcopyrite from the Chehugou porphyry Mo-Cu deposit (Northeast China) and geochemical constraints on the origin of hosting granites. Economic Geology 104, 351–363.

Wang, P.J., Liu, Z.J., Wang, S.X., Song, W.H., 2002. $^{40}Ar/^{39}Ar$ and K/Ar dating of the volcanic rocks in the Songliao basin, NE China: constraints on stratigraphy and basin dynamics. International Journal of Earth Sciences 91, 331–340.

Wang, Y., Zhao, C., Zhang, F., Liu, J., Wang, J., Peng, R., Liu, B., 2015. SIMS zircon U-Pb and molybdenite Re-Os geochronology, Hf isotope, and whole-rock geochemistry of the Wunugetushan porphyry Cu-Mo deposit and granitoids in NE China and their geological significance. Gondwana Research 28, 1228–1245.

Wu, F.Y., Han, R.H., Yang, J.H., Wilde, S.A., Zhai, M.G., Park, S.C., 2007. Initial constraints on the timing of granitic magmatism in North Korea using U-Pb zircon geochronology. Chemical Geology 238, 232–248.

Wu, H.Y., Zhang, L.C., Chen, Z.G., Wan, B., 2008. Geochemistries, tectonic setting and mineralization potentiality of the ore-bearing monzogranite in the Kulitu molybdenum (copper) deposit of Xar moron metallogetic belt, Inner Mongolia. Acta Petrologica Sinica 24, 867–878 (in Chinese with English abstract).

Wu, H.Y., Zhang, L.C., Wan, B., Chen, Z.G., Xiang, P., Pirajno, F., Du, A.D., Qu, W.J., 2011a. Re-Os and $^{40}Ar/^{39}Ar$ ages of the Jiguanshan porphyry Mo deposit, Xilamulun metallogenic belt, NE China, and constraints on mineralization events. Mineralium Deposita 46, 171–185.

Wu, H.Y., Zhang, L.C., Wan, B., Chen, Z.G., Zhang, X.J., Xiang, P., 2011b. Geochronological and geochemical constraints on Aolunhua porphyry Mo-Cu deposit, northeast China, and its tectonic significance. Ore Geology Reviews 43, 78–91.

Wu, F.Y., Sun, D.Y., Ge, W.C., Zhang, Y.B., Grant, M.L., Wilde, S.A., Jahn, B.M., 2011c.

Geochronology of the Phanerozoic granitoids in northeastern China. Journal of Asian Earth Sciences 41, 1–30.

Wu, H., Zhang, L., Pirajno, F., Xiang, P., Wan, B., Chen, Z., Zhang, X., 2014. The Jiguanshan porphyry Mo deposit in the Xilamulun metallogenic belt, northern margin of the North China Craton, U-Pb geochronology, isotope systematics, geochemistry and fluid inclusion studies: Implications for a genetic model. Ore Geology Reviews56, 549–565.

Xiao, W.J., Windley, B.F., Hao, J., Zhai, M.G., 2003. Accretion leading to collision and the Permian Solonker suture, Inner Mongolia, China: termination of the central Asian orogenic belt. Tectonics, http://dx.doi.org/10.1029/2002TC001484.

Xu, W.L., Pei, F.Q., Wang, F., Meng, E., Ji, W.Q., Yang, D.B., Wang, W., 2013. Spatial-temporal relationships of Mesozoic volcanic rocks in NE China: Constraints on tectonic overprinting and transformations between multiple tectonic regimes. Journal of Asian Earth Sciences 74, 167–193.

Yan, C., 2009. Study on LA-ICP-MS zircon U-Pb geochronology and fluid inclusions of the Banlashan Mo deposit in Arhorqin Banner, Inner Mongolia. Bachelor dissertation, Beijing, Peking University, 50 p. (in Chinese with English abstract).

Yang, Z.M., Chang, Z., Hou, Z.Q., Meffre, S., 2015. Age, igneous petrogenesis, and tectonic setting of the Bilihe gold deposit, China, and implications for regional metallogeny. Gondwana Research, http://dx.doi.org/10.1016/j.gr.2015.04.003.

Zeng, Q.D., Liu, J.M., Zhang, Z.L., Chen, W.J., Qin, F., Zhang, R.B., Yu, W.B., Zhang, X.H., Zhai, M.G., 2009a. Mineralizing types, geological characteristics and geodynamic background of molybdenum deposits in Xilamulun molybdenum polymetal metallogenic belt on northern margin of North China Craton. Acta Petrologica Sinica 25, 1225–1238 (in Chinese with English abstract).

Zeng, Q.D., Liu, J.M., Zhang, Z.L., Qin, F., Chen, W.J., Yu, C.M., Ye, J., 2009b. The ore-forming time of the Jiguanshan porphyry molybdenum deposit, northern margin of North China Craton and the Indosinian mineralization. Acta Petrologica Sinica 25, 393–398 (in Chinese with English abstract).

Zeng, Q.D., Liu, J.M., Zhang, Z.L., 2010. Re-Os geochronology of porphyry molybdenum deposit in south segment of Da Hinggan Mountains, northeastern China. Journal of Earth Sciences 21, 390–401.

Zeng, Q.D., Liu, J.M., Zhang, Z.L., Chen, W.J., Zhang, W.Q., 2011. Geology and geochronology of the Xilamulun molybdenum metallogenic belt in eastern Inner Mongolia, China. International Journal of Earth Sciences 100, 1791–1809.

Zeng, Q.D., Liu, J.M., Chu, S.X., Wang, Y.B., Sun, Y., Duan, X.X., Zhou, L.L., 2012. Mesozoic molybdenum deposits in the East Xingmeng orogenic belt, northeast China: characteristics and tectonic setting. International Geology Review 54, 1843–1869.

Zeng, Q., Liu, J., Qin, K., Fan, H., Chu, S., Wang, Y., Zhou, L., 2013. Types, characteristics, and time-space distribution of molybdenum deposits in China. International Geology Review 55, 1311–1358.

Zeng, Q., Yang, J., Zhang, Z, Liu, J., Duan, X., 2014. Petrogenesis of the Yangchang Mo-bearing granite in the Xilamulun metallogenic belt, NE China: geochemistry, zircon U-Pb ages and Sr-Nd-Pb isotopes. Geological Journal 49, 1–14.

Zhai, M.G., Santosh, M., 2011. The early Precambrian odyssey of North China Craton: a synoptic overview. Gondwana Research 20, 6–25.

Zhang, F.Q., Pang, Y.M., Yang, S.F., Dong, C.W., Chen, H.L., Shu, P., 2007a. Geochronology of zircon SHRIMP, geochemistry and its implication of the volcanic rocks from Yingcheng Formation in depression area, north of Songliao Basin. Acta Geologica Sinica 81, 1249–1259 (in Chinese with English abstract).

Zhang, S.H., Zhao, Y., Song, B., Yang, Z.Y., Hu, J.M., Wu, H., 2007b. Carboniferous granitic plutons from the northern margin of the North China block: implications for a late Paleozoic active continental margin. Journal of the Geological Society 164, 451–463.

Zhang, J.H., Ge, W.C., Wu, F.Y., Wilde, S.A., Yang, J.H., Liu, X.M., 2008. Large-scale early Cretaceous volcanic events in the northern Great Xing'an Range, northeastern China. Lithos 102, 138–157.

Zhang, L.C., Wu, H.Y., Wan, B., Chen, Z.G., 2009a. Ages and geodynamic settings of Xilamulun Mo-Cu metallogenic belt in northern part of the North China Craton. Gondwana Research 16, 243–254.

Zhang, S.H., Zhao, Y., Song, B., Hu, J.M., Liu, S.W., Yang, Y.H., Chen, F.K., Liu, X.M., Liu, J., 2009b. Contrasting Late Carboniferous and Late Permian-Middle Triassic intrusive suites from the northern margin of the North China craton: Geochronology, petrogenesis, and tectonic implications. Geological Society of America Bulletin 121, 181–200.

Zhang, S.H., Zhao, Y., Kröner, A., Liu, X.M., Xie, L.W., Chen, F.K., 2009c. Early Permian plutons from the northern North China Block: constraints on continental arc evolution and convergent margin magmatism related to the Central Asian Orogenic Belt. International Journal of Earth Sciences 98, 1441–1467.

Zhang, Z.L., Liu, J.M., Duan, X.X., Chen, W.J., 2010a. Ore-forming fluid geochemistry of Nianzigou molybdenum deposit in Xilamulun molybdenum metallogenic belt, Inner Mongolia. Acta Petrologica Sinica 26, 1375–1385 (in Chinese with English abstract).

Zhang, X.J., Zhang, L.C., Jin, X.D., Wu, H.Y., Xiang, P., Chen, Z.G., 2010b. U-Pb ages, geochemical characteristics and their implications of Banlashan Molybdenum Deposit. Acta Petrologica Sinica 26, 1411–1422 (in Chinese with English abstract).

Zhang, J.H., Gao, S., Ge, W.C., Wu, F.Y., Yang, J.H., Wilde, S.A., Li, M., 2010c. Geochronology of the Mesozoic volcanic rocks in the Great Xing'an Range, northeastern China: implications for subduction-induced delamination. Chemical Geology 276, 144–165.

Zhang, L., Gao, B., Li, W., Chen, Z., Sakyi, P.A., Jin, X., 2014. Early Mesozoic tectono-magmatic activity and mineralization in northeast China: evidence from Re-Os to U-Pb studies of the Taipingchuan porphyry Cu-Mo deposit in the Derbugan metallogenic belt. International Geology Review 56, 1837–1851.

Zhang, X., Li, T., Pu, Z., 2002a. ^{40}Ar-^{39}Ar thermochronology of two ductile shear zones from Yiwulüshan, West Liaoning Region: Age constraints on the Mesozoic tectonic events. Chinese Science Bulletin 47, 1113–1118.

Zhang, X., Li, T., Pu, Z., Wang, H., 2002b. ^{40}Ar-^{39}Ar ages of the Louzidian-Dachengzi ductile shear zone near Chifeng, Inner Mongolia and their tectonic significance. Chinese Science Bulletin 47, 1292–1297.

Zhang, Z.L., Liu, J.M., Chu, S.X., 2012. Ore-forming fluid geochemistry of Yangchang quartz vein molybdenum deposit in Xilamulun molybdenum metallogenic belt, Inner Mongolia. Acta Petrologica Sinica 28, 391–400 (in Chinese with English abstract).

Zhang, C., Li, N., 2014. Geology, geochemistry and tectonic setting of the Indosinian Mo deposits in southern Great Hinggan Range, NE China. Geological Journal 49, 537-558.

Zhou, J.B., Wilde, S.A., 2013. The crustal accretion history and tectonic evolution of the NE China segment of the Central Asian Orogenic belt. Gondwana Research 23, 1365–1377.

Zhou, Z.H., Lü, L.S., Feng, J.R., Li, C., Li, T., 2010. Molybdenite Re-Os ages of Huanggang skarn Sn-Fe deposit and their geological significance, Inner Mongolia. Acta Petrologica Sinica 26, 667–679 (in Chinese with English abstract).

Zhou, Z.H., Mao, J.W., Lyckberg, P., 2012. Geochronology and isotopic geochemistry of the A-type granites from the Huanggang Sn-Fe deposit, southern Great Hinggan Range, NE China: Implication for their origin and tectonic setting. Journal of Asian Earth Sciences 49, 272–286.

Chapter 5

Ore genesis and hydrothermal evolution of the Baiyinnuo'er zinc-lead skarn deposit, northeast China: evidence from isotopes (S, Pb) and fluid inclusions

Economic Geology, v. 108, pp. 835–860

Ore Genesis and Hydrothermal Evolution of the Baiyinnuo'er Zinc-Lead Skarn Deposit, Northeast China: Evidence from Isotopes (S, Pb) and Fluid Inclusions*

QIHAI SHU, YONG LAI,† YI SUN, CHAO WANG, AND SHU MENG

Key Laboratory of Orogenic Belt and Crustal Evolution, School of Earth and Space Sciences, Peking University, Beijing 100871, China

0361-0128/13/4118/835-26

Submitted: March 31, 2012
Accepted: November 30, 2012

95

This publication has been removed due to copyright restrictions

This publication has been removed due to copyright restrictions

This publication has been removed due to copyright restrictions

This publication has been removed due to copyright restrictions

This publication has been removed due to copyright restrictions

111

This publication has been removed due to copyright restrictions

This publication has been removed due to copyright restrictions

This publication has been removed due to copyright restrictions

This publication has been removed due to copyright restrictions

This publication has been removed due to copyright restrictions

Chapter 6

Composition and evolution of fluids forming the Baiyinnuo'er skarn Zn-Pb deposit, NE China: insights from laser ablation ICP-MS study of fluid inclusions

Composition and evolution of fluids forming the Baiyinnuo'er skarn Zn-Pb deposit, NE China: insights from laser ablation ICP-MS study of fluid inclusions

Qihai Shu[1,2,3]*, Zhaoshan Chang[1], Johannes Hammerli[1,4], Yong Lai[2], Jan-Marten Huizenga[1,5]

[1] EGRU (Economic Geology Research Centre) and Department of Earth and Oceans, College of Science, Technology and Engineering, James Cook University, Townsville, Queensland 4811, Australia

[2] Key Laboratory of Orogenic Belt and Crustal Evolution, School of Earth and Space Sciences, Peking University, Beijing 100871, China

[3] State Key Laboratory of Geological Processes and Mineral Resources, School of Earth Sciences and Resources, China University of Geosciences, Beijing 100083, China

[4] Centre for Exploration Targeting, School of Earth and Environment, The University of Western Australia, Perth, WA 6009, Australia

[5] Department of Geology, University of Johannesburg, Auckland Park, Johannesburg 2006, South Africa

*: email: qihai.shu@my.jcu.edu.au

This publication has been removed due to copyright restrictions

This publication has been removed due to copyright restrictions

This publication has been removed due to copyright restrictions

This publication has been removed due to copyright restrictions

This publication has been removed due to copyright restrictions

This publication has been removed due to copyright restrictions

This publication has been removed due to copyright restrictions

This publication has been removed due to copyright restrictions

This publication has been removed due to copyright restrictions

This publication has been removed due to copyright restrictions

This publication has been removed due to copyright restrictions

This publication has been removed due to copyright restrictions

This publication has been removed due to copyright restrictions

This publication has been removed due to copyright restrictions

This publication has been removed due to copyright restrictions

This publication has been removed due to copyright restrictions

This publication has been removed due to copyright restrictions

This publication has been removed due to copyright restrictions

This publication has been removed due to copyright restrictions

This publication has been removed due to copyright restrictions

This publication has been removed due to copyright restrictions

This publication has been removed due to copyright restrictions

Chapter 7

Summary

Summary

The NE China hosts a great number of intrusion-related deposits which can be divided into two major groups: (1) porphyry Mo-bearing deposits, and (2) skarn Zn-Pb-polymetallic deposits. This thesis studies representative deposits of both types to better understand the ore-forming processes and the geodynamic settings: (1) Five typical porphyry Mo deposits in the Xilamulun district in NE China including Haisugou, Shabutai, Yangchang, Aolunhua and Banlashan have been studied to explore the mechanisms that control the enrichment of molybdenum. The spatio-temporal framework of the Mo deposits in NE China was also constructed to infer the geodynamic setting which, furthermore, can be applied in exploration. (2) For skarns, the Baiyinnuo'er Zn-Pb deposit has been selected for a case study in terms of its mineralogy, fluid inclusions and isotopes, aiming to constrain the ore genesis, hydrothermal evolution and ore precipitation mechanism in the skarn system. The major findings of this study are summarized below.

Porphyry Mo mineralization in NE China

Three possible factors related to the enrichment of Mo have been tested in this thesis (Chapters 2 and 3): (1) the composition of the magma source region. We found that there were at least three stages of Mo mineralization during the Mesozoic (i.e., Triassic, Late Jurassic, and Early Cretaceous), and they are respectively related to magmas generated from three different source regions (see details in Chapter 3). Such a variation in the origin of the magmas from which the porphyry Mo systems were generated precludes the dependence of the formation of Mo deposit on the composition of magma sources. (2) magma fractional crystallization. We noticed that intrusions hosting porphyry Mo mineralization underwent more significant crystal fractionation when compared with intrusions hosting porphyry Cu and Cu-Mo deposits, indicating that such a process may have played a role in selective enrichment of Mo (see details in Chapter 2). (3) redox states of the magmas. We used the zircon Ce/Nd ratio as a proxy for the oxidation state of magmas and compared the zircon Ce/Nd ratios between mineralized intrusions with barren intrusions, and found that the Mo mineralization-related intrusions are associated with more oxidized magmas than the cospatial barren granites, and therefore we proposed that higher oxygen fugacity may be important for Mo enrichment and subsequent mineralization (see details in Chapter 3). In summary, the composition of the magma source region is not the key for the formation of Mo deposits, while other factors, including high oxygen fugacity and significant crystal fractionation of the magma, may have taken the fundamental role in generating Mo-rich melt and eventual Mo deposition.

The compilation of preexisting geochronological data on Mo deposits in NE China combined with

the new data from this project shows that Mesozoic ~250 to 90 Ma Mo deposits widely occur in this region. We propose that they are linked to three tectonic-magmatic events (Fig. 7-1): (1) Triassic Mo deposits (250–220 Ma) are mainly distributed along the east-west Xilamulun fault and are related to the post-collisional crustal extension following the final closure of the Paleo-Asian ocean; (2) Jurassic to Early Cretaceous Mo mineralization (200–130 Ma) displays a clear younging trend from southeast to northwest, coincides well with the regional magmatism, and is interpreted to be related to the northwestward flat-slab subduction of the Paleo-Pacific plate beneath the Eurasian continent that started from Early Jurassic (ca. 200 Ma); (3) Cretaceous Mo mineralization (130–90 Ma) shows a distinctly reversed migration trend from northwest to southeast, and can be explained by the coastward migration of slab rollback related to lower crust delamination, asthenospheric upwelling and lithospheric thinning in eastern China. Such a spatial-temporal distribution model of the Mesozoic Mo mineralization can be applied for regional exploration. Recently numerous epithermal Au (Cu, Mo) deposits have been discovered in the southeast margin of NE China. We predict that beneath these epithermal deposits, there could exist hidden porphyry/skarn systems according to this study, on which particular attention should be paid in exploration (see details in Chapter 4).

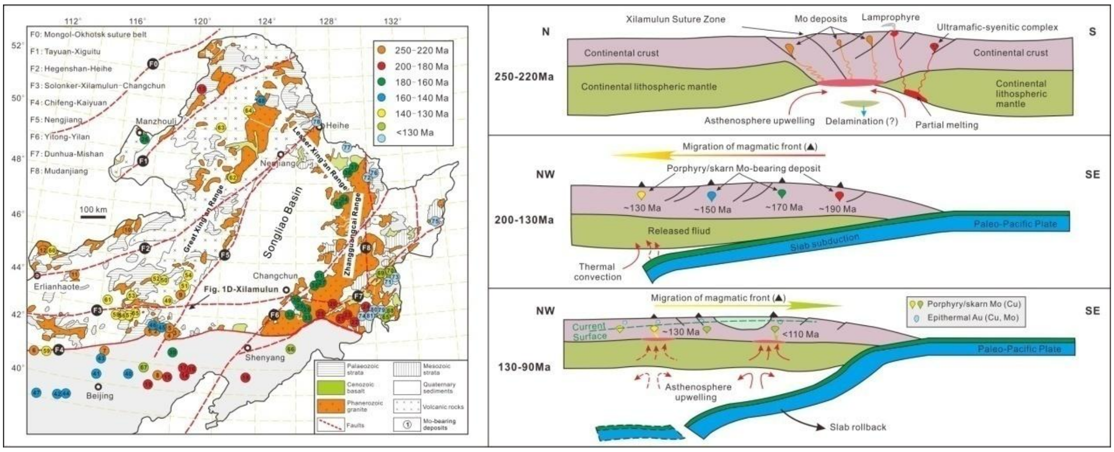

Figure 7-1.A three-stage model for Mesozoic Mo mineralization in NE China. The spatial-temporal distribution of the Mo deposits are shown in the left maps, while the geodynamic processes are illustrated in the right cartoons. The detailed description for such a model can be found in Chapter 4.

Skarn Zn-Pb mineralization in NE China

The skarn Zn-Pb mineralization in Baiyinnuo'er, a representative skarn deposit in NE China, recorded a complex sequence of hydrothermal calc-silicate minerals, sulfides, and calcite and quartz. Sulfur isotope values of the sulfides are in a narrow $\delta^{34}S$ interval (-6.1 to -4.6‰), a little lower than but in general similar to that of typical magmatic hydrothermal deposits, suggesting that the ore-forming fluid is of magmatic origin. Lead isotopic ratios also support the magmatic sources for ore-forming materials, though contribution from the Permian marble could also be significant. The Pb isotope compositions also indicate that the skarn was related to the Early Cretaceous granite rather than the Permian and Triassic intrusions nearby, based on the similarity of Pb isotopic compositions between the Early Cretaceous granite and sulfide minerals (see details in Chapter 5). Fluid inclusion study also leads to the same conclusion. In Chapter 5, systematic fluid inclusion microthermometric study indicates that the mineralization-related fluid is of magmatic origin.

From laser ablation-inductively coupled-mass spectrometry (LA-ICP-MS) compositional study of individual fluid inclusions, it has been concluded that the chemical components of fluid inclusions from different stages of skarn formation and mineralization in Baiyinnuo’er are characterized by magmatic signatures, and are distinctively different from basin brines. This reveals that all the fluids of different stages have various amount of magmatic components (more in earlier pre-ore stage and gradually less in later stages), and that there is no evolvement of basin brines. The fluid compositions also indicated that mixing with external fluid (i.e., groundwater) has occurred starting from the syn-ore stage of Zn-Pb mineralization, resulting in the significant decreases of major cations (Na, K) and halogen (Cl) in the syn- and post-ore fluids (see details in Chapter 6), consistent with the temperature-salinity trend. Microthermometric study in Chapter 5 and LA-ICP-MS study in Chapter 6 have reached an agreement that the fluids in pre-ore and syn-ore stages, from early to late, are related to two (or more) successive pluses of chemically different hydrothermal fluids exsolved from residual melt batches of a progressively downward crystallizing magma.

From LA-ICP-MS results, it has been observed that the formation of sulfides was related to the syn-ore fluid with lower metal contents other than the anomalously metal-rich fluid of the pre-ore stage. This reveals that high concentrations of metal elements in fluid will not necessarily result in sulfides deposition. Other factors, including fluid temperature, mixing with groundwater and interaction with carbonate wallrock, may have played more important roles in ore precipitation (see details in Chapter 6). Boiling occurred in the pre-ore and early part of the syn-ore stage, but no evidence indicates that it was related to metal deposition.

This study demonstrates that the fluids in skarns are similar to that in porphyry deposits in terms of their origin, composition and evolution, but differences have also been recognized (e.g., higher Ca/K ratios in skarn system), mainly due to the interaction with carbonate wall rock. The obtained data from the Baiyinnuo’er skarn Zn-Pb deposit from this study can also be applied to other skarn deposits in NE China and even worldwide, therefore helpful to understanding of the ore-forming mechanism in skarn systems.

Appendix Supplementary Materials

Appendix 1-1. Other publications I have co-authored but not included in this thesis.

Peng, H., Hou, L., **Shu, Q.**, and Zhang, C., Stable isotope and fluid inclusion constraints on the source and evolution of ore fluids in the Hongniu–Hongshan Cu skarn deposit, Yunnan Province, China (submitted to Economic Geology).

Wu, H., Zhang, L., Pirajno, F., **Shu, Q.**, Zhang, M., Zhu, M., and Xiang, P., The Caosiyao giant porphyry Mo deposit in Inner Mongolia, northern North China Craton: Re-Os and U-Pb geochronology, geochemistry and its tectonic significance (submitted to Journal of Asian Earth Sciences).

Sun, Y., Lai, Y., Chen, J., **Shu, Q.**, and Yan, C., 2013, REE and rare metal elements mobility and mineralization during magmatic and fluid evolution in alkaline granite system: evidence from fluid and melt inclusions in Baerzhe granite. Resource Geology, v. 63, p. 239–261.

Meng, S., Yan, C., Lai, Y., **Shu, Q.**, and Sun, Y., 2013, Study on the mineralization chronology and characteristics of mineralization fluid from the Chehugou porphyry Cu-Mo deposit, Inner Mongolia: Acta Petrologica Sinica, v. 29, p. 255–269.

Appendix 2-1. Ages of Mo-bearing deposits in different Mo metallogenic belts in east China.

Belt	Deposit	Genetic type	Economic metal(s)	Analytical method	Age(Ma)	References
Xilamulun						
1	Chehugou	porphyry	Cu, Mo	molybdenite Re-Os	257.5±2.5	Liu et al., 2010
2	Yuanbaoshan	porphyry	Mo	molybdenite Re-Os	248.0±2.7	Liu et al., 2010
3	Baimashi	quartz vein	Cu, Mo	molybdenite Re-Os	248.5±6.7	Zeng et al., 2012
4	Kulitu	porphyry	Cu, Mo	molybdenite Re-Os	236.0±3.3	Zhang et al., 2009
5	Laojiagou	porphyry	Mo, Cu	molybdenite Re-Os	234.9±3.1	Zeng et al., 2012
6	Nianzigou	quartz vein	Mo	molybdenite Re-Os	153.0±5.0	Zhang et al., 2009
7	Jiguanshan	porphyry	Mo	molybdenite Re-Os	155.4±1.3	Wu et al., 2011
8	Hongshanzi	quartz vein	U, Mo	asphalt rock U-Pb	130.0±8.0	Nie et al., 2007
9	Xiaodonggou	porphyry	Mo	molybdenite Re-Os	135.5±1.5	Nie et al., 2007
10	Liutiaogou	quartz vein	U, Mo	volcanic rock Rb-Sr	137.0±12	Zeng et al., 2008
11	Gangzi	porphyry	Mo	zircon U-Pb	139.1±2.3	Zhang et al., 2009
12	Huanggang	skarn	Fe, Sn, Mo	molybdenite Re-Os	135.3±0.9	Zhou et al., 2010
13	Yangchang	porphyry	Cu, Mo	molybdenite Re-Os	138.5±4.5	Zeng et al., 2010
14	Shabutai	porphyry	Mo	molybdenite Re-Os	135.3±2.6	Unpublished data
15	Haisugou	porphyry	Mo	zircon U-Pb	137.6±0.9	This study
16	Banlashan	breccias pipe	Mo	molybdenite Re-Os	136.1±6.6	Yan et al., 2011
17	Aolunhua	porphyry	Cu, Mo	molybdenite Re-Os	132.1±1.2	Ma et al., 2009
Yan-Liao						
1	Sadaigoumen	porphyry	Mo	molybdenite Re-Os	237.0±3.9	Duan et al., 2007
2	Dasuji	porphyry	Mo	molybdenite Re-Os	222.5±3.2	Nie et al., 2012
3	Yangjiazhangzi	skarn	Mo	molybdenite Re-Os	187.0±2.0	Huang et al., 1996
4	Lanjiagou	porphyry	Mo	molybdenite Re-Os	182.0±6.5	Han et al., 2009
5	Xintaimen	porphyry and skarn	Mo, Fe	molybdenite Re-Os	178.0±5.0	Zhang et al., 2009
6	Xiaojiayingzi	skarn	Mo, Fe	molybdenite Re-Os	165.5±4.6	Dai et al., 2009
7	Houyu	porphyry	Mo	molybdenite Re-Os	148.7	Du et al., 2010
8	Shouwangfen	skarn	Cu, Mo, Fe	molybdenite Re-Os	148.0±4.0	Huang et al., 1996
9	Dazhuangke	porphyry	Mo	molybdenite Re-Os	146.4±5.9	Huang et al., 1996
10	Dawang	porphyry and skarn	Mo, Cu, Zn	molybdenite Re-Os	144.4±7.4	Huang et al., 1996
11	Dacaoping	porphyry	Mo	molybdenite Re-Os	137.1±2.6	Duan et al., 2007
12	Xiaosigou	porphyry and skarn	Mo, Cu	molybdenite Re-Os	134.0±3.0	Huang et al., 1996
13	Caosiyao	porphyry	Mo	molybdenite Re-Os	130.4±2.4	Nie et al., 2012
East Qingling-Dabie [1]						
1	Huanglongpu			molybdenite Re-Os	221.5±0.3	Mao et al., 2011a
2	Xigou	quartz vein	Mo	molybdenite Re-Os	210.4	Mao et al., 2011a
3	Huangshuian	caibonatite vein	Mo, Pb	molybdenite Re-Os	209.5±4.2	Mao et al., 2011a
4	Dahu	quartz vein	Au, Mo	molybdenite Re-Os	228	Mao et al., 2011a
5	Qianfanling	quartz vein	Mo	molybdenite Re-Os	239	Mao et al., 2011a
6	Zhifang	quartz vein	Mo	molybdenite Re-Os	235	Mao et al., 2011a
7	Daxigou	quartz vein	Mo	molybdenite Re-Os	225	Mao et al., 2011a
8	Maogou	quartz vein	Mo	molybdenite Re-Os	235	Mao et al., 2011a
9	Balipo	porphyry	Mo	molybdenite Re-Os	156.3±2.2	Mao et al., 2011a

10	Shijiawan	porphyry	Mo	molybdenite Re-Os	140	Mao et al., 2011a
11	Jinduicheng	porphyry	Mo, Cu	molybdenite Re-Os	138.2±1.1	Mao et al., 2011a
12	Nannihu	porphyry and skarn	Mo, W	molybdenite Re-Os	141.8±2.1	Mao et al., 2011a
13	Shangfanggou	porphyry and skarn	Mo, Fe	molybdenite Re-Os	144.8±2.1	Mao et al., 2011a
14	Dawanggou	quartz vein	Mo	molybdenite Re-Os	144.5±2.0	Mao et al., 2011a
15	Qiushuwan	porphyry and skarn	Cu, Mo	molybdenite Re-Os	147	Mao et al., 2011a
16	Saozhoupo	quartz vein	Mo, Ag, Pb	molybdenite Re-Os	114.3±3.4	Mao et al., 2011a
17	Laojieling	quartz vein	Mo	molybdenite Re-Os	109.8±1.6	Mao et al., 2011a
18	Donggoukou	quartz vein	Mo	molybdenite Re-Os	113.4±1.9	Mao et al., 2011a
19	Shiyaogou	porphyry	Mo	molybdenite Re-Os	135.2±1.8	Mao et al., 2011a
20	Shapoling	porphyry	Mo	molybdenite Re-Os	126.8±1.7	Mao et al., 2011a
21	Yuchiling	porphyry	Mo	molybdenite Re-Os	131.2±1.4	Mao et al., 2011a
22	Leimengou	porphyry	Mo	molybdenite Re-Os	132.4±2.0	Mao et al., 2011a
23	Donggou	porphyry	Mo	molybdenite Re-Os	116.0±1.7	Mao et al., 2011a
24	Zhuyuangou	quartz vein	Mo	molybdenite Re-Os	120.9±2.3	Mao et al., 2011a
25	Tianmushan	quartz vein	Mo	molybdenite Re-Os	121.6±2.1	Mao et al., 2011a
26	Qianechong	porphyry	Mo	molybdenite Re-Os	127.8±0.9	Mao et al., 2011a
27	Dayinjian	porphyry and skarn	Mo	molybdenite Re-Os	122.1±2.4	Mao et al., 2011a
28	Tangjiaping	porphyry	Mo	molybdenite Re-Os	113.1±7.9	Mao et al., 2011a
29	Shapinggou	porphyry	Mo	molybdenite Re-Os	113.1	Mao et al., 2011a
30	Quanjiayu	quartz vein	Mo, Au	molybdenite Re-Os	130.0±1.5	Mao et al., 2011a
31	Xintianling	skarn	Mo, W, Sn	molybdenite Re-Os	161	Mao et al., 2011a
Middle–Lower Yangtze River Valley [2]						
1	Yueshan	skarn	Cu, Mo	molybdenite Os-Os	136.1±2.0	Mao et al., 2011b
2	Anqing	skarn	Cu, Au, Mo	molybdenite Re-Os	140.3±1.6	Mao et al., 2011b
3	Tongkuangli	skarn	Mo	molybdenite Re-Os	142.4±1.6	Mao et al., 2011b
4	Tongshan	skarn and stratabound	Cu, Mo	molybdenite Re-Os	147.5±2.3	Mao et al., 2011b
5	Qianjiawan	skarn	Cu, Au, Mo	molybdenite Re-Os	137.7±1.7	Mao et al., 2011b
6	Jiguanzui	skarn	Cu, Au, Mo	molybdenite Re-Os	138.2±2.2	Mao et al., 2011b
7	Ruanjiawan	skarn and stratabound	Cu, Mo	molybdenite Re-Os	143.6±1.7	Mao et al., 2011b
8	Tongshankou	porphyry	Cu, Mo	molybdenite Re-Os	143.8±2.6	Mao et al., 2011b
9	Fengshandong	porphyry, skarn and stratabound	Cu, Mo	molybdenite Re-Os	144.0±2.0	Mao et al., 2011b
10	Chengmenshan	porphyry, skarn and stratabound	Cu, Mo, Au	molybdenite Re-Os	141.0±3.0	Mao et al., 2011b
11	Wushan	skarn and stratabound	Cu, Au, Mo	molybdenite Re-Os	146.4±2.6	Mao et al., 2011b
12	Xiaotongguanshan	porphyry and skarn	Cu, Mo	molybdenite Re-Os	135.5±0.5	Mao et al., 2011b
13	Jinkouling	skarn	Cu, Au, Mo	molybdenite Re-Os	137.0±0.5	Mao et al., 2011b
14	Dongguashan	skarn and porphyry	Cu, Au, Mo	molybdenite Re-Os	137.4	Mao et al., 2011b
15	Longhushan	skarn and stratabound	Cu, Mo, Au	molybdenite Os-Os	138.0±2.5	Mao et al., 2011b
16	Qingyang	skarn	Mo	molybdenite Os-Os	138.1±2.5	Mao et al., 2011b
17	Talimu	skarn	Cu, Au, Mo	biotite Ar-Ar	138.6±0.2	Mao et al., 2011b
18	Datuanshan	skarn	Cu, Mo	molybdenite Re-Os	139.1±2.7	Mao et al., 2011b

19	Nanyangshan	skarn	Cu, Mo	molybdenite Re-Os	140.2±1.6	Mao et al., 2011b
20	Shatanjiao	skarn	Cu, Mo	molybdenite Re-Os	141.8±1.6	Mao et al., 2011b
21	Laomiaojishan	skarn	Cu, Mo	fuchsite Ar-Ar	144.9±0.4	Mao et al., 2011b
22	Tonglushan	skarn	Fe, Cu, Mo	molybdenite Re-Os	137.1±1.9	Mao et al., 2011b
23	Langyashan	skarn	Cu, Au, Mo	molybdenite Re-Os	128.6±2.2	Mao et al., 2011b
24	Mengkeng	quartz vein	Mo	molybdenite Re-Os	144.0±3.1	Mao et al., 2011b
25	Baizhanyan	skarn	Mo	molybdenite Re-Os	134.0±2.6	Mao et al., 2011b
26	Fenghuangshan	skarn	Cu, Mo	molybdenite Re-Os	141.1±1.4	Mao et al., 2011b
27	Anjishan	skarn and porphyry	Cu, Mo	molybdenite Re-Os	108.0±2.0	Mao et al., 2011b
Others						
1	Taipingchuan	porphyry	Cu, Mo	zircon U-Pb	202.0±5.7	Chen et al., 2010
2	Wunugetushan	porphyry	Cu, Mo	molybdenite Re-Os	177.6±4.5	Chen et al., 2011
3	Wulandele	porphyry	Mo, Cu	molybdenite Re-Os	134.1±3.3	Tao et al., 2009
4	Taipinggou	porphyry	Mo	molybdenite Re-Os	130.1±1.3	Wang et al., 2009
5	Xinzhangfang	quartz vein	Mo	molybdenite Re-Os	134.0±2.0	Jia et al., 2011
6	Fu’anbao	porphyry	Mo	molybdenite Re-Os	166.9±6.7	Wang et al., 2010
7	Daheishan	porphyry	Mo	molybdenite Re-Os	168.2±3.2	Wang et al., 2010
8	Xingjiashan	skarn	Mo, W	molybdenite Re-Os	157.6±3.9	Liu et al., 2011
9	Chalukou	porphyry	Mo	molybdenite Re-Os	146.9±0.8	Zeng et al., 2012
10	Xingshan	porphyry	Mo	molybdenite Re-Os	167.3±2.5	Zeng et al., 2012

Note: Xilamulun: deposit numbers corresponding to Figure 1c.
[1]Data resources for Mo-bearing deposits in the East Qinling-Dabie Belt are from Mao et al. (2011a);
[2]Data resources for Mo-bearing deposits in the Middle–Lower Yangtze River Valley Belt are from Mao et al. (2011b).

References

Chen, Z.G., Zhang, L.C., Li, Z.L., Wu, H.Y., Xiang, P., Huang, S.W., 2010. Geochronology and geochemistry of the Taipingchuan copper-molybdenum deposit in Inner Mongolia, and its geological significances (in Chinese with English abstract). Acta Petrologica Sinica 26, 1437–1449.

Chen, Z.G., Zhang, L.C., Wan, B., Wu, H.Y., Cleven, N., 2011. Geochronology and geochemistry of the Wunugetushan porphyry Cu-Mo deposit in NE China, and their geological significance: Ore Geology Reviews 43, 92–105.

Dai, J.Z., Mao, J.W., Zhao, C.S., Xie, Q.Q., Yang, F.Q., Wang, Y.T., 2009. New U-Pb and Re-Os age data and the geodynamic setting of the Xiaojiayingzi Mo (Fe) deposit, western Liaoning province, Northeastern China. Ore Geology Reviews 35, 235–244.

Du, B.F., Wei, J.H., Wang, Q., Li, Y.J., Liu, G.C., Yu, H.T., Liu, Y.L., 2010. Discussion on metallogenic setting and time difference between magmatism and mineralization of molybdenum in East China (in Chinese with English abstract). Mineral Deposits 29, 935–955.

Duan, H.C., Qin, Z.Y., Lin, X.H., Zhang, B.H., Liu, X.B., Zhang, X., Guo, P.Z., Han, F., Qin, L., Dai, J.Z., 2007. Zircon U-Pb ages of intrusive bodies in Dacaoping molybdenum ore district, Fengning Country, Hebei province (in Chinese with English abstract). Mineral Deposits 26, 634–642.

Han, C.M., Xiao, W.J., Zhao, G.C., Sun, M., Qu, W.J., Du, A.D., 2009. A Re-Os study of molybdenites from the Lanjiagou Mo deposit of North China Craton and its geological significance. Gondwana Research 16, 264–271.

Huang, D.H., Du, A.D., Wu, C.Y., Liu, L.S., Sun, Y.L., Zou, X.Q., 1996. Geochronology of molybdenum (copper) deposits in the north China platform: Re-Os age of molybdenite and its geological significance (in Chinese with English abstract). Mineral Deposits 15, 289–297.

Jia, P.P., Wei, J.H., Gong, Q.W., Zhao, W.L., Wan, L., 2011. Analysis of geological background and ore-searching prospect for copper-molybdenum deposits in the Da Hinggan Ling area (in Chinese with English abstract). Geology and Exploration 47, 151–162.

Liu, J.M., Zhao, Y., Sun, Y.L., Li, D.P., Liu, J., Chen, B.L., Zhang, S.H., Sun, W.D., 2010. Recognition of the latest Permian to Early Triassic Cu-Mo mineralization on the northern margin of the North China block and its geological significance. Gondwana Research 17, 125–134.

Liu, S.B., Wang, D.H., Chen, Y.C., Zhou, H.Q., Qu, W.J., Wang, C.H., 2011. Geological characteristics and molybdenite Re-Os age of the Xingjiashan W-Mo deposit in Yantai area, Jiaodong Peninsula, Shangdong Province (in Chinese with English abstract). Geological Bulletin of China 30, 1294–1302.

Ma, X.H., Chen, B., Lai, Y., Lu, Y.H., 2009. Petrogenesis and mineralization chronology study on the Aolunhua porphyry Mo deposit, Inner Mongolia, and its geological implications (in Chinese with English abstract). Acta Petrologica Sinica 25, 2939–2950.

Mao, J.W., Pirajno, F., Xiang, J.F., Gao, J.J., Ye, H.S., Li, Y.F., Guo, B.J., 2011a. Mesozoic molybdenum deposits in the east Qinling-Dabie orogenic belt: Characteristics and tectonic settings. Ore Geology Reviews 43, 264–293.

Mao, J.W., Xie, G.Q., Duan, C., Pirajno, F., Ishiyama, D., Chen, Y.C., 2011b. A tectono-genetic model for porphyry-skarn-stratabound Cu-Au-Mo-Fe and magnetite-apatite deposits along the Middle-Lower Yangtze River Valley, Eastern China. Ore Geology Reviews 43, 294–314.

Nie, F.J., Zhang, W.Y., Du, A.D., Jiang, S.H., Liu, Y., 2007. Re-Os isotopic dating on molybdenite separates from the Xiaodonggou porphyry Mo deposit, Hexigten Qi, Mongolia (in Chinese with English abstract). Acta Geologica Sinica 81, 898–905.

Nie, F.J., Liu, Y.F., Zhao, Y.A., Cao, Y., 2012. Discovery of Dasuji and Caosiyao large-size Mo deposits in central Inner Mongolia and its geological significances (in Chinese with English abstract). Mineral Deposits 31, 930–940.

Tao, J.X., Wang, T., Chen, Z.H., Luo, Z.Z., Xu, L.Q., Hao, X.Y., Cui, L.W., 2009. The Re-Os isotopic dating of molybdenite from the Wulandele molybdenum-copper polymetallic deposit in Sonid Zuoqi of Inner Mongolia and its geological significance. Rock and Mineral Analysis 28, 249–253.

Wang, D.H., Chen, Z.H., Chen, Y.C., Tang, J.X., Li, J.K., Ying, L.J., Wang, C.H., Liu, S.B., Li, L.X., Qin, Y., Li, H.Q., Qu, W.J., Wang, Y.B., Chen, W., Zhang, Y., 2010. New data of rock-forming and ore-forming chronology for China's important mineral resources areas (in Chinese with English abstract). Acta Geologica Sinica 84, 1030–1040.

Wang, S.W., Wang, J.G., Zhang, D., Qi, X.J., Wu, G.G., Zhao, P.Z., Yang, Z,F., Liu, Y.B., 2009. Geochronological study on Taipinggou molybdenum deposit in Da Hinggan Mountain (in Chinese with English abstract). Acta Petrologica Sinica 25, 2913–2923.

Wu, H.Y., Zhang, L.C., Wan, B., Chen, Z.G., Xiang, P., Pirajno, F., Du, A.D., Qu, W.J., 2011. Re-Os and $^{40}Ar/^{39}Ar$ ages of the Jiguanshan porphyry Mo deposit, Xilamulun metallogenic belt, NE China, and constraints on mineralization events. Mineralium Deposita 46, 171–185.

Yan, C., Sun, Y., Lai, Y., Ma, X.H., 2011. LA-ICP-MS zircon U-Pb and molybdenite Re-Os isotope ages and metallogenic geodynamic setting of Banlashan Mo deposit, Inner Mongolia (in Chinese with English abstract). Mineral Deposits 30, 616–634.

Zeng, Q.D., Liu, J.M., Qin, F., Zhang, Z.L., Chen, W.J., 2008. Preliminary research on Mesozoic four-stage Mo mineralization in Da Hinggan mountains of China. Gondwana 13, 251–252 program and abstracts.

Zeng, Q.D., Liu, J.M., and Zhang, Z.L., 2010. Re-Os geochronology of porphyry molybdenum deposit in south segment of Da Hinggan Mountains, northeastern China: Journal of Earth Sciences 21, 390–401.

Zeng, Q.D., Liu, J.M., Chu, S.X., Wang, Y.B., Sun, Y., Duan, X.X., Zhou, L.L., 2012. Mesozoic molybdenum deposits in the East Xingmeng orogenic belt, northeast China: characteristics and tectonic setting. International Geology Review 54, 1843–1869.

Zhang, L.C., Wu, H.Y., Wan, B., Chen, Z.G., 2009. Ages and geodynamic settings of Xilamulun Mo-Cu metallogenic belt in northern part of the North China Craton. Gondwana Research 16, 243–254.

Zhang, Z.Z., Wu, C.Z., Gu, L.X., Feng. H., Zheng, Y.C., Huang, J.H., Li, J., Sun, Y.L., 2009. Molybdenite Re-Os dating of Xintaimen molybdenum deposit in Yanshan-Liaoning metallogenic belt, North China (in Chinese with English abstract). Mineral Deposits 28, 313–320.

.Zhou, Z.H., Lv, L.S., Feng, J.R., Li, C., Li, T., 2010. Molybdenite Re-Os age of Huanggang skarn Sn-Fe deposit and their geological significance, Inner Mongolia (in Chinese with English abstract). Acta Petrologica Sinica 26, 667–679.

Appendix 3-1. Analytical methods

Zircon U-Pb dating and Hf isotope analyses

Zircon grains for U-Pb and Lu-Hf isotopic analyses were first separated by conventional magnetic and density techniques and purified by hand-picking under a binocular microscope afterwards. The separated zircons were mounted in epoxy resin and polished in order to expose the interiors for cathodoluminescence (CL) studies using a scanning electron microscope at the SEM Laboratory of Peking University.

Zircon U-Pb dating were performed on an Agilent 7500ce ICP-MS equipped with a 193 nm excimer laser ablation system (COMPexPro102) at the Key Laboratory of Orogenic Belts and Crustal Evolution, Peking University, following the analytical procedures described by Yuan et al., (2004). The laser beam is 36 μm in diameter and frequency is 10 Hz. U, Th and Pb concentrations were calibrated by using ^{29}Si as an internal standard and Harvard zircon 91500 as an external standard. The standard glass NIST610 was used to optimize the analytical instruments. Data reduction, isotope ratios and apparent age calculations for results obtained by LA-ICP-MS were carried out with the GLITTER 4.0 program (Macquarie University), while common Pb was corrected using the method by Anderson (2002), and U-Pb ages were calculated using the Isoplot program (Ludwig, 2003).

In-situ zircon Hf isotope analysis was carried out on a Nu Plasma HR MCICP-MS (Nu Instruments Ltd., UK) equipped with a GeoLas 2005 193 nm ArF-excimer laser-ablation system at the State Key Laboratory of Continental Dynamics in Northwest University, China. A spot size of 44 μm, a repetition rate of 10 Hz and a laser power of 100 mj $pulse^{-1}$ were used in this study. Zircon 91500, GJ-1and MON-1 were reanalyzed as the reference standard. The decay constant for ^{176}Lu (1.865×10^{-11} $year^{-1}$) proposed by Scherer et al., (2001) and the present-day chondritic ratios ($^{176}Hf/^{177}Hf$ = 0.282772 and $^{176}Lu/^{177}Hf$ = 0.0332) from Blichert-Toft and Albarède (1997) were adopted to calculate ε_{Hf} values. Single-stage model ages (T_{DM1}) were calculated relative to the depleted mantle with a present day $^{176}Hf/^{177}Hf$ ratio of 0.28325 and $^{176}Lu/^{177}Hf$ of 0.0384 (Vervoort and Blichert-Toft, 1999), while Two-stage Hf model ages (T_{DM2}) were calculated on the assumption that the parent magma was produced from average continental crust with $^{176}Lu/^{177}Hf$ = 0.015 (Griffin et al., 2000).

Sr-Nd-Pb isotopes

Dissolution of whole rock samples and the separation and purification of Rb, Sr, Sm and Nd were carried out in the ultraclean lab of the Key Laboratory of Orogenic Belts and Crustal Evolution, Peking University. Isotopic compositions were analyzed using Triton thermal ionization mass spectrometry (TIMS) at Tianjin Institute of Geology and Mineral Resources. The $^{87}Rb/^{86}Sr$ and $^{147}Sm/^{144}Nd$ ratios were calculated with the concentrations of Rb, Sr, Sm and Nd measured by ICP-MS. The mass fractionation was corrected by normalizing the measured $^{87}Sr/^{86}Sr$ and $^{143}Nd/^{144}Nd$ ratios against $^{86}Sr/^{88}Sr$ ratio of 0.1194 and $^{146}Nd/^{144}Nd$ ratio of 0.7219, respectively. The repeated analyses of the NBS-987 Sr standard and the Shin Etsu JNdi-1 Nd standard respectively yielded $^{87}Sr/^{86}Sr$ = 0.71025 and $^{143}Nd/^{144}Nd$ = 0.512115. The USGS reference material BCR-2 was analyzed to monitor the precision of the analytical procedures, which yielded $^{87}Sr/^{86}Sr$ = 0.705042 ± 8 (2σ) and $^{143}Nd/^{144}Nd$ = 0.512628 ± 2 (2σ).

Lead isotope measurements were performed on a Finnigan MAT-262 thermal ionization mass spectrometer (TIMS) at the Institute of Geology and Geophysics, Chinese Academy of Science in Beijing. About 150 mg for each sample were weighed into 248 Teflon capsules and dissolved in distilled HF+HNO_3 at 150 °C for seven days and then separated and purified using anion-exchange columns with diluted HBr as eluant. Procedural blanks were <0.2 ng for Pb. Lead was loaded with a mixture of Si-gel and H_3PO_4 onto a single-Re filament and analyzed at 1300 °C. Measured Pb isotopic ratios were corrected for instrumental mass fractionation of 0.11% per atomic mass unit by references to repeated analysis of NBS-981 Pb standard.

References

Anderson, T., 2002. Correlation of common lead in U-Pb analyses that do not report ^{204}Pb. Chemical Geology 192, 59–79.

Blichert-Toft, J., Albarède, F., 1997. The Lu-Hf isotope geochemistry of chondrites and the evolution of the mantle-crust system. Earth and Planetary Science Letters 148, 243–258.

Griffin, W.L., Pearson, N.J., Belousova, E., Jackson, S.E., van Achterbergh, E., O'Reilly, S.Y., Shee, S.R., 2000. The Hf isotope composition of cratonic mantle: LAM-MC-ICPMS analysis of zircon megacrysts in kimberlites. Geochimica et Cosmochimica Acta 64:133–147.

Ludwig, K.R., 2003. User’s Manual for Isoplot 3.0, A geochronological toolkit for Microsoft Excel. Berkeley Geochronology Center Special Publications 4, 1–70.

Scherer, E., Munker, C., Mezger, K., 2001. Calibration of the lutetium-hafnium clock. Science 293, 683–687.

Vervoort, J.D., Blichert-Toft, J., 1999. Evolution of the depleted mantle: Hf isotope evidence from juvenile rocks through time. Geochimica et Cosmochimica Acta 63, 533–556.

Yuan, H.L., Gao, S., Liu, X.M., Li, H.M., Günther, D., Wu, F.Y., 2004. Accurate U-Pb age and trace element determinations of zircon by laser ablation inductively coupled plasma mass spectrometry. Geostandards and Geoanalytical Research 28, 353–370.

Appendix 3-2. Zircon U-Pb and in-situ Hf data for the monzogranite samples from Yangchang (YC32) and Shabutai (SB0).

Spot no.	Pb (ppm)	^{238}U (ppm)	^{232}Th (ppm)	$^{232}Th/^{238}U$	$^{207}Pb/^{206}Pb$	1σ	$^{207}Pb/^{235}U$	1σ	$^{206}Pb/^{238}U$	1σ	$^{206}Pb/^{238}U$ ages (Ma)	1σ	$^{176}Yb/^{177}Hf$	$^{176}Lu/^{177}Hf$	$^{176}Hf/^{177}Hf$	$^{176}Hf/^{177}Hf$ (corrected)	$2\sigma_m$	$\varepsilon_{Hf}(0)$	$\varepsilon_{Hf}(t)$	T_{DM1}(Ma)	T_{DM2}(Ma)	$f_{Lu/Hf}$
Shabutai																						
SB001	82.6	739.1	474.6	0.64	0.04836	0.00119	0.14394	0.00347	0.02159	0.00044	138	3	0.018650	0.000744	0.282854	0.282859	5	3.1	6.1	553	804	-0.98
SB002	91.0	844.9	327.2	0.39	0.04928	0.00120	0.14779	0.00354	0.02176	0.00044	139	3	0.035080	0.001336	0.282900	0.282905	8	4.7	7.6	497	704	-0.96
SB003	127.9	1218.1	415.3	0.34	0.04853	0.00111	0.14288	0.00323	0.02136	0.00043	136	3	0.021108	0.000847	0.282845	0.282850	9	2.8	5.8	568	825	-0.97
SB004	54.3	433.2	167.5	0.39	0.04844	0.00125	0.14557	0.00369	0.02180	0.00045	139	3	0.028990	0.001090	0.282882	0.282888	8	4.1	7.1	517	741	-0.97
SB005	104.5	910.4	272.6	0.30	0.04782	0.00116	0.14349	0.00343	0.02177	0.00044	139	3	0.018095	0.000707	0.282875	0.282881	7	3.9	6.9	521	753	-0.98
SB006	185.5	1759.6	600.7	0.34	0.04861	0.00108	0.14587	0.00321	0.02177	0.00044	139	3	0.032325	0.001215	0.282916	0.282921	9	5.3	8.2	471	666	-0.96
SB008	50.4	463.4	188.9	0.41	0.04947	0.00131	0.14650	0.00381	0.02148	0.00044	137	3	0.029436	0.001141	0.282917	0.282923	10	5.3	8.3	469	662	-0.97
SB011	173.3	1495.5	1648.6	1.10	0.04827	0.00108	0.14503	0.00320	0.02180	0.00044	139	3	0.019515	0.000760	0.282848	0.282853	8	2.9	5.9	562	818	-0.98
SB012	36.7	301.1	154.9	0.51	0.04881	0.00143	0.14593	0.00418	0.02169	0.00045	138	3	0.033799	0.001279	0.282830	0.282836	9	2.3	5.2	594	859	-0.96
SB013	82.6	708.5	307.7	0.43	0.04818	0.00121	0.14561	0.00361	0.02192	0.00045	140	3	0.024936	0.000961	0.282838	0.282844	9	2.6	5.5	577	838	-0.97
SB014	193.0	1697.2	1091.8	0.64	0.04825	0.00115	0.14394	0.00337	0.02164	0.00044	138	3	0.036226	0.001348	0.282853	0.282859	8	2.0	5.0	601	872	-0.97
SB016	231.2	1972.2	1976.1	1.00	0.04808	0.00111	0.14527	0.00332	0.02192	0.00044	140	3	0.043742	0.001639	0.282914	0.282919	8	5.2	8.1	480	673	-0.95
SB017	31.1	255.4	112.1	0.44	0.04880	0.00197	0.14600	0.00576	0.02171	0.00048	138	3	0.031423	0.001229	0.282880	0.282886	7	4.0	7.0	522	746	-0.96
SB018	71.3	641.2	339.6	0.53	0.04797	0.00126	0.14402	0.00371	0.02178	0.00045	139	3	0.020683	0.000907	0.282938	0.282943	8	6.0	9.0	437	616	-0.97
SB019	318.6	2823.3	2241.1	0.79	0.04804	0.00108	0.14290	0.00317	0.02158	0.00044	138	3	0.025790	0.000985	0.282847	0.282852	8	2.8	5.8	567	822	-0.97
SB020	51.7	467.4	212.1	0.45	0.04839	0.00132	0.14335	0.00384	0.02149	0.00044	137	3	0.044700	0.001679	0.282862	0.282867	7	3.4	6.3	556	792	-0.95
Yangchang																						
YC32-01	24.6	212.2	95.1	0.45	0.04866	0.00150	0.14734	0.00442	0.02197	0.00045	140	3	0.023877	0.001020	0.282816	0.282821	7	1.7	4.7	611	892	-0.97
YC32-02	31.0	242.7	155.4	0.64	0.04936	0.00184	0.14863	0.00543	0.02185	0.00046	139	3	0.032463	0.001420	0.282822	0.282827	7	1.9	4.9	609	881	-0.96
YC32-03	64.4	536.1	349.4	0.65	0.04957	0.00166	0.14826	0.00486	0.02170	0.00045	138	3	0.031713	0.001350	0.282851	0.282857	8	3.0	5.9	565	812	-0.96
YC32-04	63.4	546.9	531.0	0.97	0.04932	0.00149	0.14789	0.00433	0.02176	0.00045	139	3	0.030432	0.001316	0.282832	0.282838	7	2.3	5.3	591	855	-0.96
YC32-05	46.5	416.3	207.9	0.50	0.04926	0.00127	0.14848	0.00375	0.02187	0.00044	139	3	0.040564	0.001734	0.282800	0.282806	8	1.2	4.1	645	930	-0.95
YC32-06	18.8	104.1	105.1	1.01	0.04944	0.00399	0.14748	0.01180	0.02164	0.00048	138	3	0.028820	0.001235	0.282821	0.282826	10	1.9	4.8	608	883	-0.96
YC32-08	34.3	290.7	229.6	0.79	0.04962	0.00144	0.14911	0.00423	0.02180	0.00044	139	3	0.030158	0.001297	0.282848	0.282854	9	2.9	5.8	569	819	-0.96
YC32-10	40.7	343.3	278.6	0.81	0.04915	0.00155	0.14577	0.00449	0.02152	0.00044	137	3	0.027879	0.001199	0.282829	0.282834	8	2.2	5.1	596	864	-0.96
YC32-11	60.2	518.1	474.0	0.91	0.04931	0.00125	0.14851	0.00368	0.02185	0.00044	139	3	0.041477	0.001724	0.282882	0.282887	9	4.1	7.0	527	747	-0.95
YC32-12	50.3	437.8	301.3	0.69	0.04699	0.00283	0.13822	0.00780	0.02133	0.00045	136	3	0.066807	0.002820	0.282857	0.282862	9	3.2	6.0	580	809	-0.92
YC32-14	53.4	409.8	226.0	0.55	0.05073	0.00202	0.15153	0.00592	0.02167	0.00045	138	3	0.032023	0.001324	0.282765	0.282770	9	-0.1	2.8	690	1010	-0.96
YC32-16	60.6	548.5	421.2	0.77	0.04843	0.00126	0.14110	0.00359	0.02114	0.00043	135	3	0.037979	0.001607	0.282819	0.282824	8	1.8	4.7	616	888	-0.95
YC32-17	78.0	693.6	837.8	1.21	0.04984	0.00131	0.14230	0.00364	0.02072	0.00042	132	3	0.041288	0.001775	0.282846	0.282852	9	2.8	5.7	579	827	-0.95
YC32-18	36.0	315.2	204.3	0.65	0.04986	0.00146	0.14922	0.00427	0.02171	0.00045	138	3	0.033468	0.001408	0.282823	0.282828	9	2.0	4.9	607	878	-0.96
YC32-19	39.8	267.9	197.2	0.74	0.04985	0.00207	0.14919	0.00611	0.02171	0.00045	138	3	0.055547	0.002346	0.282884	0.282889	9	4.1	7.0	534	746	-0.93
YC32-20	40.9	367.8	262.9	0.71	0.04987	0.00141	0.14395	0.00396	0.02094	0.00043	134	3	0.037460	0.001577	0.282854	0.282860	8	3.1	6.0	564	808	-0.95

Appendix 3-3. A summary of Sr-Nd-Pb isotopic data for the Mo deposits in the northern Xilamulun district.

Deposit	Sample no.	$^{87}Rb/^{86}Sr$	$^{87}Sr/^{86}Sr$	$(^{87}Sr/^{86}Sr)_i$	$^{147}Sm/^{144}Nd$	$^{143}Nd/^{144}Nd$	$\varepsilon_{Nd}(t)$	$f_{Sm/Nd}$	T_{DM}(Ma)	$^{206}Pb/^{204}Pb$	$^{207}Pb/^{204}Pb$	$^{208}Pb/^{204}Pb$	$(^{206}Pb/^{204}Pb)_i$	$(^{207}Pb/^{204}Pb)_i$	$(^{208}Pb/^{204}Pb)_i$
Aolunhua	H-31	0.750	0.706443	0.7050	0.1036	0.512631	1.4	-0.47	808	N.d.	N.d.	N.d.	N.d.	N.d.	N.d.
Aolunhua	H-32	0.529	0.706018	0.7050	0.1118	0.512612	0.9	-0.43	849	N.d.	N.d.	N.d.	N.d.	N.d.	N.d.
Aolunhua	H-54	0.647	0.706092	0.7049	0.1094	0.512628	1.3	-0.44	820	N.d.	N.d.	N.d.	N.d.	N.d.	N.d.
Aolunhua	H-56	0.907	0.706645	0.7049	0.1312	0.512605	0.5	-0.33	886	N.d.	N.d.	N.d.	N.d.	N.d.	N.d.
Aolunhua	H-63	0.430	0.705964	0.7052	0.1099	0.512613	1.0	-0.44	845	N.d.	N.d.	N.d.	N.d.	N.d.	N.d.
Haisugou	HSG01	1.010	0.706016	0.7040	0.1272	0.512657	1.6	-0.35	799	19.084	15.588	38.759	18.030	15.537	37.953
Haisugou	HSG02	0.996	0.706894	0.7049	0.1281	0.512633	1.1	-0.35	838	19.014	15.568	38.603	18.155	15.527	38.035
Haisugou	HSG03	1.078	0.707063	0.7050	0.1199	0.512609	0.8	-0.39	865	19.099	15.589	38.834	18.279	15.549	38.073
Haisugou	HSG09	0.939	0.707892	0.7061	0.1362	0.512623	0.8	-0.31	865	N.d.	N.d.	N.d.	N.d.	N.d.	N.d.
Haisugou	HSG41	1.106	0.708776	0.7066	0.1320	0.512609	0.6	-0.33	882	19.097	15.583	38.671	18.560	15.557	38.172
Haisugou	HSG42	1.007	0.707284	0.7053	0.1264	0.512625	1.0	-0.36	849	18.975	15.521	38.474	18.187	15.483	37.716
Haisugou	HSG43	1.029	0.709450	0.7074	0.1237	0.512583	0.2	-0.37	911	19.115	15.575	38.638	18.461	15.543	38.066
Haisugou	HSG44	0.969	0.707230	0.7053	0.1354	0.512655	1.4	-0.31	813	N.d.	N.d.	N.d.	N.d.	N.d.	N.d.
Haisugou	HSG45	1.300	0.707041	0.7045	0.1287	0.512619	0.8	-0.35	861	N.d.	N.d.	N.d.	N.d.	N.d.	N.d.
Haisugou	HSG46	2.422	0.712098	0.7074	0.1268	0.512595	0.4	-0.36	897	N.d.	N.d.	N.d.	N.d.	N.d.	N.d.
Haisugou	HSG47	1.083	0.709454	0.7073	0.1309	0.512593	0.3	-0.33	906	N.d.	N.d.	N.d.	N.d.	N.d.	N.d.
Haisugou	HSG48	1.624	0.707249	0.7041	0.1187	0.512607	0.8	-0.40	866	N.d.	N.d.	N.d.	N.d.	N.d.	N.d.
Shabutai	SB03	1.110	0.707955	0.7057	0.1545	0.512610	-3.0	-0.21	912	19.013	15.578	38.613	18.542	15.555	38.244
Shabutai	SB04	1.567	0.708898	0.7058	0.1525	0.512609	-3.0	-0.22	911	19.142	15.586	38.670	18.511	15.555	38.123
Shabutai	SB11	1.291	0.707977	0.7054	0.1455	0.512596	-3.0	-0.26	922	N.d.	N.d.	N.d.	N.d.	N.d.	N.d.
Shabutai	SB12	2.472	0.710049	0.7051	0.1330	0.512592	-2.5	-0.32	910	19.105	15.579	38.720	18.314	15.541	38.022
Shabutai	SB14	1.909	0.708919	0.7051	0.1231	0.512580	-2.4	-0.37	915	19.091	15.578	38.671	18.512	15.550	38.275
Shabutai	SB15	1.123	0.707680	0.7054	0.1442	0.512611	-2.6	-0.27	896	N.d.	N.d.	N.d.	N.d.	N.d.	N.d.
Shabutai	SB16	1.251	0.707665	0.7052	0.1420	0.512597	-2.8	-0.28	915	N.d.	N.d.	N.d.	N.d.	N.d.	N.d.
Shabutai	SB17	1.028	0.707577	0.7055	0.1442	0.512597	-2.9	-0.27	918	18.942	15.541	38.602	18.071	15.499	37.821
Yangchang	1-16	0.799	0.707109	0.7055	0.0982	0.512459	-1.8	-0.50	914	18.833	15.561	38.826	18.410	15.541	37.945
Yangchang	2-31	0.921	0.707281	0.7055	0.1007	0.512476	-1.5	-0.49	911	N.d.	N.d.	N.d.	N.d.	N.d.	N.d.
Yangchang	2-32	0.956	0.706443	0.7046	0.1007	0.512461	-1.8	-0.49	931	18.805	15.540	38.817	18.411	15.521	37.842
Yangchang	3-3	0.737	0.706914	0.7055	0.1010	0.512453	-1.9	-0.49	944	18.983	15.566	39.212	18.375	15.537	37.790

Yangchang	3-4	0.914	0.707331	0.7055	0.0964	0.512457	-1.8	-0.51	903	18.783	15.540	38.951	18.376	15.520	37.929
Yangchang	3-5	0.877	0.707174	0.7055	0.0999	0.512457	-1.8	-0.49	931	18.727	15.555	38.844	18.359	15.537	37.982
Yangchang	4-23	0.761	0.707000	0.7055	0.0998	0.512447	-2.0	-0.49	942	18.788	15.585	38.898	18.256	15.559	38.066
Yangchang	5-8	0.949	0.707378	0.7055	0.0990	0.512454	-1.9	-0.50	927	18.824	15.550	38.821	18.234	15.522	38.025
Yangchang	6-7	0.659	0.706916	0.7056	0.1021	0.512452	-2.0	-0.48	955	18.749	15.536	38.658	18.150	15.507	37.983
Yangchang	8-7	0.505	0.706546	0.7056	0.1006	0.512460	-1.8	-0.49	932	18.777	15.572	38.822	18.269	15.548	38.065
Yangchang	SD-1	8.774	0.720093	0.7043	0.0951	0.512364	-3.7	-0.52	1012	18.709	15.598	38.537	18.437	15.585	38.126
Yangchang	SD-2	N.d.	N.d.	N.d.	N.d.	N.d.	N.d.	N.d.	N.d.	18.593	15.548	38.493	18.237	15.531	37.907
Yangchang	SX-1	N.d.	N.d.	N.d.	N.d.	N.d.	N.d.	N.d.	N.d.	18.558	15.531	38.438	18.158	15.512	37.830
Yangchang	SX-2	N.d.	N.d.	N.d.	N.d.	N.d.	N.d.	N.d.	N.d.	18.479	15.531	38.456	18.190	15.517	37.940
Huanggang	HG-1-7	30.53	0.761554	0.7021	0.1089	0.512520	-0.8	-0.45	993	19.239	15.583	39.316	18.669	15.556	38.194
Huanggang	HG-1-21	22.89	0.748748	0.7042	0.0842	0.512538	0.0	-0.57	929	18.974	15.554	38.925	18.307	15.522	37.998
Huanggang	HG-1-10	N.d.	N.d.	N.d.	N.d.	N.d.	N.d.	N.d.	N.d.	19.599	15.593	38.894	18.879	15.558	37.873
Huanggang	HG-4-1	66.82	0.833072	0.7039	0.1980	0.512634	-0.1	0.01	939	N.d.	N.d.	N.d.	N.d.	N.d.	N.d.
Huanggang	HG-3-20	35.60	0.776607	0.7073	0.1201	0.512617	0.9	-0.39	855	19.171	15.569	38.944	18.863	15.554	37.956

Note: N.d. = no data. The Sr-Nd-Pb isotopes for Shabutai, and Pb isotopes for Haisugou are from this study. Other data for Yangchang, Huanggang, Aolunhua and Haisugou are respectively from Zeng et al. (2014), Zhou et al. (2012), Ma et al. (2013) and Shu et al. (2014). Parameters employed to calculation are the same as in Shu et al. (2014).

References

Ma, X., Chen, B., Yang, M., 2013. Magma mixing origin for the Aolunhua porphyry related to Mo-Cu mineralization, eastern Central Asian Orogenic Belt. Gondwana Research 24, 1152–1171.

Shu, Q., Lai, Y., Wang, C., Xu, J., Sun, Y., 2014. Geochronology, geochemistry and Sr-Nd-Hf isotopes of the Haisugou porphyry Mo deposit, northeast China, and their geological significance. Journal of Asian Earth Sciences 79, 777–791.

Zeng, Q., Yang, J., Zhang, Z., Liu, J., Duan, X., 2014. Petrogenesis of the Yangchang Mo-bearing granite in the Xilamulun metallogenic belt, NE China: geochemistry, zircon U-Pb ages and Sr-Nd-Pb isotopes. Geological Journal 49, 1–14.

Zhou, Z.H., Mao, J.W., Lyckberg, P., 2012. Geochronology and isotopic geochemistry of the A-type granites from the Huanggang Sn-Fe deposit, southern Great Hinggan Range, NE China: Implication for their origin and tectonic setting. Journal of Asian Earth Sciences 49, 272–286.

Appendix 4-1. Basic characteristics of the Mesozoic Mo-bearing deposits in NE China.

No.	Deposit	Geographic Location	Deposit type and metal assemblage	Host rocks and ages (Ma)	Molybdenite Re-Os age (Ma)	Mo tonnage and grade	References
250-220 Ma							
1	Chehugou	42°25'N, 118°31'E	Porphyry Cu-Mo	Granitic porphyry (U-Pb, 251.6 ± 3.2)	250.2 ± 7.2	120 Kt Mo @ 0.1%	Liu et al., 2010; Zeng et al., 2012
2	Yuanbaoshan	42°24'N, 118°47'E	Porphyry Mo	Quartz monzonite (U-Pb, 269 ± 3)	248.0 ± 2.7	*N.d.*	Liu et al., 2010; Zeng et al., 2012
3	Kulitu	42°25'N, 119°50'E	Porphyry Mo-Cu	Monzogranite (U-Pb, 249.1 ± 1.6)	245.1 ± 1.3	7.4 Kt Mo @ 0.05%	Zhang et al., 2009a; Zeng et al., 2012
4	Baituyingzi	42°23'N, 119°48'E	Porphyry Mo-Cu	Monzogranite porphyry	248.0 ± 10	Mo @ 0.08-0.18%	Sun et al., 2013
5	Baimashi	42°27'N, 119°45'E	Porphyry Cu-Mo	Porphyritic granite (U-Pb, 249.4 ± 2.2)	248.6 ± 6.7	22 Kt Mo @ 0.08%	Zeng et al., 2012; Sun et al., 2013
6	Dasuji	40°44'N, 112°43'E	Porphyry Mo	Quartz porphyry and granite porphyry	222.5 ± 3.2	69 Kt Mo @ 0.133%	Zhang et al., 2009b
7	Sadaigoumen	41°16'N, 116°35'E	Porphyry Mo	Monzogranite (U-Pb, 227.1 ± 2.7)	236.5 ± 2.2	187 Kt Mo @ 0.076%	Duan et al., 2007; Jiang et al., 2014
8	Hekanzi	40°38'N, 119°12'E	Porphyry Mo-Cu	Biotite-orthoclase granite (U-Pb, 235.3 ± 1.0)	224.0 ± 1.3	*N.d.*	Liu et al., 2012
9	Laojiagou	43°46'N, 120°03'E	Porphyry Mo	Monzogranite porphyry (U-Pb, 238.6 ± 1.8)	234.9 ± 3.1	135 Kt Mo @ 0.07%	Zeng et al., 2012
10	Shamai	45°58'N, 116°56'E	Greisen type Mo-W	Biotite granite (U-Pb, 226 ± 1.5)	224.0 ± 6.2	50 Kt Mo @ 0.08%	Nie and Jiang, 2011
11	Bogda Uul	44°05'N, 114°28'E	Porphyry Mo-W	Granite porphyry (U-Pb, 235.2 ± 2.3)	232.5 ± 2.3	120 Kt Mo @ 0.09%	Nie and Jiang, 2011
12	Ulandler	44°50'N, 112°51'E	Porphyry Mo-Cu	K-feldspar granite (U-Pb, 241.0 ± 2.5)	239.6 ± 3.0	100 Kt Mo @ 0.1%	Nie and Jiang, 2011
200-180 Ma							
13	Taipingchuan	51°28'N, 120°27'E	Porphyry Cu-Mo	Granodiorite porphyry (U-Pb, 202.4 ± 5.8)	200.1 ± 2.5	12.8 Kt Mo @ 0.09%	Zhang et al., 2014
14	Yangjiazhangzi	40°48'N, 120°33'E	Skarn Mo	Porphyritic granite and granite porphyry	187.0 ± 2.0	262 Kt Mo @ 0.14%	Huang et al., 1996; Chen et al., 2012
15	Yangmadian	40°34'N, 119°45'E	Porphyry Mo	Granite (U-Pb, 189.3 ± 3.3)	*N.d.*	23.7 Kt Mo @ 0.12%	Feng et al., 2012
16	Lanjiagou	40°52'N, 120°37'E	Porphyry Mo	Porphyritic granite (K-Ar, 178-186)	181.6 ± 6.5	217 Kt Mo @ 0.13%	Han et al., 2009
17	Xintaimen	40°51'N, 120°25'E	Porphyry Mo	Granite porphyry (U-Pb, 181 ± 2)	183.0 ± 3.0	*N.d.*	Zhang et al., 2009c
18	Yaojiagou	40°45'N, 123°36'E	Skarn Mo	Granite (U-Pb, 184.5±1.6)	*N.d.*	*N.d.*	Yu et al., 2009
19	Sibozi-Liubozi	40°15'N, 118°44'E	Porphyry Mo-Cu	Wubazi granite porphyry (U-Pb, 189.8 ± 0.7)	187.8 ± 4.5	Mo @ 0.1%	Li et al., 2012
20	Dashihe	43°46'N, 127°51'E	Porphyry Mo	Granodiorite porphyry	186.7 ± 5.0	100 Kt Mo @ 0.07%	Ju et al., 2012
21	Liushengdian	43°01'N, 128°16'E	Porphyry Mo	Granodiorite porphyry	185.0 ± 12	22.1 Kt Mo @ 0.08%	Wang et al., 2011; Zeng et al., 2012
22	Dongfeng	42°57'N, 128°59'E	Skarn Pb-Zn-Mo	Quartz monzodiorite	194.6 ± 3.9	28.5 Kt Mo @ 0.08%	Zeng et al., 2012; Zhang et al., 2013a
23	Sanchazi	43°05'N, 128°26'E	Porphyry Mo	Granodiorite porphyry (K-Ar, 195)	*N.d.*	325 Kt Mo @ 0.07%	Zeng et al., 2012; Zhang et al., 2013b
24	Jiapigou	43°21'N, 129°49'E	Porphyry Mo	Biotite monzogranite (U-Pb, 193.1 ± 1.0)	188.6 ± 4.7	Mo @ 0.095%	Wang et al., 2013
25	Dabinghugou	43°20'N, 127°18'E	Porphyry Mo	Granodiorite	192.0 ± 3.0	*N.d.*	Di et al., 2011
180-160 Ma							
26	Wunugetu	49°28'N, 117°20'E	Porphyry Cu-Mo	Monzogranite porphyry (Ar-Ar, 177.6 ± 4.5)	179.0 ± 1.9	450 Kt Mo @ 0.46%	Chen et al., 2011
27	Fu'anpu	44°24'N, 127°17'E	Porphyry Mo	Granite porphyry (Rb-Sr, 170)	166.9 ± 6.7	230 Kt Mo @ 0.13%	Li et al., 2009
28	Badaohezi	43°19'N, 126°31'E	Porphyry Mo	Granite porphyry (U-Pb, 177.4 ± 0.6)	178.3 ± 4.4	Mo @ 0.07-0.28%	Wang, 2012
29	Daheishan	43°29'N, 126°19'E	Porphyry Mo	Granodiorite porphyry (U-Pb, 170 ± 3)	168.0 ± 4.4	1090 Kt Mo @ 0.06%	Han et al., 2014
30	Xingshan	43°35'N, 126°16'E	Porphyry Mo	Granite (U-Pb, 170.9 ± 4.6)	167.3 ± 2.5	11 Kt Mo @ 0.12%	Zhou et al., 2013
31	Chang'anpu	44°28'N, 127°18'E	Porphyry Mo	Granodiorite (U-Pb, 166.9 ± 1.5)	*N.d.*	Mo @ 0.07-0.12%	Zhang et al., 2013b
32	Houdaomu	43°14'N, 125°40'E	Porphyry Mo	Plagiogranite, alkali granite, and granodiorite	167.5 ± 1.2	Mo @ 0.074%	Zhang et al., 2013b
33	Xinhualong	43°06'N, 126°38'E	Porphyry Mo	Granodiorite porphyry (U-Pb, 183.8 ± 1.1)	171.6 ± 1.6	28.5 Kt Mo @ 0.08%	Zeng et al., 2012; Zhang, 2013b
34	Cuiling	47°24'N, 128°38'E	Porphyry Mo	Monzogranite porphyry (U-Pb, 178.2 ± 0.7)	*N.d.*	Mo @ 0.07%	Yang et al., 2012
35	Luming	47°22'N, 128°34'E	Porphyry Mo	Granite porphyry (U-Pb, 187.1 ± 1.2)	177.4 ± 3.5	752 Kt Mo @ 0.09%	Tan et al., 2012; Zeng et al., 2012

36	Cuihongshan	48°29'N, 128°45'E	Skarn W-Mo-Zn	Granite porphyry (U-Pb, 172.3 ± 1.5)	*N.d.*	90 Kt Mo @ 0.134%	Liu, 2009; Hu et al., 2014
37	Huojihe	48°31'N, 128°56'E	Porphyry Mo	Monzogranite (U-Pb, 178 ± 2)	*N.d.*	100 Kt Mo @ 0.07%	Sun, 2010; Zeng et al., 2012
38	Jidetun	44°18'N, 127°07'E	Porphyry Mo	Granodiorite (U-Pb, 170.9 ± 0.8)	168.0 ± 2.5	430 Kt Mo @ 0.09%	Zeng et al., 2012; Zhang et al., 2013b
39	Xiaojiayingzi	41°32'N, 119°51'E	Skarn Mo-Fe	Diorite (U-Pb, 169.9 ± 1.4)	165.5 ± 4.6	105 Kt Mo @ 0.23%	Dai et al., 2009
160-140 Ma							
40	Shouwangfen	40°37'N, 117°50'E	Skarn Cu-Fe-Mo	Granodiorite	148.0 ± 4.0	2.1 Kt Mo @ 0.13%	Dai et al., 2006
41	Dazhuangke	40°25'N, 116°14'E	Porphyry Mo	Quartz monzonite (U-Pb, 269 ± 3)	146.4 ± 3.4	10.4 Kt Mo @ 0.08%	Huang et al., 1996; Dai et al., 2006
42	Dawan	39°20'N, 114°45'E	Porphyry-skarn Mo	Rhyolite porphyry	144.4 ± 7.4	250 Kt Mo @ 0.04%	Huang et al., 1996; Song et al., 2014
43	Dacaoping	41°01'N, 116°34'E	Porphyry Mo	Granodiorite (U-Pb, 140 ± 1.5)	140.1 ± 3.4	*N.d.*	Duan et al., 2007; Jiang et al., 2014
44	Mujicun	39°21'N, 114°51'E	Porphyry Cu-Mo	Porphyry diorite (U-Pb, 144.1 ± 1.2)	140.3 ± 3.9	10.4 Kt Mo @ 0.052%	Dong et al., 2013
45	Jiguanshan	42°25'N, 119°06'E	Porphyry Mo	Granite porphyry (U-Pb, 156.0 ± 1.3)	155.3 ± 0.9	100 Kt Mo @ 0.1%	Wu et al., 2011a, 2014; Zeng et al., 2012
46	Nianzigou	42°25'N, 118°40'E	Porphyry Mo	Monzonitic granite (U-Pb, 152.4 ± 1.6)	154.3 ± 3.6	15 Kt Mo @ 0.39%	Zeng et al., 2011
47	Houyu	39°09'N, 113°37'E	Porphyry Mo	Quartz porphyry	148.7	*N.d.*	Du et al., 2010
48	Chalukou	51°10'N, 123°51'E	Porphyry Mo	Granite porphyry (U-Pb, 149 ± 5)	148.0 ± 1.0	1780 Kt Mo @ 0.09%	Liu et al., 2014
140-130 Ma							
49	Yangchang	43°32'N, 119°05'E	Porphyry Mo-Cu	Monzogranite (U-Pb, 137.4 ± 2.1)	138.5 ± 4.5	Mo @ 0.07%	Zeng et al., 2010, 2014; Shu et al., 2015
50	Haisugou	44°18'N, 119°03'E	Porphyry Mo	Granodiorite and granite (U-Pb, 137.6 ± 0.9)	136.4 ± 0.8	*N.d.*	Shu et al., 2014, 2015; This study
51	Banlashan	44°03'N, 120°07'E	Porphyry Mo	Granodiorite porphyry (U-Pb, 133.5 ± 1.7)	136.1 ± 6.6	51 Kt Mo @ 0.03%	Yan, 2009; Zhang et al., 2010
52	Shabutai	44°20'N, 119°01'E	Porphyry Mo	Monzogranite (U-Pb, 138.4 ± 1.5)	135.3 ± 2.6	*N.d.*	Shu et al., 2015; This study
53	Huanggang	43°35'N, 117°29'E	Skarn Fe-Sn-Mo	Granite porphyry (U-Pb, 136.8 ± 0.57)	135.3 ± 0.9	*N.d.*	Zhou et al., 2012; This study
54	Aolunhua	44°32'N, 120°13'E	Porphyry Cu-Mo	Monzogranite porphyry (U-Pb, 131.9 ± 0.5)	129.4 ± 3.4	32 Kt Mo @ 0.05%	Wu et al., 2011b; Ma et al., 2013; This study
55	Gangzi	42°57'N, 117°53'E	Porphyry Mo	Porphyritic granite (U-Pb, 139.1 ± 2.3)	*N.d.*	Mo @ 0.01-0.06%	Zeng et al., 2011, 2012
56	Xiaodonggou	43°01'N, 117°44'E	Porphyry Mo	Porphyritic granite (U-Pb, 142.2 ± 2)	135.5 ± 1.5	32 Kt Mo @ 0.11%	Qin et al., 2008, 2009
57	Liutiaogou	43°01'N, 117°45'E	Volcanic hydrothermal vein Mo-U	Tuff (Rb-Sr, 137 ± 12)	*N.d.*	Mo @ 0.29%	Zhang et al., 2009a; Zeng et al., 2012
58	Hongshanzi	42°53'N, 117°24'E	Volcanic hydrothermal vein Mo-U	Rhyolite porphyry (U-Pb, 130 ± 8)	*N.d.*	4.5 Kt Mo @ 0.65%	Zhang et al., 2009a; Zeng et al., 2012
59	Caosiyao	40°49'N, 113°52'E	Porphyry Mo	Granite porphyry (U-Pb, 131-134)	130.4 ± 2.4	1328 Kt Mo @ 0.102%	Nie et al., 2013; Hao et al., 2014
60	Ulandler	44°50'N, 112°51'E	Porphyry Mo-Cu	Monzonitic granite (U-Pb, 131.4 ± 1.6)	134.1 ± 3.3	100 Kt Mo @ 0.1%	Tao et al., 2009; Nie and Jiang, 2011
61	Chamuhan	43°15'N, 116°47'E	Porphyry Mo	Biotite granite	139.3 ± 1.5	Mo @ 0.085%	Wang and He, 2013
62	Taipinggou	48°09'N, 123°20'E	Porphyry Mo	Granite porphyry (U-Pb, 131.5 ± 1.1)	129.4 ± 3.9	49.1 Kt Mo @ 0.07%	Wang et al., 2009; Zeng et al., 2012
63	Xinzhangfang	50°02'N, 121°40'E	Greisen type Mo	Xinzhangfang granite	134.0 ± 2.0	*N.d.*	She et al., 2009
64	Xing'a	50°43'N, 123°42'E	Porphyry Mo-Cu	Monzogranite porphyry (U-Pb, 131 ± 1)	*N.d.*	310 Kt Mo @ 0.106%	Zhang et al., 2013c
<130 Ma							
65	Nongping	42°55'N, 130°47'E	Porphyry Cu-Au-Mo	Granodiorite (U-Pb, 96.9 ± 1.4)	*N.d.*	*N.d.*	Han et al., 2013
66	Ermi	41°47'N, 125°50'E	Porphyry Cu-Au-Mo	Granite porphyry (U-Pb, 95.7 ± 0.3)	*N.d.*	*N.d.*	Han et al., 2013
67	Xiaosigou	40°57'N, 118°31'E	Porphyry Cu-Mo	Granite porphyry (K-Ar, 122.8 ± 2.5)	*N.d.*	59.8 Kt Mo @ 0.09%	Dai et al., 2010
68	Xiaoxinancha	43°13'N, 130°53'E	Porphyry Cu-Au-Mo	Granite (U-Pb, 102-112)	111.1 ± 3.1	*N.d.*	Ren et al., 2011
69	Kanchuangou	44°40'N, 130°13'E	Porphyry Mo-Cu	Granite porphyry (U-Pb, 111.8 ± 1.4)	*N.d.*	Mo @ 0.02-0.48%	Liu, 2010
70	Jinchanggou	44°52'N, 131°03'E	Porphyry Mo	Granodiorite (U-Pb, 114.0 ± 2.2)	*N.d.*	3.9 Kt Mo @ 0.061%	Kong, 2012
Total						>9.23 Mt Mo	

Note: The deposit no. are the same as in Fig. 4-1C. N.d. = not data.

References

Chen, Z., Zhang, L., Wan, B., Wu, H., Cleven, N., 2011. Geochronology and geochemistry of the Wunugetushan porphyry Cu-Mo deposit in NE china, and their geological significance. Ore Geology Reviews 43, 92–105.

Chen, Y.J., Zhang, C., Li, N., Yang, Y.F., Deng, K., 2012. Geology of the Mo deposits in northeast China. Journal of Jilin University (Earth Science Edition) 42, 1223–1268 (in English with Chinese abstract).

Dai, J., Mao, J., Yang, F., Ye, H., Zhao, C., Xie, G., Zhang, C., 2006. Geological characteristics and geodynamic background of molybdenum (copper) deposits along Yanshan-Liaoning metallogenic belt on the northern margin of North China block. Mineral Deposits 25, 598-612 (in Chinese with English abstract).

Dai, J.Z., Mao, J.W., Zhao, C.S., Xie, Q.Q., Yang, F.Q., Wang, Y.T., 2009. New U-Pb and Re-Os age data and the geodynamic setting of the Xiaojiayingzi Mo (Fe) deposit, western Liaoning province, Northeastern China. Ore Geology Reviews 35, 235–244.

Dai, X.L., Peng, S.L., Hu, X.Z., 2010. Adakite in Xiaosigou porphyry copper-molybdenum deposit, Hebei Province: age, geochemical characteristics and geological implications. Mineral Deposits 29, 517-528 (in Chinese with English abstract).

Di, X., Bi, X.G., Jia, H.M., Li, D., 2011. Qianjin rock body zircon U-Pb ages of Jiaohe region to the molybdenum mineralization of central part of Jilin province-Yanbian region. Jilin Geology 30, 25–28 (in Chinese with English abstract).

Dong, G., Santosh, M., Li, S., Shen, J., Mo, X., Scott, S., Qu, K., Wang, X., 2013. Mesozoic magmatism and metallogenesis associated with the destruction of the North China Craton: Evidence from U-Pb geochronology and stable isotope geochemistry of the Mujicun porphyry Cu-Mo deposit. Ore Geology Reviews 53, 434-445.

Du, B.F., Wei, J.H., Wang, Q., Li, Y.J., Liu, G.C., Yu, H.T., Liu, Y.L., 2010. Discussion on metallogenic setting and time difference between magmatism and mineralization of molybdenum deposits n east China. Mineral Deposits 29, 935-955 (in Chinese with English abstract).

Duan, H., Qin, Z., Lin, X., Zhang, B., Liu, X., Zhang, X., Guo, P., Han, F., Qin, L., Dai, J., 2007. Zircon U-Pb ages of intrusive bodies in Dacaoping molybdenum ore district, Fengning County, Hebei Province. Mineral Deposits 26, 634–642 (in Chinese with English abstract).

Feng, H., Wu, C. Z., Zheng, Y., Gu, L., Jiang, S. Y., Sun, H. T., Gao, L., 2012. Geochronology, Geochemistry and Petrogenic & Metallogenic Settings of the Yangmadian Porphyry Molybdenum Deposit in the Yanshan-Liaoning Metallogenic Belt, North China. Journal of Jilin University (Earth Science Edition) 42, 1711–1729 (in Chinese with English abstract).

Han, C.M., Xiao, W.J., Zhao, G.C., Sun, M., Qu, W.J., Du, A.D., 2009. A Re-Os study of molybdenites from the Lanjiagou Mo deposit of North China Craton and its geological significance. Gondwana Research 16, 264–271.

Han, S.J., Sun, J.G., Bai, L.A., Xing, S.W., Chai, P., Zhang, Y., Yang, F., Meng, L.J., Li, Y.X., 2013. Geology and ages of porphyry and medium-to high-sulphidation epithermal gold deposits of the continental margin of Northeast China. International Geology Review 55, 287–310.

Han, C., Xiao, W., Windley, B. F., Zhao, G., Su, B., Ao, S., Zhang, J., Zhang, Z., Wan, B., Cui, B., Qu, W., Du, A., 2014. Re-Os Age of Molybdenite from the Daheishan Mo Deposit in the Eastern Central Asian Orogenic Belt, NE China. Resource Geology 64, 379-386.

Hao, Z., Fei, H., Liu, L., Hao, Q., Turner, S., 2014. World's Third–Largest Molybdenum Deposit Discovered in Caosiyao Area, Xinghe County, Inner Mongolia. Acta Geologica Sinica (English Edition) 88, 1615-1616.

Hou, W.R., 2011. Contrast study on the Houdamengou gold deposit and Jinchanggouliang gold deposit, Inner Mongolia. Unpublished Ph. D. dissertation, Beijing, Chinese Academy of Geological Sciences, 213 p. (in Chinese with English abstract).

Hu, X.L., Ding, Z.J., He, M.C., Yao, S.Z., Zhu, B.P., Shen, J., Chen, B., 2014. Two epochs of magmatism and metallogeny in the Cuihongshan Fe-polymetallic deposit, Heilongjiang Province, NE China: Constrains from U–Pb and Re–Os geochronology and Lu–Hf isotopes. Journal of Geochemical Exploration 143, 116–126.

Huang, D.H., Du, A.D., Wu, C.Y., Liu, L.S., Sun, Y.L., Zou, X.Q., 1996. Geochronology of molybdenum (copper) deposits in the north China platform: Re-Os age of molybdenite and its geological significance. Mineral Deposits 15, 289–297 (in Chinese with English abstract).

Jiang, S.H., Liang, Q.L., Bagas, L., 2014. Re-Os ages for molybdenum mineralization in the Fengning region of northern Hebei Province, China: New constraints on the timing of mineralization and geodynamic setting. Journal of Asian Earth Sciences 79, 873–883.

Ju, N., Ren, Y.S., Wang, C., Wang, H., Zhao, H.L., Qu, W.J., 2012. Ore genesis and molybdenite Re-Os dating of Dashihe molybdenum deposit in Dunhua, Jilin. Global Geology 31, 68–76 (in Chinese with English abstract).

Kong, S., 2012. Analysis on the metallogenic geological, geochemical characteristics and metallogenic conditions of the Jinchanggou molybdenum deposit in Jidong County, Heilongjiang province. unpublished Master dissertation, Changchun, Jilin University, 61 p. (in Chinese with English abstract).

Li, L.X., Song, Q.H., Wang, D.H., Wang, C.H., Qu, W.J., Wang, Z.G., Bi, S.Y., Yu, C., 2009. Re-Os isotopic dating of molybdenite from the Fuanpu molybdenum deposit of Jilin Province and discussion on its metallogenesis. Rock and Mineral Analysis 28, 283–287 (in Chinese with English abstract).

Li, Q., Meng, X.Y., Wu, F., Yang, F.Q., Liu, F., Zhang, Z.X., 2012. LA-ICP-MS zircon U-Pb dating of intrusive rocks and its metallogenic significance in Sibozi-Liubozi molybdenum-copper deposit of Qinglong County, Hebei Province. Mineral Deposits 31, 255–270 (in Chinese with English abstract).

Liu, Z.H., 2009. Geological characteristics and origin of deposit in Cuihongshan W, Mo, Zn polymetalic deposit. unpublished Master dissertation, Changchun, Jilin University, 84 p. (in Chinese with English abstract).

Liu, J.M., Zhao, Y., Sun, Y.L., Li, D.P., Liu, J., Chen, B.L., Zhang, S.H., Sun, W.D., 2010. Recognition of the latest Permian to Early Triassic Cu-Mo mineralization on the northern margin of the North China block and its geological significance. Gondwana Research 17, 125–134.

Liu, L., 2010. Ore-forming geological conditions and prospecting of Kanchuangou Mo-Cu deposit in Muling area, Heilongjiang. unpublished Master dissertation, Changchun, Jilin University, 56 p. (in Chinese with English abstract).

Liu, Y., Nie, F.J., Fang, J.Q., 2012. Isotopic age dating of the alkaline intrusive complex and its related molybdenum polymetallic deposit at Hekanzi, western Liaoning Province. Mineral Deposits 31, 1326–1336 (in Chinese with English abstract).

Liu, J., Mao, J., Wu, G., Wang, F., Luo, D., Hu, Y., 2014. Zircon U-Pb and molybdenite Re-Os dating of the Chalukou porphyry Mo deposit in the northern Great Xing’an Range, China and its geological significance. Journal of Asian Earth Sciences 79, 696–709.

Ma, X., Chen, B., Yang, M., 2013. Magma mixing origin for the Aolunhua porphyry related to Mo–Cu mineralization, eastern Central Asian Orogenic Belt. Gondwana Research 24, 1152–1171.

Nie, F. J., Jiang, S. H., 2011. Geological Setting and Origin of Mo–W–Cu Deposits in the Honggor–Shamai District, Inner Mongolia, North China. Resource geology 61, 344–355.

Nie, F. J., Li, X. Z., Li, C., Zhao, Y. A., Li, Y. F, 2013. Re-Os isotopic age dating of the molybdenite separated from the Caosiyao giant molybdenum deposit, Xinghe County, Inner Mongolia, and its geological significance. Geological Review 59, 175–181 (in English with Chinese abstract).

Qin, F., Liu, J.M., Zeng, Q.D., Zhang, R.B., 2008. The metallogenic epoch and source of ore-forming materials of the Xiaodonggou porphyry molybdenum deposit, Inner Mongolia. Geoscience 22, 173–180 (in Chinese with English abstract).

Qin, F., Liu, J.M., Zeng, Q., Luo, Z., 2009. Petrogenetic and metallogenic mechanism of the Xiaodonggou porphyry molybdenum deposit in Hexigten Banner, Inner Mongolia. Acta Petrologica Sinica 25, 3357–3368 (in Chinese with English abstract).

Ren, Y.S., Wang, H., Qu, W.J., Zhao, H.L., Chu, G.Q., 2011. Re-Os isotopic dating of molybdenite from Xiaoxi’nancha copper-gold deposit in the Yanbian area and its geological significance. Earth Science–Journal of China University of Geosciences 36, 721–728 (in Chinese with English abstract).

She, H., Li, H., Li, J., Zhao, S., Tan, G., Zhang, D., Jin, J., Dong, Y., Feng, C., 2009. The metallogenetical characteristics and prospecting direction of the copper-lead-zinc polymetal deposits in the northern-central Daxing’anling Mountain, Inner Mongolia. Acta Geologica Sinica 83, 1456–1473 (in Chinese with English abstract).

Shu, Q., Lai, Y., Wang, C., Xu, J., Sun, Y., 2014. Geochronology, geochemistry and Sr–Nd–Hf isotopes of the Haisugou porphyry Mo deposit, northeast China, and their geological significance. Journal of Asian Earth Sciences 79, 777–791.

Shu, Q., Lai, Y., Zhou, Y., Xu, J., Wu, H., 2015. Zircon U-Pb geochronology and Sr-Nd-Pb-Hf isotopic constraints on the timing and origin of Mesozoic granitoids hosting the Mo deposits in northern Xilamulun district, NE China. Lithos http://dx. doi:10.1016/j.lithos.2015.09.014.

Song, Y., Wang, R. J., Nie, F. J., HU JZ, S. C., Zhang, S., 2011. The discovery of the Indosinian metallogenesis in the Jinchangyu gold deposit and its geological significance. Acta Geoscientica Sinica 32, 125–128 (in Chinese with English abstract).

Song, Y., Ding, H. Y., Qu, X. M., Wang, R. J., Zhou, W., Wang, S. Z., 2014. Re–Os and U–Pb Geochronology of the Dawan Mo–Zn–Fe Deposit in Northern Taihang Mountains, China. Resource Geology 64, 117–135.

Sun, Z.J., 2010. The mineralization and geochemical features of Stone Forest Park Mo (W) in Xiaoxing’anling. unpublished Master dissertation, Changchun, Jilin University, 66 p. (in Chinese with English abstract).

Sun, Y., Liu, J.M., Zeng, Q.D., Chu, X.S., Zhou, L.L., Wu, G.B., Gao, Y.Y., Shen, W.J., 2013. Geological characteristics and molybdenite Re-Os ages of the Baituyingzi Mo-Cu field, eastern Inner Mongolia and their geological implications. Acta Petrologica Sinica 29, 241–254.

Tao, J.X., Wang, T., Chen, Z.H., Luo, Z.Z., Xu, L.Q., Hao, X.Y., Cui, L.W., 2009. The Re-Os isotopic dating of molybdenite from the Wulandele molybdenum-copper polymetallic deposit in Sonid Zuoqi of Inner Mongolia and its geological significance. Rock and Mineral Analysis 28, 249–253 (in Chinese with English abstract).

Tan, H.Y., Shu, G.L., Lue, J.C., Han, R.P., Zhang, S., Kou, L.L., 2012. LA-ICP-MS zircon U-Pb and molybdenite Re-Os dating for the Luming large-scale molybdenum deposit in Xiao Hinggan Mountains and its geological implication. Journal of Jilin University (Earth Science Edition) 42, 1757–1770 (in Chinese with English abstract).

Wang, S.W., Wang, J.G., Zhang, D., Qi, X.J., Wu, G.G., Zhao, P.Z., Yang, Z,F., Liu, Y.B., 2009. Geochronological study on Taipinggou molybdenum deposit in Da Hinggan Mountain. Acta Petrologica Sinica 25, 2913–2923 (in Chinese with English abstract).

Wang, H., Ren, Y.S., Zhao, H.L., Ju, N., Qu, W.J., 2011. Re-Os dating of molybdenite from the Liushengdian molybdenum deposit in Antu area of Jilin Province and its geological significance. Acta Geoscientica Sinica 32, 707-715 (in Chinese with English abstract).

Wang, Z.G., 2012. Study on metallogenesis of Mesozoic endogenetic metal deposits in the eastern part of Jilin province. unpublished Ph. D. dissertation, Changchun, Jilin University, 205 p. (in Chinese with English abstract).

Wang, H., Ren, Y.S., Sun, Z.M., Hao, Y.J., Li, C., 2013. Metallogenic epoch and tectonic setting of Jiapigou porphyry molybdenum deposit in Wangqing area, Jilin Province. Mineral Deposits 32, 489–500 (in Chinese with English abstract).

Wang, M., He, L., 2013. Re-Os dating of molybdenites from Chamuhan W-Mo deposit, Inner Mongolia and its geological implications. Geotectonica et Metallogenia 37, 49–56 (in Chinese with English abstract).

Wu, H.Y., Zhang, L.C., Wan, B., Chen, Z.G., Xiang, P., Pirajno, F., Du, A.D., Qu, W.J., 2011a. Re-Os and 40Ar/39Ar ages of the Jiguanshan porphyry Mo deposit, Xilamulun metallogenic belt, NE China, and constraints on mineralization events. Mineralium Deposita 46, 171–185.

Wu, H.Y., Zhang, L.C., Wan, B., Chen, Z.G., Zhang, X.J., Xiang, P., 2011b. Geochronological and geochemical constraints on Aolunhua porphyry Mo-Cu deposit, northeast China, and its tectonic significance. Ore Geology Reviews 43, 78–91.

Wu, H., Zhang, L., Pirajno, F., Xiang, P., Wan, B., Chen, Z., Zhang, X., 2014. The Jiguanshan porphyry Mo deposit in the Xilamulun metallogenic belt, northern margin of the North China Craton, U-Pb geochronology, isotope systematics, geochemistry and fluid inclusion studies: Implications for a genetic model. Ore Geology Reviews 56, 549–565.

Yan, C., 2009. Study on LA-ICP-MS zircon U-Pb geochronology and fluid inclusions of the Banlashan Mo deposit in Arhorqin Banner, Inner Mongolia. Bachelor dissertation, Beijing, Peking University, 50 p. (in Chinese with English abstract).

Yang, Y.C., Han, S.J., Sun, D.Y., Gao, J., Zhang, S.J., 2012. Geological and geochemical features and geochronology of porphyry molybdenum deposits in the Lesser Xing'an range-Zhangguangcai range metallogenic belt. Acta Petrologica Sinica 28, 379–390 (in Chinese with English abstract).

Yu, G., Chen, J., Xue, C., Chen, Y., Chen, F., Du, X., 2009. Geochronological framework and Pb, Sr isotope geochemistry of the Qingchengzi Pb-Zn-Ag-Au orefield, Northeastern China. Ore Geology Reviews 35, 367-382.

Zeng, Q.D., Liu, J.M., Zhang, Z.L., 2010. Re-Os geochronology of porphyry molybdenum deposit in south segment of Da Hinggan Mountains, northeastern China. Journal of Earth Sciences 21, 390–401.

Zeng, Q.D., Liu, J.M., Zhang, Z.L., Chen, W.J., Zhang, W.Q., 2011. Geology and geochronology of the Xilamulun molybdenum metallogenic belt in eastern Inner Mongolia, China. International Journal of Earth Sciences 100, 1791–1809.

Zeng, Q.D., Liu, J.M., Chu, S.X., Wang, Y.B., Sun, Y., Duan, X.X., Zhou, L.L., 2012. Mesozoic molybdenum deposits in the East Xingmeng orogenic belt, northeast China: characteristics and tectonic setting. International Geology Review 54, 1843–1869.

Zeng, Q., Yang, J., Zhang, Z, Liu, J., Duan, X., 2014. Petrogenesis of the Yangchang Mo-bearing granite in the Xilamulun metallogenic belt, NE China: geochemistry, zircon U-Pb ages and Sr-Nd-Pb isotopes. Geological Journal 49, 1–14.

Zhang, L.C., Wu, H.Y., Wan, B., Chen, Z.G., 2009a. Ages and geodynamic settings of Xilamulun Mo-Cu metallogenic belt in northern part of the North China Craton. Gondwana Research 16, 243–254.

Zhang, T., Chen, Z.Y., Xu, L.Q., Chen, Z.H., 2009b. The Re-Os isotopic dating of molybdenite from the Dasuji molybdenum deposit in Zhuozi County of Inner Mongolia and its geological significance. Rock and Mineral Analysis 28, 279–282 (in Chinese with English abstract).

Zhang, Z., Wu, C., Gu, L., Feng, H., Zheng, Y., Huang, J., Li, J., Sun, Y., 2009c. Molybdenite Re-Os dating of Xintaimen molybdenum deposit in Yanshan-Liaoning metallogenic belt, North China. Mineral Deposits 28, 313–320 (in Chinese with English abstract).

Zhang, X.J., Zhang, L.C., Jin, X.D., Wu, H.Y., Xiang, P., Chen, Z.G., 2010. U-Pb ages, geochemical characteristics and their implications of Banlashan Molybdenum Deposit. Acta Petrologica Sinica 26, 1411–1422 (in Chinese with English abstract).

Zhang, Y., Sun, J.G., Xing, S.W., Zhao, K.Q., Zhang, Z.J., Ma, Y.B., 2013a. Re-Os dating of molybdenite from Tianbaoshan polymetallic orefield in Yanbian and its geological significance. Mineral Deposits 32, 427-435 (in Chinese with English abstract).

Zhang, Y., Sun, J.G., Chen, Y.J., Zhao, K.Q., Gu, A.L., 2013b. Re-Os and U-Pb geochronology of porphyry Mo deposits in central Jilin Province: Mo ore-forming stages in northeast China. International Geology Review 55, 1763–1785.

Zhang, C., Li, N., Chen, Y.J., Zhao, X.C., 2013c. Zircon U-Pb ages and Hf isotopic compositions of the intrusive rocks in the Xing'a Mo-Cu deposit, Inner Mongolia. Acta Petrologica Sinica 29, 217–230 (in Chinese with English abstract).

Zhang, L., Gao, B., Li, W., Chen, Z., Sakyi, P.A., Jin, X., 2014. Early Mesozoic tectono-magmatic activity and mineralization in northeast China: evidence from Re-Os to U-Pb studies of the Taipingchuan porphyry Cu-Mo deposit in the Derbugan metallogenic belt. International Geology Review 56, 1837–1851.

Zhao, Y., Sun, J., Wang, Q., Men, L., Li, Y., Guo, J., Cui, P., 2010. $^{40}Ar/^{39}Ar$ laser probe dating and discussion on metallogenic epoch of epithermal Au-Cu deposit in Yanbian area of Jilin. Earth Science Frontiers 17, p. 156–169 (in Chinese with English abstract).

Zhou, Z.H., Mao, J.W., Lyckberg, P., 2012. Geochronology and isotopic geochemistry of the A-type granites from the Huanggang Sn-Fe deposit, southern Great Hinggan Range, NE China: Implication for their origin and tectonic setting. Journal of Asian Earth Sciences 49, 272–286.

Zhou, L.L., Zeng, Q.D., Liu, J.M., Friis, H., Zhang, Z.L., Duan, X.X., 2013. Geochronology of the Xingshan molybdenum deposit, Jilin Province, NE China, and its Hf isotope significance. Journal of Asian Earth Sciences 75, 58-70.

Appendix 4-2. Locations and ore-forming ages of the epithermal Au (Mo, Cu) deposits in NE China.

No.	Deposit	Geographic Location	Metals	Sample description	Method	Age (Ma)	References
71	Jinchang	44°15'N, 130°49'E	Cu-Ag	Beresite	Pyrite Rb-Sr	110.0 ± 2.6	Li et al., 2009
72	Wulaga	48°22'N, 130°15'E	Au	Gold-bearing pyrite	Pyrite Rb-Sr	113.8 ± 4.4	Wang et al., 2014
73	sishanlinchang	44°55'N, 131°05'E	Au-Ag	Gold-bearing molybdenite-quartz vein	Molybdenite Re-Os	111.3 ± 1.6	Huang, 2010
74	Wuxingshan	43°05'N, 129°28'E	Ag-Au	Gold-bearing pyrite-quartz vein	Fluid inclusion Ar-Ar	123 ± 7	Zhao et al., 2010
75	Sipingshan	46°21'N, 133°33'E	Ag-Au	Sulfide-quartz vein	Zircon U-Pb	96.7 ± 2.6	Sun et al., 2013
76	Tuanjiegou	48°22'N, 130°16'E	Au	Pyrite-quartz veins and brecciated ore	Zircon U-Pb	102.5 ± 1.7	Sun et al., 2013
77	Dong'an	49°20'N, 129°01'E	Ag-Au	Gold-bearing sericitolite	Sericite Ar-Ar	107.2 ± 0.6	Sun et al., 2013
78	Sandaowanzi	50°23'N, 127°02'E	Au-Te	Pyrite in altered trachyandesites	Pyrite Rb-Sr	119.1 ± 3.9	Zhai et al., 2015
79	Duhuangling	43°18'N, 130°42'E	Cu-Au	Gold-bearing pyrite-quartz vein	Fluid inclusion Ar-Ar	107 ± 11	Chai et al., 2014
80	Jiusangou	43°19'N, 130°35'E	Au	Porphyritic diorite	Zircon U-Pb	105.8 ± 1.8	Han et al., 2013
81	Naozhi	43°11'N, 129°41'E	Cu-Au	Gold-bearing sulfide-quartz vein	Sericite Ar-Ar	123.6 ± 2.5	Meng et al., 2001

Note: The deposit no. are the same as in Fig. 4-6C.

References

Chai, P., Sun, J.G., Xing, S.W., Men, L.J., Han, J.L., 2015. Early Cretaceous arc magmatism and high-sulphidation epithermal porphyry Cu–Au mineralization in Yanbian area, Northeast China: the Duhuangling example. International Geology Review 57, 1267–1293.

Han, S.J., Sun, J.G., Bai, L.A., Xing, S.W., Chai, P., Zhang, Y., Yang, F., Meng, L.J., Li, Y.X., 2013. Geology and ages of porphyry and medium-to high-sulphidation epithermal gold deposits of the continental margin of Northeast China. International Geology Review 55, 287–310.

Huang, Y., 2010. Study on metallogenetic regularities and ore-forming forecast of epithermal gold deposits in Wanda mountain and Taiping mountain Belts in southeast of Heilongjiang Province. unpublished Ph. D. dissertation, Beijing, China University of Geosciences, 169 p. (in Chinese with English abstract).

Li, Z.Z., Li, S.R., Zhang, H.F., 2009. Wall rock alteration and metallogenic chronology of Jinchang gold deposit in Dongning County, Heilongjiang Province. Mineral Deposits 28, 83–92 (in Chinese with English abstract).

Meng, Q.L., Zhou, Y.C., Chai, S.L., 2001. The porphyry and hydrothermal lode gold and copper deposits in Eastern Yanbian region of China. Changchun, Jilin Science and Technology Press, 162 p (in Chinese with English abstract).

Sun, J.G., Zhang, Y., Han, S.J., Men, L.J., Li, Y.X., Chai, P., Yang, F., 2013b. Timing of formation and geological setting of low-sulphidation epithermal gold deposits in the continental margin of NE China. International Geology Review 55, 608–632.

Wang, Y., Zeng, Q., Liu, J., 2014. Rb-Sr Dating of Gold-bearing Pyrites from Wulaga Gold Deposit and its Geological Significance. Resource Geology 64 , 262-270.

Zhai, D., Liu, J., Ripley, E.M., Wang, J., 2015. Geochronological and He-Ar-S Isotopic Constraints on the Origin of the Sandaowanzi Gold-Telluride Deposit, Northeastern China. Lithos 212–215, 338–352.

Appendix 5-1. Microthermometric data of fluid inclusions in Baiyinnuo'er.

Pre-ore stage

Thin section no.	FI type	P&S	Homogenization temperature of the H_2O phases	Dissolution temperature of halite	Salinity	Pressure
B10-3 (Cpx)	S1	P	459	385	45.9	337
		P	466	374	44.8	362
		P	461	384	45.7	337
		P	446	341	41.6	322
		P	451	407	48.2	302
		P	458	381	45.4	332
		P	535	355	42.9	482
		P	540	345	41.9	502
		P	487	341	41.6	432
		P	472	357	43.1	392
		P	464	369	44.3	352
		P	483	328	40.4	442
		P	411	369	44.2	232
		P	415	345	41.9	237
	V	P	413			
		P	482			
		P	522			
		P	458			
		P	463			
		P	412			
		P	515			
	S2	S	400	411	48.7	386
		S	361	366	43.9	795
		S	365	378	45.1	191
		S	353	402	47.7	304
		S	267	387	46.0	2155
		S	315	375	44.8	981
		S	291	378	45.1	1500
		S	341	380	45.3	613
B19-21 (Cpx)	S1	P	467	372	44.5	372
		P	476	366	44.0	402
		P	478	354	42.8	412
		P	478	346	42.1	417
		P	389	323	40.0	180
		P	432	342	41.6	342
		P	417	391	46.5	227
		P	432	355	42.9	322
		P	411	336	41.1	232
		P	489	362	43.5	432
		P	480	351	42.4	422
		P	522	371	44.4	568
B9 (Cpx)	S1	P	483	367	44.1	412
		P	459	336	41.2	362
		P	481	378	45.2	402
		P	456	363	43.7	342
		P	472	424	50.1	342
		P	478	413	48.9	342
		P	479	387	46.1	387

		P	563	393	46.7	606
		P	547	395	46.9	587
		P	480	401	47.6	382
		P	452	296	37.8	357
		P	462	306	38.6	382
		P	441	377	45.0	312
		P	456	367	44.0	337
		P	443	341	41.6	317
		P	449	337	41.2	322
		P	512	365	43.8	482
		P	518	348	42.2	572
		P	487	368	44.1	422
		P	500	332	40.8	482
		P	491	349	42.3	442
		P	507	355	42.9	472
		P	499	323	40.0	492
		P	493	349	42.3	447
B10-41 (Cpx)	S1	P	479	398	47.3	382
		P	471	378	45.2	372
		P	475	339	41.4	402
		P	466	373	44.7	362
		P	472	344	41.8	382
		P	505	342	41.6	507
		P	499	327	40.4	482
		P	484	353	42.7	412
		P	476	314	39.3	402
		P	466	362	43.5	362
		P	464	371	44.5	347
		P	450	306	38.6	342
		P	470	317	39.5	392
		P	465	355	42.9	352
		P	471	333	40.9	402
		P	494	359	43.2	442
		P	455	394	46.8	342
		P	472	291	37.5	422
		P	496	376	44.9	452
		P	507	368	44.2	492
	V	P	516			
		P	485			
		P	520			
		P	393			
B10-4 (Cpx)	S1	P	481	353	42.7	412
		P	503	365	43.8	462
		P	508	388	46.1	472
		P	524	404	47.8	492
		P	472	349	42.3	382
		P	490	381	45.4	422
		P	516	393	46.7	482
		P	494	359	43.2	442
		P	487	379	45.2	412
		P	371	325	40.2	150
		P	456	323	40.0	352

		P	450	337	41.3	332
		P	415	294	37.7	252
B12-8 (Qz)	S1	P	460	358	43.2	400
		P	476	404	47.9	305
		P	467	347	42.1	410
		P	453	355	42.9	310
		P	389	386	45.9	320
		P	398	390	46.3	415
		P	412	380	45.4	305
		P	414	385	45.8	315
		P	371	320	39.7	150
		P	508	382	45.6	605
		P	487	376	44.9	370
		P	491	364	43.8	565
	V	P	488			
		P	440			
		P	509			
		P	456			
		P	465			
	S2	P	316	432	51.1	1262
		P	347	453	53.7	1363
		P	380	439	51.9	645
		P	349	427	50.4	1910
		P	302	379	45.2	171
		S	307	388	46.1	1961
		S	217	379	45.2	1762
		S	363	411	48.7	967
		S	284	397	47.1	1304
		S	348	389	46.2	2942
		S	215	352	42.5	777
		S	295	406	48.1	1982
		S	330	337	41.2	2651
		S	313	367	44.0	879
		S	273	368	44.0	1732
B12-7 (Qz)	S2	P	322	385	45.9	1737
		P	296	402	47.7	205
		P	294	394	46.8	741
		S	341	363	43.6	355
		S	274	358	43.2	1049
		S	328	375	44.8	1526
		S	294	436	51.5	2422
		S	315	400	47.5	1415
		S	309	410	48.6	1724
		S	362	390	46.4	491
		S	362	368	44.1	1029
		S	304	367	44.0	1844

Syn-ore stage

Thin section no.	FI type	P&S	Final melting temperature	Homogenization temperature	Salinity	Pressure
B9 (Sph)	L	P	-6.5	419	9.9	320
		P	-7.2	338	10.7	130
		P	-6.8	402	10.2	280
		P	-5.0	312	7.9	100
		P	-2.4	389	4.0	250
		P	-3.8	372	6.2	200
		P	-3.3	372	5.4	135
		P	-3.5	318	5.7	110
		P	-4.3	327	6.9	120
		P	-3.1	323	5.1	115
		P	-3.3	335	5.4	120
		P	-3.3	315	5.4	105
		P	-3.6	347	5.9	150
		P	-1.7	368	2.9	205
		P	-1.4	207	2.4	15
		P	-2.3	335	3.9	130
		P	-1.9	328	3.2	125
		P	-2.3	332	3.9	130
		P		389		
		P		364		
		P		393		
		P		368		
		P		364		
		P		308		
		P		329		
		P		260		
		P		197		
		P		345		
		P		339		
		P		357		
		P		327		
		P		365		
		P		377		
	V	P	-0.3	365	0.5	200
		P	-0.8	355	1.4	175
		P		382		
		P		374		
B11-5 (Sph)	L	P	-4.7	287	7.4	85
		P	-4.9	342	7.7	141
		P	-2.2	306	3.7	100
		P	-5.7	298	8.8	90
		P	-2.4	312	4.0	105
		S	-5.7	247	8.8	50
		S	-1.2	262	2.1	60
	V	P	-1.4	407	2.4	280
		P	-0.4	355	0.7	180
B16-11 (Qz)	L	P	-7.6	365	11.2	185
		P	-8.4	363	12.2	180
		P	-8.0	358	11.7	180

		P	-9.4	380	13.3	210
		P	-5.1	402	8.0	270
		P	-5.4	398	8.4	270
		P	-5.5	406	8.5	310
		P	-4.4	355	7.0	170
		P	-3.8	354	6.2	160
		P	-4.5	381	7.2	220
		S	-5.2	226	8.1	30
		S	-3.7	247	6.0	50
		S	-1.5	227	2.6	30
		S	-1.3	220	2.2	30
		P		322		
	V	P	-0.9	402	1.6	270
		P		348		
B16-12 (Qz)	L	P	-7.6	377	11.2	210
		P	-8.2	373	11.9	200
		P	-7.3	363	10.9	180
		P	-1.7	306	2.9	100
		P	-2.8	295	4.6	80
		P	-0.9	238	1.6	35
		P	-1.1	242	1.9	40
		P	-3.9	375	6.3	210
		P	-3.7	371	6.0	200
		P	-6.9	328	10.4	120
		P	-3.2	339	5.3	140
		P	-4.8	337	7.6	130
		P	-5.4	312	8.4	95
	V	P	-0.9	380	1.6	230
		P		393		
		P		371		
B12-4 (Qz)	L	P		376		
		P		351		
		P		378		
		P		382		
		P		327		
B19-26 (Cc)	L	P	-3.8	326	6.2	120
		P	-5.3	396	8.3	270
		P	-4.7	379	7.4	220
		P	-3.5	358	5.7	180
		P	-4.0	318	6.4	110
		P	-2.0	334	3.4	135
		P	-2.4	313	4.0	100
		P		347		
		P		322		
		P		367		
		P		364		
		P		372		
		P		331		
		P		338		
		P		321		
		P		439		
		P		431		

Post-ore stage L-type inclusions

Thin section no.	P&S	Final melting temperature	Homogenization temperature	Salinity
B13-1 (Cc)	P	-0.8	240	1.4
	P	-1.3	238	2.2
	P	-0.7	223	1.2
	P	-0.6	217	1.1
	P	-0.4	153	0.7
	P	-0.8	375	1.4
	P	-0.9	188	1.6
	P	-1.4	187	2.4
	P	-0.8	207	1.4
	P	-0.4	198	0.7
	P	-0.7	194	1.2
	P	-1.1	204	1.9
	P	-1.2	233	2.1
	P	-0.8	234	1.4
	P	-3.1	237	5.1
	S	-2.3	233	3.9
	S	-1.1	239	1.9
	S	-0.8	152	1.4
	S	-0.9	160	1.6
	S	-0.8	159	1.4
	S	-0.5	159	0.9
	S		325	
	S		162	
	S		246	
	S		241	
B14-18 (Cc)	S	-0.3	148	0.5
	S	-0.6	152	1.1
	S	-0.9	230	1.6
	S	-1.2	192	2.1
	S		144	
	S		124	
B13-2 (Cc)	P	-1.8	229	3.1
	P	-0.9	213	1.6
	P	-1.6	198	2.7
	P	-1.2	208	2.1
	P	-0.9	204	1.6
	P	-1.4	213	2.4
	P	-2.7	232	4.5
	P	-1.3	215	2.2
	P	-1.1	210	1.9
	P	-0.9	215	1.6
	P	-1.4	196	2.4
	P	-1.1	258	1.9
	S	-1.3	239	2.2
	S	-1.4	242	2.4
	S	-1.3	220	2.2
	P		146	
	P		231	
	P		201	

Post-ore stage Lc-type inclusions

Thin section no.	P&S	Eutectic temperature	Hydrohalite melting temperature	Final melting temperature	Homogenization temperature	Salinity	X_{NaCl}
B11-5 (Sph)	S		-31.3	-14.2	117	17.0	0.30
	S		-28.4	-14.5	121	16.9	0.41
	S			-13.8	134	17.6	
	S				165		
B19-26 (Cc)	S	-36.7	-29.1	-3.2	162	6.1	0.38
	S	-39.4			128		
	S	-44.7	-25.3	-3.6	143	6.6	0.59
	S		-25.3	-6.2	226	10.1	0.59
	S		-26.8	-5.8	214	9.6	0.49
	S			-5.7	164	8.8	
	S			-4.9	196	7.7	
	S			-5.6	189	8.7	
	S				207		
	S			-10.4	217	14.4	
	S		-29.0	-9.0	221	13.1	0.38
	S		-27.5	-7.7	145	11.8	0.45
	S				194		
B13 (Cc)	P	-47.4	-27.9	-13.9	160	16.8	0.43
	P		-24.3	-14.7	173	16.1	0.67
	P	-52.2	-25.1	-11.4	206	15.0	0.60
	P		-26.6	-10.4	212	14.5	0.50
	P		-27.1	-12.7	195	16.8	0.48
	P		-28.4	-16.7	152	18.7	0.41
	P		-29.1	-19.5	175	18.6	0.38
	P		-25.2	-20.2	219	12.9	0.60
B16-12 (Qz)	S	-50.1	-25.1	-3.3	241	6.1	0.60
	S		-24.7	-4.0	234	7.2	0.64
	S		-27.6	-8.9	187	13.1	0.45
	S			-10.2	168	14.1	

FI (fluid inclusion) types are defined in the text. Host mineral abbreviations are the same as in Fig. 5-7.

Temperature values are reported in degrees Celsius (°C), salinity values as wt percent NaCl equiv (wt % NaCl eqv) and pressure values as bars. $X_{NaCl} = NaCl/(NaCl + CaCl_2)$. P = primary, S = secondary.

Appendix 6-1. EMPA analyses of sphalerite.

Sample No.	Fe	As	S	Co	Pb	Ni	Ag	Cu	Cd	Zn	Sb	Au	Total
B13-3-1.3	7.19	0.01	33.19	0.00	0.10	0.04	0.00	0.04	0.28	59.82	0.00	0.01	100.68
B13-3-1.1	7.14	0.00	33.21	0.00	0.12	0.03	0.00	0.00	0.32	59.61	0.00	0.16	100.59
B13-3-1.2	7.03	0.00	32.99	0.00	0.01	0.01	0.00	0.03	0.30	59.59	0.00	0.03	99.97
B13-3-2.3	6.22	0.00	33.36	0.00	0.11	0.00	0.00	0.00	0.26	60.47	0.00	0.08	100.50
B13-3-2.2	6.21	0.00	33.02	0.00	0.00	0.00	0.00	0.00	0.25	60.35	0.00	0.27	100.10
B13-3-3.2	6.96	0.01	33.28	0.00	0.00	0.00	0.00	0.03	0.25	60.29	0.00	0.15	100.95
B13-3-2.1	5.26	0.00	32.57	0.00	0.03	0.00	0.00	0.02	0.28	60.70	0.00	0.16	99.01
B13-3-3.1	5.95	0.00	33.27	0.00	0.05	0.00	0.00	0.00	0.23	60.23	0.00	0.00	99.73
B13-3-3.4	6.08	0.08	33.50	0.00	0.04	0.00	0.00	0.01	0.21	60.19	0.01	0.00	100.12
B13-3-3.3	4.94	0.13	33.21	0.00	0.12	0.01	0.00	0.03	0.29	61.05	0.01	0.00	99.79
B14-2.2	8.25	0.01	33.45	0.00	0.02	0.00	0.00	0.00	0.14	57.84	0.00	0.00	99.71
B14-3.2	7.51	0.00	33.42	0.00	0.00	0.03	0.00	0.00	0.18	58.72	0.00	0.18	100.03
B14-1.2	8.61	0.02	33.38	0.00	0.00	0.00	0.00	0.02	0.14	57.43	0.00	0.16	99.76
B14-2.1	9.39	0.06	33.62	0.00	0.09	0.00	0.00	0.02	0.21	56.42	0.00	0.27	100.08
B14-3.1	9.40	0.00	33.39	0.00	0.04	0.00	0.00	0.02	0.17	56.40	0.00	0.09	99.51
B14-1.3	9.38	0.00	33.40	0.00	0.03	0.02	0.01	0.01	0.22	56.38	0.00	0.00	99.44
B14-1.1	7.59	0.00	33.14	0.00	0.07	0.00	0.00	0.02	0.19	58.27	0.00	0.00	99.28
B14-2.3	7.33	0.00	33.36	0.00	0.07	0.00	0.00	0.00	0.23	58.22	0.01	0.26	99.49
B14-3.3	7.50	0.00	33.41	0.00	0.04	0.00	0.00	0.00	0.21	58.17	0.03	0.01	99.36
Average	7.26	0.02	33.27	0.00	0.05	0.01	0.00	0.01	0.23	58.96	0.00	0.10	99.90
SD	1.32	0.04	0.23	0.00	0.04	0.01	0.00	0.01	0.05	1.55	0.01	0.10	0.52

Appendix 6-2. EMPA analyses of pyroxene.

Sample No.	SiO_2	TiO_2	Al_2O_3	Cr_2O_3	FeO	MnO	NiO	MgO	CaO	Na_2O	K_2O	Total
B16-11.9	51.38	0.00	0.00	0.00	11.78	3.32	0.05	9.34	24.40	0.04	0.00	100.30
B13-3-a2	52.27	0.05	0.00	0.03	9.35	3.89	0.07	10.37	24.67	0.00	0.00	100.69
B16-3-b6	50.98	0.07	0.02	0.05	14.95	2.98	0.00	7.85	23.84	0.03	0.00	100.78
B16-3-a12	50.77	0.01	0.01	0.00	15.52	2.95	0.00	7.22	23.52	0.02	0.00	100.02
B16-3-a13	48.37	0.02	0.08	0.05	25.49	2.66	0.00	1.24	22.91	0.08	0.01	100.91
B17-1.1	48.59	0.00	0.13	0.03	17.38	11.94	0.03	0.24	20.99	0.34	0.00	99.67
B17-1.3	47.90	0.00	0.60	0.01	22.93	5.47	0.00	0.04	22.51	0.13	0.02	99.60
B16-3-b7	48.45	0.01	0.14	0.00	25.41	3.28	0.08	0.33	22.41	0.11	0.01	100.23
B16-3-1.15	48.51	0.01	0.10	0.00	24.11	2.91	0.02	1.26	22.70	0.07	0.00	99.69
B16-3-2.1	48.77	0.03	0.19	0.02	22.87	4.42	0.00	0.79	22.38	0.09	0.00	99.55
B16-3-2.2	48.73	0.04	0.28	0.00	23.70	3.81	0.05	0.99	22.42	0.09	0.00	100.11
B16-3-2.3	48.98	0.00	0.04	0.02	23.41	3.27	0.00	1.21	22.82	0.11	0.02	99.87
B16-3-2.4	48.73	0.00	0.04	0.00	22.96	3.65	0.01	1.11	22.70	0.12	0.00	99.31
B16-3-2.5	50.70	0.03	0.00	0.03	14.21	2.94	0.00	7.90	23.47	0.05	0.00	99.32
B16-3-2.6	51.18	0.04	0.00	0.03	14.00	3.07	0.00	7.96	23.66	0.01	0.00	99.95
B16-3-2.7	50.83	0.02	0.01	0.00	14.27	3.02	0.00	7.76	23.66	0.14	0.02	99.74
B16-3-2.8	50.88	0.00	0.01	0.00	14.34	3.17	0.00	7.19	24.13	0.04	0.03	99.79
B16-3-2.9	50.89	0.00	0.01	0.02	14.23	3.42	0.04	7.54	23.74	0.00	0.00	99.89
Average	49.83	0.02	0.09	0.02	18.38	3.90	0.02	4.46	23.16	0.08	0.01	99.97
SD	1.36	0.02	0.15	0.02	5.32	2.11	0.03	3.85	0.90	0.08	0.01	0.47

Appendix 6-3. Full data of fluid inclusion compositions and selected element ratios from LA-ICP-MS analyses.

Assemblages	Sample No.	Th	Salinity	Li	Na	K	Ca	Cu	Zn	As	Rb	Sr	Ag	Cs	Ba	Pb	Cl	Br	K/Na	Ca/K	Rb/Na	Zn/Na	Zn/Cl	Pb/Cl	Cl/Br
		°C	wt. % NaCl	ppm	wt.%	wt.%	wt.%	ppm	ppm	ppm	ppm	ppm	ppm	ppm	ppm	ppm	wt.%	ppm							
Pre-ore Pyroxene																									
B4-1a	1			950	12.6	11.3	NA	520	7440	410	980	380	110	810	280	12600	40.9	<1250	0.89	NA	0.0078	0.0591	0.0182	0.0308	NA
	2			1660	12.0	12.6	NA	380	9950	280	1310	1130	60	670	920	11700	37.5	1400	1.05	NA	0.0109	0.0829	0.0265	0.0311	269
	3			<1500	10.6	14.9	NA	590	22400	<350	1480	1010	100	1380	740	12700	34.9	1380	1.40	NA	0.0139	0.2114	0.0643	0.0363	253
	4			<1200	11.4	12.8	NA	320	22000	410	950	1030	90	850	740	13400	34.5	1050	1.13	NA	0.0084	0.1933	0.0638	0.0389	329
	N	9	9	2	4	4	NA	4	4	3	4	4	4	4	4	4	4	3	4	NA	4	4	4	4	3
	Average	441	44.4	1300	11.6	12.9	NA	450	15500	360	1180	890	90	930	670	12600	36.9	1270	1.12	NA	0.0102	0.1367	0.0432	0.0343	284
	SD	18	2.2	500	0.8	1.5	NA	130	7880	80	250	350	20	310	270	710	3.0	200	0.21	NA	0.0028	0.0768	0.0243	0.0040	40
B4-1b	1			<3590	12.3	13.6	NA	<800	10000	<910	1240	710	110	540	230	11300	37.3	<5120	1.11	NA	0.0101	0.0814	0.0269	0.0304	NA
	2			<1490	13.0	11.6	NA	<340	12700	<370	1150	1070	50	520	620	9740	38.7	<3070	0.89	NA	0.0088	0.0973	0.0327	0.0252	NA
	3			<2230	13.4	10.9	NA	<530	8820	1030	1120	650	60	960	240	10100	42.5	<4060	0.81	NA	0.0083	0.0658	0.0208	0.0237	NA
	4			<1220	11.9	13.6	NA	430	16200	<320	1230	840	140	1510	750	16200	38.1	<2300	1.14	NA	0.0103	0.1358	0.0425	0.0426	NA
	5			<1460	12.4	13.4	NA	<320	8360	<370	1330	1130	80	760	780	14500	32.7	<2500	1.08	NA	0.0107	0.0675	0.0255	0.0442	NA
	N	12	12	0	5	5	NA	1	5	1	5	5	5	5	5	5	5	0	5	NA	5	5	5	5	0
	Average	432	46.1	NA	12.6	12.6	NA	430	11200	1030	1210	880	90	860	520	12400	37.9	NA	1.01	NA	0.0096	0.0895	0.0297	0.0332	NA
	SD	13	2.8	NA	0.6	1.3	NA	0	3250	0	80	210	40	410	270	2860	3.5	NA	0.15	NA	0.0010	0.0288	0.0083	0.0097	NA
B4-1c	1			<1690	13.5	9.5	NA	<370	<500	1100	950	590	50	690	240	3060	35.6	<2770	0.70	NA	0.0070	NA	NA	0.0086	NA
	2			<2140	13.6	8.5	NA	<500	3960	<570	490	500	80	400	230	6400		<4330	0.62	NA	0.0036	0.0291	NA	NA	NA
	3			<2090	10.3	16.0	NA	<510	12200	700	1730	890	110	730	1270	14500	39.5	<3240	1.56	NA	0.0169	0.1191	0.0309	0.0368	NA
	4			<3680	<10.0	14.3	NA	520	23100	1030	1250	1540	140	400	1280	39800	40.8	1990	NA	NA	NA	NA	0.0565	0.0974	205
	5			2830	10.7	13.5	NA	320	18600	340	1320	1370	140	700	510	24500	44.2	1830	1.27	NA	0.0124	0.1744	0.0420	0.0555	242
	N	8	8	1	4	5	NA	2	4	4	5	5	5	5	5	5	4	2	4	NA	4	3	3	4	2
	Average	469	43.6	2830	12.0	12.4	NA	420	14500	790	1150	870	100	580	710	17700	40.0	1910	1.04	NA	0.0100	0.1075	0.0431	0.0496	223
	SD	10	3.0	0	1.8	3.2	NA	140	8290	350	460	610	40	170	530	14900	3.6	120	0.45	NA	0.0059	0.0733	0.0128	0.0373	26
B7-1	1			<1420	12.3	6.3	NA	<350	3390	370	520	260	70	460	100	5960	31.4	<3480	0.51	NA	0.0042	0.0275	0.0108	0.0190	NA

	2			<780	11.2	8.4	NA	<190	8520	<230	830	770	<10	740	350	9300	33.4	1470	0.75	NA	0.0074	0.0758	0.0255	0.0278	228
	3			<1900	9.7	11.4	NA	690	9770	730	1620	1470	110	1650	680	22100	39.0	1660	1.18	NA	0.0168	0.1008	0.0250	0.0566	236
	4			<3600	12.9	<1.9	NA	<950	15700	<900	280	810	110	530	1280	27700	38.7	<4200	NA	NA	0.0022	0.1216	0.0406	0.0714	NA
	N	4	4	0	4	3	NA	1	4	2	4	4	3	4	4	4	4	2	3	NA	4	4	4	4	2
	Average	484	38.1	NA	11.6	8.7	NA	690	9360	550	810	830	100	850	600	16300	35.6	1560	0.81	NA	0.0076	0.0814	0.0255	0.0437	232
	SD	6	0.9	NA	1.4	2.6	NA	0	5080	250	590	490	30	550	510	10300	3.8	130	0.34	NA	0.0065	0.0406	0.0122	0.0245	5
B9-3a	1			<2920	10.1	13.3	NA	<720	11200	<850	950	1790	110	790	780	12200	43.5	<3950	1.31	NA	0.0094	0.1106	0.0257	0.0280	NA
	2			<930	10.2	12.0	NA	<210	15400	<270	1780	1680	<10	380	790	22800	38.7	1000	1.18	NA	0.0175	0.1516	0.0398	0.0590	387
	3			1060	11.6	14.5	NA	320	4450	280	850	850	200	1190	920	23400	40.7	1210	1.25	NA	0.0073	0.0382	0.0109	0.0575	337
	4			2260	9.6	13.8	NA	<950	<2220	<1120	1390	1770	<60	990	780	28300	36.6	<7850	1.43	NA	0.0144	NA	NA	0.0775	NA
	5			5440	13.6	9.3	NA	300	9750	<230	980	1060	80	930	290	16200	37.4	1210	0.69	NA	0.0072	0.0719	0.0261	0.0433	310
	6			990	12.3	14.1	NA	240	1900	450	1020	790	90	940	400	8900	36.3	1530	1.15	NA	0.0083	0.0154	0.0052	0.0245	238
	N	8	8	4	6	6	NA	3	5	2	6	6	4	6	6	6	6	4	6	NA	6	5	5	6	4
	Average	504	45.5	2440	11.2	12.8	NA	290	8540	360	1160	1320	120	870	660	18600	38.9	1240	1.17	NA	0.0107	0.0775	0.0216	0.0483	318
	SD	14	1.8	2090	1.5	1.9	NA	40	5400	120	350	470	50	270	250	7440	2.8	220	0.26	NA	0.0042	0.0548	0.0137	0.0203	63
B9-3b	1			<2070	14.2	7.7	NA	<450	7090	<510	950	760	50	1440	<16	6900	30.2	<3520	0.54	NA	0.0067	0.0499	0.0235	0.0229	NA
	2			5170	12.2	11.6	NA	340	11500	200	1170	1520	90	810	360	21100	41.4	1430	0.96	NA	0.0096	0.0945	0.0278	0.0511	289
	3			<4100	12.4	15.3	NA	<930	11660	<1100	1420	1090	90	1270	420	12000	41.5	<3990	1.24	NA	0.0114	0.0939	0.0281	0.0289	NA
	4			4980	12.1	11.5	NA	340	14000	<310	1200	1380	80	1160	290	21700	45.1	1730	0.95	NA	0.0099	0.1159	0.0311	0.0481	261
	5			<1890	14.0	8.1	NA	<410	9180	<460	850	790	50	1280	<16	6380	33.4	<3480	0.58	NA	0.0061	0.0655	0.0275	0.0191	NA
	N	11	11	2	5	5	NA	2	5	1	5	5	5	5	3	5	5	2	5	NA	5	5	5	5	2
	Average	448	44.7	5080	13.0	10.9	NA	340	10700	200	1120	1110	70	1190	360	13600	38.3	1580	0.85	NA	0.0087	0.0839	0.0276	0.0340	275
	SD	20	3.2	140	1.0	3.1	NA	2	2650	0	220	340	20	240	70	7460	6.3	210	0.29	NA	0.0023	0.0261	0.0027	0.0147	20
B27	1			540	12.4	12.1	NA	<220	<240	<280	1940	750	50	470	200	3430	32.8	<2210	0.97	NA	0.0157	NA	NA	0.0104	NA
	2			3360	13.2	8.7	NA	<190	<180	2220	1230	1260	100	700	580	18100	40.6	1550	0.66	NA	0.0093	NA	NA	0.0446	263
	3			1230	12.7	10.1	NA	750	<570	<710	1260	1150	120	970	650	16900	36.3	1850	0.79	NA	0.0098	NA	NA	0.0464	197
	4			7060	9.2	18.4	NA	340	<270	500	1710	1760	60	420	600	34300	42.0	2120	2.00	NA	0.0186	NA	NA	0.0817	198
	N	7	7	4	4	4	NA	2	0	2	4	4	4	4	4	4	4	3	4	NA	4	0	0	4	3
	Average	465	43.2	3050	11.9	12.3	NA	550	NA	1360	1530	1230	80	640	510	18200	37.9	1850	1.11	NA	0.0133	NA	NA	0.0458	219

	SD	9	1.8	2930	1.8	4.3	NA	290	NA	1220	350	420	40	250	210	12600	4.2	290	0.61	NA	0.0045	NA	NA	0.0291	38
B25-1	1			3530	9.8	10.8	NA	210	<61	260	1490	1390	50	2440	820	20100	39.9	1380	1.11	NA	0.0153	NA	NA	0.0505	288
	2			2480	11.5	6.4	NA	<950	<1050	<1430	730	690	50	730	190	17700	<26.3	<4800	0.56	NA	0.0064	NA	NA	NA	NA
	3			1050	10.7	8.6	NA	<380	<420	530	1120	1210	80	1790	630	14800	29.8	<3250	0.81	NA	0.0104	NA	NA	0.0498	NA
	N	4	4	3	3	3	NA	1	0	2	3	3	3	3	3	3	2	1	3	NA	3	0	0	2	1
	Average	492	36.5	2350	10.7	8.6	NA	210	NA	400	1120	1100	60	1650	550	17600	34.8	1380	0.82	NA	0.0107	NA	NA	0.0501	288
	SD	7	0.3	1250	0.9	2.2	NA	0	NA	190	380	360	16	870	330	2660	7.1	0	0.28	NA	0.0045	NA	NA	0.0005	0
B28a	1			1140	<12.6	9.2	NA	<290	9560	<320	1080	1260	60	770	600	16900	38.2	<2930	NA	NA	NA	NA	0.0250	0.0443	NA
	2			1150	13.9	6.7	NA	<230	<520	<260	1140	640	30	1260	360	3450	34.6	<2370	0.48	NA	0.0082	NA	NA	0.0100	NA
	3			2850	13.7	5.1	NA	210	8230	280	680	720	90	720	170	18700	28.8	1210	0.37	NA	0.0050	0.0600	0.0286	0.0648	239
	4			2790	<21.6	7.3	NA	<480	7210	620	950	1090	90	970	240	19000	31.7	<5990	NA	NA	NA	NA	0.0227	0.0599	NA
	N	15	15	4	2	4	NA	1	3	2	4	4	4	4	4	4	4	1	2	NA	2	1	3	4	1
	Average	497	41.9	1980	13.8	7.1	NA	210	8330	450	960	930	70	930	340	14500	33.3	1210	0.43	NA	0.0066	0.0600	0.0254	0.0447	239
	SD	26	4.6	970	0.1	1.7	NA	0	1180	240	200	290	30	250	190	7430	4.0	0	0.08	NA	0.0023	0.0000	0.0030	0.0248	0
B28b	1			1890	13.4	4.7	NA	<290	13900	<310	530	770	80	600	190	12700	38.8	<2860	0.35	NA	0.0039	0.1036	0.0358	0.0327	NA
	2			6830	<17.3	10.3	NA	550	18000	480	1320	1360	130	1380	300	28500	36.1	<3390	NA	NA	NA	NA	0.0498	0.0790	NA
	3			<4950	16.1	<8.6	NA	350	<11300	220	<350	<100	30	<50	<230	<50	30.8	2200	NA	NA	NA	NA	NA	NA	140
	N	8	8	2	2	2	NA	2	2	2	2	2	3	2	2	2	3	1	1	NA	1	1	2	2	1
	Average	471	40.9	4360	14.7	7.5	NA	450	16000	350	920	1070	80	990	240	20600	35.2	2200	0.35	NA	0.0039	0.1036	0.0428	0.0558	140
	SD	18	1.5	3490	1.9	3.9	NA	140	2880	190	560	420	50	550	80	11200	4.1	0	0.00	NA	0.0000	0.0000	0.0099	0.0328	0
B16-1a	1			3410	8.5	15.8	NA	200	17600	470	460	900	110	930	1290	13800	28.1	1230	1.86	NA	0.0054	0.2076	0.0628	0.0491	227
	2			250	14.5	4.1	NA	<170	1630	<190	480	1050	<6	820	440	6030	27.5	1560	0.28	NA	0.0033	0.0113	0.0059	0.0220	176
	3			1560	12.6	7.1	NA	180	12500	270	830	840	120	860	210	19600	34.6	1190	0.57	NA	0.0066	0.0993	0.0362	0.0566	291
	4			3050	11.9	9.1	NA	280	7710	260	1870	1320	140	700	1290	23600	31.8	1500	0.76	NA	0.0157	0.0647	0.0242	0.0744	212
	5			3490	13.4	5.6	NA	220	9180	310	790	770	80	770	140	13900	26.2	<2050	0.42	NA	0.0059	0.0684	0.0351	0.0531	NA
	N	8	8	5	5	5	NA	4	5	4	5	5	4	5	5	5	5	4	5	NA	5	5	5	5	4
	Average	454	41.1	2350	12.2	8.4	NA	220	9730	330	890	980	110	820	670	15400	29.6	1370	0.78	NA	0.0074	0.0902	0.0329	0.0510	227
	SD	23	1.8	1410	2.3	4.6	NA	50	5920	100	580	220	20	90	570	6670	3.5	190	0.63	NA	0.0048	0.0728	0.0207	0.0189	48
B16-2a	1			610	15.5	2.6	NA	<210	3950	<230	400	590	120	730	280	18000	29.8	<2470	0.17	NA	0.0026	0.0256	0.0133	0.0603	NA

	2			1970	14.0	6.1	NA	330	8090	<230	720	710	100	730	180	16700	30.6	1560	0.44	NA	0.0051	0.0578	0.0265	0.0547	195
	N	5	5	2	2	2	NA	1	2	0	2	2	2	2	2	2	2	1	2	NA	2	2	2	2	1
	Average	474	43.4	1290	14.7	4.4	NA	330	6020	NA	560	650	110	730	230	17300	30.2	1560	0.30	NA	0.0038	0.0417	0.0199	0.0575	195
	SD	9	0.4	960	1.0	2.5	NA	0	2930	NA	230	90	14	0	70	880	0.6	0	0.19	NA	0.0018	0.0228	0.0093	0.0040	0
B16-1b	1			3170	<12.5	9.5	NA	260	11400	<320	1300	1040	140	360	280	26000	32.3	1450	NA	NA	NA	NA	0.0352	0.0804	223
	2			5110	13.1	6.7	NA	210	10900	210	820	910	90	880	220	19200	29.1	1050	0.51	NA	0.0063	0.0832	0.0375	0.0660	279
	3			1360	12.7	8.3	NA	170	7570	130	920	870	80	710	400	16300	34.9	1070	0.65	NA	0.0072	0.0595	0.0217	0.0467	328
	N	9	9	3	2	3	NA	3	3	2	3	3	3	3	3	3	3	3	2	NA	2	2	3	3	3
	Average	493	42.2	3210	12.9	8.2	NA	210	9950	170	1010	940	100	650	300	20500	32.1	1190	0.58	NA	0.0067	0.0713	0.0314	0.0644	277
	SD	15	2.1	1880	0.3	1.4	NA	50	2070	50	250	90	30	270	90	4970	2.9	230	0.10	NA	0.0007	0.0168	0.0085	0.0169	52
B16-2b	1			<250	13.5	5.5	NA	<270	14600	350	670	920	70	680	230	15500	26.0	<3120	0.40	NA	0.0049	0.1079	0.0561	0.0597	NA
	2			4030	13.1	7.0	NA	240	10300	230	860	780	100	880	130	17200	33.4	1200	0.54	NA	0.0066	0.0790	0.0309	0.0515	278
	3			1960	<35.7	10.6	NA	<740	18000	<820	1200	1390	110	1220	320	33600	30.8	<5170	NA	NA	NA	NA	0.0587	0.1092	NA
	N	3	3	2	2	3	NA	1	3	2	3	3	3	3	3	3	3	1	2	NA	2	2	3	3	1
	Average	476	37.8	3000	13.3	7.7	NA	240	14300	290	910	1030	90	930	220	22100	30.1	1200	0.47	NA	0.0057	0.0934	0.0486	0.0735	278
	SD	3	1.1	1460	0.3	2.6	NA	0	3870	80	270	320	20	270	90	9980	3.7	0	0.09	NA	0.0012	0.0204	0.0153	0.0312	0
Syn-ore Sphalerite																									
B13-3a	1			<130	1.6	1.1	1.1	<40	NA	<40	350	190	<2	300	90	590	5.6	250	0.68	1	0.0227	NA	NA	0.0105	225
	2			320	1.4	0.3	0.3	<30	NA	50	120	30	1220	120	5	120	3.1	<340	0.23	0.90	0.0085	NA	NA	0.0038	NA
	3			<1320	<1.5	<0.8	<0.3	<440	NA	<360	150	<14	970	270	<30	620	4.3	<830	NA	NA	NA	NA	NA	0.0144	NA
	N	6	6	1	2	2	2	0	NA	1	3	2	2	3	2	3	3	1	2	2	2	0	0	3	1
	Average	348	6.6	320	1.5	0.7	0.7	NA	NA	50	210	110	1100	230	50	440	4.3	250	0.45	0.97	0.0156	NA	NA	0.0096	225
	SD	9	0.8	0	0.1	0.5	0.6	NA	NA	0	130	110	180	100	60	280	1.3	0	0.32	0.10	0.0100	NA	NA	0.0053	0
B13-3b	1			<1170	2.5	<0.6	<2.8	<1070	NA	40	<12	<5	<70	<2	<13	<30	<7.4	<3690	NA	NA	NA	NA	NA	NA	NA
	2			<300	2.1	2.0	0.9	210	NA	<80	160	30	280	<1	4	1220	6.9	290	0.95	0.43	0.0074	NA	NA	0.0179	237
	3			<70	1.6	1.8	1.6	150	NA	60	490	130	1660	520	50	1090	9.1	500	1.12	0.89	0.0300	NA	NA	0.0120	183
	N	3	3	0	3	2	2	2	NA	2	2	2	2	1	2	2	2	2	2	2	2	0	0	2	2
	Average	359	9.4	NA	2.1	1.9	1.3	180	NA	50	320	80	970	520	30	1160	8.0	390	1.03	0.66	0.0187	NA	NA	0.0149	210
	SD	30	0.9	NA	0.4	0.1	0.5	40	NA	18	240	70	980	0	30	100	1.6	150	0.12	0.32	0.0160	NA	NA	0.0042	38

B13-3c	1			<60	1.1	1.1	0.9	<20	NA	<16	160	23	1250	90	4	0	<0.6	110	1.04	0.81	0.0152	NA	NA	NA	NA
	2			<100	1.3	1.2	0.8	50	NA	<30	360	130	20	460	40	6	5.1	200	0.91	0.70	0.0277	NA	NA	0.0001	255
	3			100	1.0	1.2	1.0	<30	NA	20	170	10	540	70	3	60	5.0	<180	1.13	0.84	0.0161	NA	NA	0.0013	NA
	N	7	7	1	3	3	3	1	NA	1	3	3	3	3	3	3	2	2	3	3	3	0	0	2	1
	Average	336	5.6	100	1.1	1.2	0.9	50	NA	20	230	60	600	210	16	20	5.0	160	1.03	0.78	0.0197	NA	NA	0.0007	255
	SD	5	2.1	0	0.1	0.0	0.1	0	NA	0	110	70	620	220	20	30	0.1	60	0.11	0.08	0.0070	NA	NA	0.0008	0
B13-3d	1			60	1.2	1.6	1.6	<10	NA	30	270	200	440	220	100	310	7.2	250	1.26	1.05	0.0222	NA	NA	0.0044	287
	2			120	1.3	1.5	1.3	<5	NA	<6	310	220	70	260	110	820	8.5	360	1.20	0.88	0.0248	NA	NA	0.0097	236
	N	3	3	2	2	2	2	0	NA	1	2	2	2	2	2	2	2	2	2	2	2	0	0	2	2
	Average	368	7.1	90	1.2	1.5	1.5	NA	NA	30	290	210	250	240	110	570	7.8	300	1.23	0.97	0.0235	NA	NA	0.0070	262
	SD	25	0.5	40	0.0	0.0	0.2	NA	NA	0	30	11	260	30	6	360	0.9	80	0.04	0.12	0.0019	NA	NA	0.0037	36
B-2	1			40	1.6	1.5	1.0	<7	NA	16	250	50	660	90	6	40	6.3	<60	0.89	0.70	0.0157	NA	NA	0.0006	NA
	N	6	6	1	1	1	1	0	NA	1	1	1	1	1	1	1	1	0	1	1	1	0	0	1	0
	Average	323	7.8	40	1.6	1.5	1.0	NA	NA	16	250	50	660	90	6	40	6.3	NA	0.89	0.70	0.0157	NA	NA	0.0006	NA
	SD	5	1.8	0	0	0	0	NA	NA	0	0	0	0	0	0	0	0	NA	0.00	0.00	0.0000	NA	NA	0.0000	NA
B30a	1			280	<2.6	1.9	<0.7	370	NA	<60	650	200	1940	830	70	620	8.5	<620	NA	NA	NA	NA	NA	0.0074	NA
	2			160	2.3	1.6	0.5	220	NA	40	520	150	2500	670	40	630	6.9	350	0.68	0.29	0.0224	NA	NA	0.0092	195
	N	2	2	2	1	2	1	2	NA	1	2	2	2	2	2	2	2	1	1	1	1	0	0	2	1
	Average	345	8.3	220	2.3	1.8	0.5	300	NA	40	580	180	2220	750	60	630	7.7	350	0.68	0.29	0.0224	NA	NA	0.0083	195
	SD	7	0.5	80	0.0	0.2	0.0	100	NA	0	87	30	390	120	17	7	1.1	0	0.00	0.00	0.0000	NA	NA	0.0013	0
B30b	1			170	<2.1	<1.9	0.7	<30	NA	<50	240	140	30	620	50	150	7.4	<610	NA	NA	NA	NA	NA	0.0021	NA
	2			60	2.0	0.6	<0.5	<40	NA	<50	240	100	890	280	20	290	5.8	<540	0.31	NA	0.0118	NA	NA	0.0049	NA
	3			50	<2.4	0.5	<0.6	100	NA	<60	150	70	510	240	20	400	<3.0	<660	NA	NA	NA	NA	NA	NA	NA
	N	3	3	3	1	2	1	1	NA	0	3	3	3	3	3	3	2	0	1	0	1	0	0	2	0
	Average	311	4.9	90	2.0	0.6	0.7	100	NA	NA	210	100	480	380	30	280	6.6	NA	0.31	NA	0.0118	NA	NA	0.0035	NA
	SD	9	0.4	70	0.0	0.1	0.0	0	NA	NA	50	30	430	210	15	120	1.1	NA	0.00	NA	0.0000	NA	NA	0.0020	NA
B14-1	1			40	1.8	1.1	0.5	<10	NA	13	340	50	480	230	15	580	5.4	140	0.61	0.50	0.0192	NA	NA	0.0107	381
	2			40	1.3	1.1	1.2	<14	NA	24	270	40	110	190	12	360	5.8	250	0.80	1.10	0.0201	NA	NA	0.0062	234
	N	4	4	2	2	2	2	0	NA	2	2	2	2	2	2	2	2	2	2	2	2	0	0	2	2

	Average	328	6.3	40	1.6	1.1	0.9	NA	NA	18	300	50	300	210	14	470	5.6	200	0.70	0.80	0.0197	NA	NA	0.0085	307
	SD	23	0.6	0	0.3	0.0	0.5	NA	NA	8	50	7	270	30	2	160	0.3	70	0.13	0.42	0.0006	NA	NA	0.0032	104
B14-2	1			20	<0.5	0.0	<0.2	<10	NA	<11	130	20	560	60	3	40	<0.5	<110	NA	NA	NA	NA	NA	NA	NA
	2			180	1.2	0.6	<0.2	140	NA	40	120	30	870	180	10	50	3.2	130	0.53	NA	0.0100	NA	NA	0.0016	248
	N	1	1	2	1	2	0	1	NA	1	2	2	2	2	2	2	1	1	1	0	1	0	0	1	1
	Average	319	3.9	100	1.2	0.3	NA	140	NA	40	120	20	715	120	6	50	3.2	130	0.53	NA	0.0100	NA	NA	0.0016	248
	SD	0	0	120	0.0	0.4	NA	0	NA	0	9	6	220	80	5	9	0.0	0	0.00	NA	0.0000	NA	NA	0.0000	0
Syn-ore Calcite																									
B19a	1			70	2.4	0.7	NA	<50	<60	<50	270	NA	<1	340	34	<3	5.3	<450	0.30	NA	0.0111	NA	NA	NA	NA
	2			450	2.5	0.7	NA	<70	<80	<70	110	NA	<3	140	<6	<1	6.1	<950	0.27	NA	0.0046	NA	NA	NA	NA
	3			790	2.6	0.3	NA	<40	500	<50	60	NA	40	410	<3	<1	6.0	<750	0.12	NA	0.0023	0.0193	0.0084	NA	NA
	4			380	1.9	1.9	NA	210	1110	<12	350	NA	24	390	70	540	6.5	270	1.00	NA	0.0184	0.0581	0.0170	0.0082	245
	5			190	2.2	0.9	NA	130	710	<20	280	NA	10	160	50	490	6.4	<290	0.42	NA	0.0124	0.0316	0.0111	0.0077	NA
	6			<170	2.3	1.1	NA	170	400	<180	300	NA	60	170	40	670	<5.8	<200	0.49	NA	0.0131	0.0175	NA	NA	NA
	N	4	4	5	6	6	NA	3	4	0	6	NA	4	6	4	3	5	1	6	NA	6	4	3	2	1
	Average	338	6.9	380	2.3	0.9	NA	170	680	NA	230	NA	30	270	50	570	6.1	270	0.43	NA	0.0103	0.0316	0.0122	0.0080	245
	SD	33	0.9	270	0.2	0.5	NA	40	320	NA	120	NA	20	130	17	90	0.5	0	0.30	NA	0.0059	0.0187	0.0044	0.0004	0
B14-3	1			280	2.0	1.1	NA	10	500	<3	380	NA	<1	230	50	150	6.0	160	0.54	NA	0.0190	0.0252	0.0084	0.0026	374
	2			330	1.9	1.4	NA	<50	580	40	430	NA	<1	240	50	130	6.4	<340	0.73	NA	0.0229	0.0312	0.0091	0.0020	NA
	3			390	2.3	0.5	NA	<40	<40	40	190	NA	<2	190	<2	<1	5.7	<550	0.22	NA	0.0083	NA	NA	NA	NA
	4			80	1.9	1.2	NA	70	510	<8	240	NA	25	170	30	300	4.1	120	0.64	NA	0.0122	0.0265	0.0126	0.0074	327
	5			300	2.3	0.4	NA	<13	<150	<14	170	NA	<1	310	6	<1	4.7	200	0.16	NA	0.0076	NA	NA	NA	228
	6			420	2.1	0.8	NA	<20	360	<25	210	NA	<1	240	3	<7	5.6	280	0.37	NA	0.0096	0.0166	0.0064	NA	197
	7			200	2.3	0.3	NA	<30	280	35	230	NA	20	370	50	260	<2.9	<470	0.13	NA	0.0098	0.0121	NA	NA	NA
	N	7	7	7	7	7	NA	2	5	3	7	NA	2	7	6	4	6	4	7	NA	7	5	4	3	4
	Average	329	6.2	290	2.1	0.8	NA	40	450	40	260	NA	23	250	30	210	5.4	190	0.40	NA	0.0128	0.0223	0.0091	0.0040	281
	SD	19	0.6	120	0.2	0.4	NA	40	120	4	100	NA	3	70	20	80	0.9	70	0.24	NA	0.0059	0.0078	0.0026	0.0030	83
B13-3e	1			130	2.5	1.2	NA	270	1320	40	420	NA	80	370	16	760	5.6	290	0.49	NA	0.0167	0.0525	0.0234	0.0135	195
	2			440	2.9	0.5	NA	240	<50	<40	190	NA	<20	280	11	<1	7.5	<650	0.18	NA	0.0066	NA	NA	NA	NA

	3			<10	2.7	0.9	NA	<20	460	50	370	NA	41	200	14	830	5.9	<950	0.32	NA	0.0139	0.0170	0.0078	0.0141	NA
	N	5	5	2	3	3	NA	2	2	2	3	NA	2	3	3	2	3	1	3	NA	3	2	2	2	1
	Average	355	7.8	280	2.7	0.9	NA	250	890	40	330	NA	60	280	14	800	6.3	290	0.33	NA	0.0124	0.0348	0.0156	0.0138	195
	SD	17	1.5	220	0.2	0.4	NA	16	610	9	120	NA	30	90	2	50	1.0	0	0.15	NA	0.0052	0.0251	0.0111	0.0005	0
B19b	1			420	1.7	0.5	NA	<90	90	<90	190	NA	40	160	30	60	4.4	<130	0.30	NA	0.0115	0.0054	0.0020	0.0013	NA
	2			200	1.7	0.5	NA	<40	60	<34	150	NA	<1	180	5	30	3.6	<280	0.27	NA	0.0090	0.0033	0.0015	0.0009	NA
	3			260	1.6	0.6	NA	<70	60	<60	190	NA	<1	220	4	60	3.6	<360	0.36	NA	0.0119	0.0038	0.0017	0.0016	NA
	4			230	1.6	0.5	NA	<30	<20	<24	190	NA	<1	210	6	30	6.4	290	0.33	NA	0.0115	NA	NA	0.0005	225
	5			420	1.6	0.6	NA	<30	<30	<28	250	NA	<1	290	10	35	5.9	<230	0.40	NA	0.0158	NA	NA	0.0006	NA
	N	5	5	5	5	5	NA	0	3	0	5	NA	1	5	5	5	5	1	5	NA	5	3	3	5	1
	Average	316	4.7	300	1.6	0.5	NA	NA	70	NA	200	NA	40	210	11	40	4.8	290	0.33	NA	0.0120	0.0041	0.0018	0.0010	225
	SD	17	1.5	110	0.0	0.1	NA	NA	18	NA	40	NA	0	50	11	13	1.3	0	0.05	NA	0.0024	0.0011	0.0002	0.0005	0
B21	1			70	0.8	0.2	NA	<17	<15	<16	60	NA	<1	70	3	3	2.2	<220	0.23	NA	0.0082	NA	NA	0.0001	NA
	2			90	0.8	0.2	NA	<17	<15	<15	80	NA	<1	90	1	1	2.1	<190	0.26	NA	0.0102	NA	NA	0.0001	NA
	3			210	0.7	0.3	NA	<30	<20	<24	130	NA	<1	150	<1	<1	2.3	<240	0.47	NA	0.0185	NA	NA	NA	NA
	N	3	3	3	3	3	NA	0	0	0	3	NA	0	3	2	2	3	0	3	NA	3	0	0	2	0
	Average	291	2.1	120	0.7	0.2	NA	NA	NA	NA	90	NA	NA	100	2	2	2.2	NA	0.32	NA	0.0123	NA	NA	0.0001	NA
	SD	25	0.3	70	0.0	0.1	NA	NA	NA	NA	40	NA	NA	40	1	1	0.1	NA	0.13	NA	0.0055	NA	NA	0.0001	NA
Post-ore Calcite																									
B39a	1			70	1.1	0.2	NA	<30	<30	<30	70	NA	<1	70	<2	<1	2.6	<460	0.18	NA	0.0063	NA	NA	NA	NA
	2			<3	1.2	0.5	NA	20	20	<6	30	NA	<1	<1	1	3	3.2	<150	0.45	NA	0.0023	0.0017	0.0006	0.0001	NA
	3			<2	1.2	0.5	NA	12	90	<5	30	NA	<1	<1	1	5	4.2	<260	0.44	NA	0.0024	0.0079	0.0022	0.0001	NA
	4			230	1.1	0.4	NA	<30	<26	<27	120	NA	<1	160	<2	<1	5.2	<420	0.34	NA	0.0111	NA	NA	NA	NA
	5			200	1.0	0.5	NA	<50	<50	<50	170	NA	<2	190	<2	3	5.0	<600	0.49	NA	0.0165	NA	NA	0.0001	NA
	6			280	1.0	0.6	NA	<100	<100	<100	160	NA	<3	200	<8	3	<5.5	<320	0.59	NA	0.0156	NA	NA	NA	NA
	N	3	3	4	6	6	NA	2	2	0	6	NA	0	4	2	4	5	0	6	NA	6	2	2	3	0
	Average	210	1.9	200	1.1	0.5	NA	15	60	NA	100	NA	NA	150	1	3	4.0	NA	0.41	NA	0.0090	0.0048	0.0014	0.0001	NA
	SD	7	0.3	90	0.1	0.1	NA	5	50	NA	60	NA	NA	60	0	1	1.1	NA	0.14	NA	0.0063	0.0044	0.0011	0.0000	NA
B39b	1			<30	0.7	<0.2	NA	<60	<50	<60	40	NA	<2	40	<3	16	3.5	<750	NA	NA	0.0058	NA	NA	0.0005	NA

2			160	0.7	0.2	NA	<8	<7	7	70	NA	<1	90	1	<1	2.3	100	0.28	NA	0.0101	NA	NA	NA	233
3			160	0.7	0.2	NA	<14	13	<14	50	NA	<1	70	3	<1	3.3	130	0.23	NA	0.0080	0.0019	0.0004	NA	255
4			90	0.7	0.1	NA	<20	<19	<19	50	NA	15	60	3	<1	2.8	<350	0.18	NA	0.0078	NA	NA	NA	NA
5			60	0.7	<0.3	NA	<90	<80	<80	40	NA	<3	40	<3	<1	4.8	<950	NA	NA	0.0049	NA	NA	NA	NA
6			50	0.7	0.2	NA	<3	24	8	30	NA	<1	7	12	83	1.6	50	0.23	NA	0.0043	0.0035	0.0015	0.0051	349
N	4	4	5	6	4	NA	0	2	2	6	NA	1	6	4	2	6	3	4	NA	6	2	2	2	3
Average	248	3.1	100	0.7	0.2	NA	NA	19	7	50	NA	15	50	5	50	3.0	90	0.23	NA	0.0068	0.0027	0.0009	0.0028	279
SD	15	0.2	50	0.0	0.0	NA	NA	8	0	14	NA	0	30	5	47	1.1	40	0.04	NA	0.0022	0.0011	0.0008	0.0033	62

Note: Concentrations are reported in wt. % or ppm; temperature values in degrees Celsius (°C), and salinity values as wt percent NaCl equiv (wt. % NaCl eqv). Data are also reported as assemblage averages with 1 standard deviation (SD).

N = the number of available data for each assemblage, and NA = not applicable.

Appendix 6-4. Microthermometric results from this study.

Pre-ore Pyroxene

Assemblages	FI type	P&S	Homogenization temperature	Halite dissolution temperature	Salinity
B4-1a	S	P	464	370	44.4
B4-1a	S	P	458	407	48.2
B4-1a	S	P	416	345	41.9
B4-1a	S	P	409	341	41.6
B4-1a	S	P	437	366	44.0
B4-1a	S	P	450	354	42.8
B4-1a	S	P	452	381	45.4
B4-1a	S	P	445	391	46.5
B4-1a	S	P	440	378	45.2
N			9	9	9
Average			441	370	44.4
SD			18	22	2.2
B4-1b	S	P	438	379	45.2
B4-1b	S	P	410	352	42.5
B4-1b	S	P	450	439	51.9
B4-1b	S	P	424	391	46.5
B4-1b	S	P	418	379	45.2
B4-1b	S	P	427	388	46.1
B4-1b	S	P	414	367	44.0
B4-1b	S	P	446	411	48.7
B4-1b	S	P	439	397	47.1
B4-1b	S	P	445	389	46.2
B4-1b	S	P	434	406	48.1
B4-1b	S	P	434	337	41.2
N			12	12	12
Average			432	386	46.1
SD			13	27	2.8
B4-1c	S	P	451	323	40.0
B4-1c	S	P	464	366	43.9
B4-1c	S	P	463	378	45.1
B4-1c	S	P	476	296	37.8
B4-1c	S	P	478	387	46.0
B4-1c	S	P	467	378	45.2
B4-1c	S	P	469	378	45.1
B4-1c	S	P	480	380	45.3
N			8	8	8
Average			469	361	43.6
SD			10	33	3.0
B7-1	S	P	490	293	37.6
B7-1	S	P	478	314	39.3
B7-1	S	P	487	290	37.4
B7-1	S	P	480	311	38.1
N			4	4	4
Average			484	302	38.1
SD			6	12	0.9

B9-3a	S	P	486	385	45.9
B9-3a	S	P	489	368	44.1
B9-3a	S	P	531	400	47.5
B9-3a	S	P	504	402	47.7
B9-3a	S	P	514	394	46.8
B9-3a	S	P	509	375	44.8
B9-3a	S	P	497	363	43.6
B9-3a	S	P	503	358	43.2
N			8	8	8
Average			504	381	45.5
SD			14	17	1.8
B9-3b	S	P	483	406	48.1
B9-3b	S	P	477	337	41.2
B9-3b	S	P	438	327	40.4
B9-3b	S	P	435	349	42.3
B9-3b	S	P	436	411	48.7
B9-3b	S	P	459	352	42.5
B9-3b	S	P	465	379	45.2
B9-3b	S	P	439	368	44.0
B9-3b	S	P	429	427	50.4
B9-3b	S	P	432	367	44.0
B9-3b	S	P	432	379	45.2
N			11	11	11
Average			448	373	44.7
SD			20	32	3.2
B27	S	P	468	353	42.7
B27	S	P	472	378	45.1
B27	S	P	458	339	41.4
B27	S	P	466	341	41.6
B27	S	P	456	375	44.8
B27	S	P	479	339	41.4
B27	S	P	455	380	45.3
N			7	7	7
Average			465	358	43.2
SD			9	19	1.8
B25-1	S	P	500	281	36.6
B25-1	S	P	484	284	36.8
B25-1	S	P	490	273	36.1
B25-1	S	P	493	277	36.3
N			4	4	4
Average			492	279	36.5
SD			7	5	0.3
B28a	S	P	510	333	40.9
B28a	S	P	525	453	53.7
B28a	S	P	530	327	40.4
B28a	S	P	538	427	50.4
B28a	S	P	481	296	37.8
B28a	S	P	465	314	39.3
B28a	S	P	467	306	38.6

B28a	S	P	471	379	45.2
B28a	S	P	478	323	40.0
B28a	S	P	526	337	41.2
B28a	S	P	496	368	44.0
B28a	S	P	518	314	39.3
B28a	S	P	468	325	40.2
B28a	S	P	476	317	39.5
B28a	S	P	500	306	38.6
N	S		15	15	15
Average	S		497	342	41.9
SD	S		26	46	4.6
B28b	S	P	463	345	41.9
B28b	S	P	497	327	40.4
B28b	S	P	471	314	39.3
B28b	S	P	444	323	40.0
B28b	S	P	476	328	40.4
B28b	S	P	495	369	44.2
B28b	S	P	463	332	40.8
B28b	S	P	462	327	40.4
N			8	8	8
Average			471	333	40.9
SD			18	17	1.5
B16-1a	S	P	446	353	42.7
B16-1a	S	P	436	365	43.8
B16-1a	S	P	419	325	40.2
B16-1a	S	P	485	307	38.8
B16-1a	S	P	479	317	39.5
B16-1a	S	P	437	355	42.9
B16-1a	S	P	463	332	40.8
B16-1a	S	P	464	327	40.4
N			8	8	8
Average			454	335	41.1
SD			23	20	1.8
B16-2a	S	P	473	359	43.2
B16-2a	S	P	488	363	43.7
B16-2a	S	P	464	364	43.8
B16-2a	S	P	472	360	43.4
B16-2a	S	P	472	353	42.7
N			5	5	5
Average			474	360	43.4
SD			9	4	0.4
B16-1b	S	P	477	325	40.2
B16-1b	S	P	501	323	40.0
B16-1b	S	P	508	337	41.3
B16-1b	S	P	506	351	42.4
B16-1b	S	P	470	393	46.7
B16-1b	S	P	488	359	43.2
B16-1b	S	P	479	336	41.2
B16-1b	S	P	506	337	41.3

B16-1b	S	P	503	363	43.7
N			9	9	9
Average			493	347	42.2
SD			15	22	2.1
B16-2b	S	P	476	284	36.8
B16-2b	S	P	470	294	37.7
B16-2b	S	P	482	310	39.0
N			3	3	3
Average			476	296	37.8
SD			6	13	1.1

Syn-ore Sphalerite

Assemblages	FI type	P&S	Final melting temperature	Homogenization temperature	Salinity
B13-3a	L	P	-3.8	353	6.2
B13-3a	L	P	-4.5	341	7.2
B13-3a	L	P	-5.2	342	8.1
B13-3a	L	P	-3.7	343	6.0
B13-3a	L	P	-3.9	345	6.3
B13-3a	L	P	-3.7	364	6.0
N			6	6	6
Average			-4.1	348	6.6
SD			0.6	9	0.8
B13-3b	L	P	-5.4	344	8.4
B13-3b	L	P	-6.8	394	10.2
B13-3b	L	P	-6.2	340	9.5
N			3	3	3
Average			-6.1	359	9.4
SD			0.7	30	0.9
B13-3c	L	P	-2.8	336	4.6
B13-3c	L	P	-1.1	327	1.9
B13-3c	L	P	-3.9	333	6.3
B13-3c	L	P	-3.1	334	5.1
B13-3c	L	P	-3.2	345	5.3
B13-3c	L	P	-4.8	337	7.6
B13-3c	L	P	-5.4	338	8.4
N			7	7	7
Average			-3.5	336	5.6
SD			1.4	5	2.1
B13-3d	L	P	-4.2	340	6.7
B13-3d	L	P	-4.4	387	7.0
B13-3d	L	P	-4.8	377	7.6
N			3	3	3
Average			-4.5	368	7.1
SD			0.3	25	0.5
B-2	L	P	-5.0	322	7.9
B-2	L	P	-5.4	321	8.4
B-2	L	P	-7.3	331	10.9
B-2	L	P	-4.4	325	7.0

B-2	L	P	-3.5	322	5.7
B-2	L	P	-4.3	315	6.9
N			6	6	6
Average			-5.0	323	7.8
SD			1.3	5	1.8
B30a	L	P	-5.0	340	7.9
B30a	L	P	-5.5	350	8.6
N			2	2	2
Average			-5.3	345	8.3
SD			0.4	7	0.5
B30b	L	P	-2.8	317	4.6
B30b	L	P	-3.2	315	5.3
B30b	L	P	-2.9	301	4.8
N			3	3	3
Average			-3.0	311	4.9
SD			0.2	9	0.4
B14-1	L	P	-3.6	351	5.8
B14-1	L	P	-4.1	330	6.6
B14-1	L	P	-4.3	296	6.9
B14-1	L	P	-3.6	335	5.8
N			4	4	4
Average			-3.9	328	6.3
SD			0.4	23	0.6
B14-2	L	P	-2.3	319	3.9
N			1	1	1
Average			-2.3	319	3.9
SD			0.0	0	0.0

Syn-ore Calcite

Assemblages	FI type	P&S	Final melting temperature	Homogenization temperature	Salinity
B19a	L	P	-3.9	349	6.3
B19a	L	P	-3.7	288	6.0
B19a	L	P	-4.5	361	7.2
B19a	L	P	-5.2	352	8.1
N			4	4	4
Average			-4.3	338	6.9
SD			0.7	33	0.9
B14-3	L	P	-3.8	332	6.2
B14-3	L	P	-4.5	305	7.2
B14-3	L	P	-3.7	321	6.0
B14-3	L	P	-3.9	305	6.3
B14-3	L	P	-3.7	348	6.0
B14-3	L	P	-4.0	350	6.5
B14-3	L	P	-3.2	344	5.3
N			7	7	7
Average			-3.8	329	6.2
SD			0.4	19	0.6
B13-3e	L	P	-6.9	376	10.4

B13-3e	L	P	-4.5	350	7.2
B13-3e	L	P	-4.8	369	7.6
B13-3e	L	P	-4.6	346	7.3
B13-3e	L	P	-4.1	334	6.7
N			5	5	5
Average			-5.0	355	7.8
SD			1.1	17	1.5
B19b	L	P	-3.7	326	6.0
B19b	L	P	-3.5	321	5.7
B19b	L	P	-2.4	319	4.0
B19b	L	P	-3.3	327	5.4
B19b	L	P	-1.4	287	2.4
N			5	5	5
Average			-2.9	316	4.7
SD			1.0	17	1.5
B21	L	P	-1.7	268	2.9
B21	L	P	-1.9	318	3.2
B21	L	P	-1.9	288	3.2
N			3	3	3
Average			-1.8	291	3.1
SD			0.1	25	0.2

Post-ore Calcite

Assemblages	FI type	P&S	Final melting temperature	Homogenization temperature	Salinity
B39a	L	S	-1.3	204	2.2
B39a	L	S	-1.4	209	2.4
B39a	L	S	-1.0	218	1.8
N			3	3	3
Average			-1.2	210	2.1
SD			0.2	7	0.3
B39b	L	S	-1.2	270	2.1
B39b	L	S	-0.9	240	1.6
B39b	L	S	-1.0	245	1.8
B39b	L	S	-1.3	238	2.2
N			4	4	4
Average			-1.1	248	1.9
SD			0.2	15	0.3

Note: FI (fluid inclusion) types are defined in the text. N = number; SD = 1 standard deviation. Temperature values are reported in degrees Celsius (°C), salinity values as wt percent NaCl equiv (wt % NaCl eqv) and pressure values as bars. P&S represent primary and secondary inclusions, respectively.

Appendix 6-5. Chemical compositions of host minerals from LA-ICP-MS analyses.

Sample No.	Li	Na	Mg	Si	Cl	K	Ca	Mn	Fe	Cu	Zn	As	Br	Rb	Sr	Ag	Cs	Ba	Pb
Pre-ore Pyroxene																			
B4-1a	BD	1877	7155	NA	BD	BD	165809	39164	205462	BD	650	BD	BD	1.12	5.0	BD	1.14	BD	4.5
B4-1a	BD	241	10359	NA	BD	28	165809	137949	145912	BD	454	BD	BD	0.23	4.2	BD	0.15	BD	3.4
B4-1a	BD	1123	11136	NA	BD	BD	165809	41963	174102	BD	641	BD	BD	BD	5.2	BD	0.21	BD	4.8
B4-1a	BD	320	8358	NA	BD	BD	165809	33320	164462	BD	565	BD	BD	BD	4.3	BD	0.02	BD	3.7
B4-1a	BD	811	9522	NA	BD	BD	165809	40818	166128	BD	600	BD	BD	BD	4.4	BD	0.20	BD	2.5
B4-1a	40	1196	10110	NA	BD	BD	165809	32959	147461	BD	424	BD	BD	0.51	5.1	BD	0.65	BD	8.3
B4-1a	BD	970	5744	NA	BD	BD	165809	37238	154462	BD	451	BD	BD	BD	4.1	BD	BD	BD	0.8
B4-1a	BD	889	10753	NA	BD	BD	165809	36413	160485	BD	576	BD	BD	BD	4.7	BD	0.06	BD	1.1
B4-1a	BD	903	9909	NA	BD	BD	165809	36826	151926	BD	831	BD	BD	BD	4.3	BD	0.04	BD	1.2
B4-1a	BD	756	6023	NA	BD	BD	165809	24438	169030	BD	539	BD	BD	BD	5.4	BD	0.14	BD	0.9
B4-1b	BD	577	9442	NA	BD	BD	165809	34652	159453	BD	456	BD	BD	BD	4.2	BD	BD	BD	1.1
B4-1b	BD	2550	4710	NA	BD	BD	165809	34538	193143	BD	586	BD	BD	0.59	5.6	BD	1.09	BD	8.9
B4-1b	BD	3560	11745	NA	BD	BD	165809	42962	187775	BD	645	BD	BD	2.94	6.6	BD	0.65	BD	2.5
B4-1b	BD	1760	8635	NA	BD	BD	165809	44291	171533	BD	497	BD	BD	1.65	4.8	BD	0.71	BD	16.2
B4-1b	BD	1209	13236	NA	BD	BD	165809	37272	171008	BD	499	BD	BD	0.68	5.0	BD	0.75	0.41	16.0
B4-1b	BD	5330	15572	NA	BD	461	165809	52819	201461	BD	900	BD	BD	1.32	15.4	BD	0.48	1.71	2.6
B4-1b	BD	742	15519	NA	BD	BD	165809	35991	163290	BD	487	BD	BD	0.43	4.9	BD	0.37	BD	2.9
B4-1b	BD	948	14701	NA	BD	BD	165809	40061	154188	BD	592	BD	BD	0.32	5.3	BD	0.43	BD	4.9
B4-1c	BD	983	8120	NA	BD	174	165809	28101	171744	BD	818	BD	BD	0.97	10.2	BD	0.58	0.65	1.0
B4-1c	BD	1105	12136	NA	BD	BD	165809	38945	162470	BD	512	BD	BD	BD	5.1	BD	0.13	BD	8.9
B4-1c	BD	1800	9800	NA	BD	BD	165809	42289	166646	BD	510	BD	BD	BD	4.2	BD	0.10	BD	2.7
B4-1c	BD	2301	9875	NA	BD	BD	165809	43915	180874	BD	522	BD	BD	BD	4.7	BD	0.28	BD	3.5
B4-1c	BD	2101	9678	NA	BD	BD	165809	48458	188813	BD	633	BD	BD	2.05	6.1	BD	0.77	1.31	17.5
B4-1c	BD	1126	8288	NA	BD	BD	165809	36778	170562	BD	535	BD	BD	0.22	5.8	BD	0.26	0.30	14.9
B4-1c	BD	2634	11434	NA	BD	BD	165809	47453	182868	BD	554	BD	BD	BD	5.4	BD	0.45	BD	3.6

B4-1c	BD	3795	10639	NA	BD	BD	165809	48891	189992	BD	462	BD	BD	BD	6.6	BD	0.32	BD	6.3
B4-1c	19	1134	7576	NA	BD	BD	165809	30404	176880	BD	595	BD	BD	BD	6.1	BD	0.38	BD	5.2
B4-1c	BD	442	9740	NA	3497	BD	165809	31915	149233	BD	437	BD	BD	0.15	4.1	BD	0.05	BD	2.0
B7-1	6	276	5755	NA	2392	BD	165809	23046	135221	BD	487	BD	BD	BD	3.9	BD	BD	BD	0.8
B7-1	BD	671	7723	NA	BD	BD	165809	35523	160311	BD	487	BD	BD	BD	4.2	BD	0.03	BD	1.4
B7-1	BD	371	8615	NA	181	BD	165809	31347	138402	BD	450	BD	BD	BD	3.8	BD	0.04	BD	1.5
B7-1	BD	1734	7865	NA	5439	BD	165809	39616	180297	BD	624	BD	BD	BD	4.6	BD	0.17	BD	3.0
B7-1	BD	1382	9630	NA	6937	BD	165809	37656	157399	BD	809	BD	BD	0.73	5.4	BD	1.13	0.31	10.2
B9-3a	BD	694	BD	NA	3382	BD	165809	3018	167215	BD	BD	BD	BD	BD	5.3	BD	BD	0.86	5.7
B9-3a	BD	536	4965	NA	BD	63	165809	27783	171921	BD	567	BD	BD	1.09	6.9	BD	1.02	0.61	9.9
B9-3a	BD	419	6638	NA	BD	BD	165809	25771	155997	BD	498	BD	BD	BD	5.0	BD	BD	BD	0.7
B9-3a	BD	1522	6908	NA	3262	BD	165809	34464	194846	BD	604	BD	BD	BD	5.8	BD	0.11	BD	3.2
B9-3a	BD	412	5800	NA	BD	BD	165809	23244	156495	BD	492	BD	BD	0.07	5.1	BD	0.37	0.43	0.9
B9-3a	BD	647	7501	NA	25	BD	165809	26039	157804	BD	548	BD	BD	0.47	7.9	BD	0.60	0.52	6.4
B9-3a	31	1014	10443	NA	1543	BD	165809	30577	180413	BD	533	BD	BD	BD	5.6	BD	BD	BD	3.0
B9-3a	BD	629	9229	NA	BD	BD	165809	28445	154932	BD	488	BD	BD	BD	5.2	BD	BD	BD	1.4
B9-3a	BD	860	7809	NA	654	BD	165809	30532	162363	BD	496	BD	BD	BD	5.3	BD	0.14	0.11	2.2
B9-3a	BD	801	11375	NA	648	BD	165809	30424	171564	BD	531	BD	BD	BD	5.6	BD	BD	BD	0.9
B9-3a	35	1031	12088	NA	1584	BD	165809	34220	187897	BD	549	BD	BD	BD	6.7	BD	0.30	BD	3.4
B9-3b	BD	498	9109	NA	8	103	165809	29057	171702	BD	497	BD	BD	1.94	7.6	BD	1.08	1.34	1.6
B9-3b	BD	909	10658	NA	390	BD	165809	28613	163552	BD	501	BD	BD	BD	5.2	BD	0.06	0.51	1.8
B9-3b	BD	700	11198	NA	459	BD	165809	33210	180311	BD	566	BD	BD	BD	5.3	BD	0.07	BD	1.8
B9-3b	BD	1024	9754	NA	805	BD	165809	30877	167957	BD	526	BD	BD	BD	5.2	BD	0.07	0.13	1.4
B9-3b	BD	1085	9508	NA	1131	BD	165809	30866	179572	BD	558	BD	BD	BD	6.2	BD	BD	BD	1.1
B27	9	434	7558	NA	BD	56	165809	NA	180349	BD	449	BD	BD	0.52	5.7	BD	0.41	0.25	11.4
B27	6	302	7784	NA	153	BD	165809	NA	170064	BD	482	BD	BD	0.42	6.3	BD	0.64	0.36	6.8
B27	8	409	10588	NA	214	BD	165809	NA	177840	BD	467	BD	BD	BD	5.4	BD	0.39	0.23	4.8
B27	7	290	10987	NA	400	BD	165809	NA	181091	BD	465	BD	BD	BD	5.4	BD	0.03	BD	1.6
B25-1	8	317	10176	NA	12	BD	165809	NA	163665	BD	454	BD	BD	0.34	5.3	BD	0.40	0.13	10.7

B25-1	11	682	10602	NA	3035	BD	165809	NA	208533	BD	618	BD	BD	BD	8.4	BD	0.44	BD	2.6
B25-1	8	361	10511	NA	BD	BD	165809	NA	172996	BD	495	BD	BD	BD	6.6	BD	0.03	BD	1.1
B28a	5	BD	7598	232798	BD	BD	124162	NA	152624	BD	433	BD	BD	BD	4.0	BD	0.12	BD	1.6
B28a	6	BD	6267	232798	BD	BD	158095	NA	169838	BD	478	BD	BD	1.51	6.5	BD	1.17	1.07	1.7
B28a	7	BD	10429	232798	BD	BD	171346	NA	174784	BD	474	BD	BD	BD	7.1	BD	0.02	BD	0.7
B28a	10	BD	8132	232798	BD	BD	141961	NA	176272	BD	497	BD	BD	BD	4.1	BD	0.17	BD	3.3
B28a	11	BD	7029	232798	BD	BD	122451	NA	145606	BD	454	BD	BD	0.37	4.6	BD	0.39	0.29	8.5
B28b	2	BD	7634	232798	BD	BD	165991	NA	185761	BD	236	BD	BD	BD	2.4	BD	0.02	BD	0.7
B28b	8	BD	6702	232798	BD	BD	153630	NA	177077	BD	266	BD	BD	0.31	2.5	BD	0.11	BD	1.4
B28b	2	BD	9008	232798	BD	BD	149429	NA	165242	BD	227	BD	BD	BD	2.4	BD	0.02	BD	0.4
B28b	8	BD	7885	232798	BD	227	148257	NA	158768	BD	473	BD	BD	2.21	6.9	BD	0.13	0.98	2.6
B28b	6	BD	6713	232798	BD	BD	139500	NA	163254	BD	439	BD	BD	BD	4.3	BD	0.10	BD	2.8
B28b	10	BD	9066	232798	BD	BD	138367	NA	163036	BD	486	BD	BD	0.64	7.2	BD	0.77	BD	3.8
B28b	7	BD	8616	232798	BD	BD	141344	NA	170255	BD	628	BD	BD	0.28	5.5	BD	0.66	0.77	1.9
B28b	7	BD	8881	232798	BD	BD	165031	NA	170804	BD	505	BD	BD	BD	5.5	BD	0.27	0.84	1.3
B28b	6	BD	10629	232798	BD	BD	184804	NA	178882	BD	472	BD	BD	BD	5.4	BD	BD	BD	0.8
B16-1a	4	BD	8010	232798	BD	BD	130954	NA	152252	BD	436	BD	BD	BD	4.7	BD	0.14	BD	2.1
B16-1a	7	BD	10782	232798	BD	BD	178979	NA	175327	BD	482	BD	BD	0.39	6.9	BD	0.62	0.13	7.0
B16-1a	7	BD	8735	232798	BD	70	148982	NA	166922	BD	475	BD	BD	0.87	6.0	BD	0.59	0.45	13.6
B16-1a	8	BD	6984	232798	BD	BD	121045	NA	147094	BD	418	BD	BD	BD	4.4	BD	0.35	BD	8.5
B16-1a	7	BD	9746	232798	BD	BD	155662	NA	154696	BD	459	BD	BD	BD	5.5	BD	BD	BD	12.6
B16-2a	3	BD	9463	232798	BD	BD	156479	NA	151321	BD	403	BD	BD	BD	5.5	BD	0.10	0.52	4.9
B16-2a	9	BD	9938	232798	BD	BD	160421	NA	160707	BD	453	BD	BD	BD	5.8	BD	0.06	0.08	1.7
B16-2a	5	BD	11487	232798	BD	BD	179796	NA	182234	BD	486	BD	BD	BD	5.3	BD	0.06	0.22	1.9
B16-2a	8	BD	11608	232798	BD	BD	165324	NA	169331	BD	440	BD	BD	BD	4.3	BD	0.11	BD	4.6
B16-1b	4	BD	8288	232798	BD	BD	171836	NA	166988	BD	415	BD	BD	BD	4.9	BD	BD	0.26	0.9
B16-1b	7	BD	8587	232798	BD	BD	165012	NA	169998	BD	495	BD	BD	0.15	5.5	BD	0.15	0.51	5.1
B16-1b	8	BD	9983	232798	BD	BD	164928	NA	157288	BD	632	BD	BD	0.60	7.0	BD	0.92	0.49	2.1
B16-2b	5	BD	6760	232798	BD	BD	134949	NA	159857	BD	431	BD	BD	BD	4.1	BD	0.06	BD	2.2

B16-2b	11	BD	7812	232798	BD	BD	129212	NA	138822	BD	361	BD	BD	BD	4.9	BD	0.12	BD	3.8
B16-2b	4	BD	8054	232798	BD	BD	132208	NA	160290	BD	400	BD	BD	BD	3.5	BD	0.04	BD	1.6
Syn-ore Sphalerite																			
B13-3d	BD	119	BD	NA	287	BD	BD	833	2382	8.0	590000	BD	BD	BD	BD	8.3	BD	BD	0.3
B13-3d	BD	133	BD	NA	238	BD	BD	792	2471	13.3	590000	BD	BD	BD	BD	13.7	BD	BD	2.2
B13-3d	BD	306	BD	NA	852	BD	BD	585	1945	10.5	590000	BD	BD	BD	BD	10.6	BD	BD	1.9
B13-3d	BD	361	BD	NA	528	BD	BD	747	2295	11.2	590000	BD	BD	BD	BD	8.2	BD	BD	1.0
B13-3a	BD	59	BD	NA	BD	BD	BD	576	10638	2.9	590000	BD	BD	BD	BD	4.0	BD	BD	0.3
B13-3a	BD	182	BD	NA	199	BD	BD	711	12740	4.2	590000	BD	BD	BD	BD	6.5	BD	BD	0.6
B13-3a	BD	121	BD	NA	112	BD	BD	702	11982	3.7	590000	BD	BD	BD	BD	15.7	BD	BD	2.9
B13-3a	BD	101	BD	NA	-28	BD	BD	685	12225	2.0	590000	BD	BD	BD	BD	6.0	BD	BD	0.5
B13-3a	BD	96	BD	NA	198	BD	BD	714	12591	2.3	590000	BD	BD	BD	BD	5.8	BD	BD	0.5
B13-3a	BD	62	BD	NA	BD	BD	BD	697	12084	4.0	590000	BD	BD	BD	BD	6.8	BD	BD	1.0
B13-3b	BD	94	BD	NA	911	BD	BD	562	3230	15.6	590000	BD	BD	BD	BD	14.2	BD	BD	1.0
B13-3b	BD	91	BD	NA	BD	BD	BD	700	3765	5.4	590000	BD	BD	BD	BD	8.7	BD	BD	0.7
B13-3b	BD	163	BD	NA	665	BD	BD	615	3311	14.4	590000	BD	BD	BD	BD	13.8	BD	BD	0.9
B13-3b	BD	185	BD	NA	914	BD	BD	1059	5727	15.2	590000	BD	BD	BD	BD	5.6	BD	BD	0.8
B13-3b	BD	469	BD	NA	3883	BD	BD	668	3919	11.2	590000	BD	BD	BD	BD	6.1	BD	BD	0.7
B13-3c	BD	146	BD	NA	631	BD	BD	1171	4688	11.8	590000	BD	BD	BD	BD	6.9	BD	BD	1.7
B13-3c	BD	106	BD	NA	BD	BD	BD	1203	5184	16.1	590000	BD	BD	BD	BD	8.2	BD	BD	0.7
B13-3c	BD	321	BD	NA	2497	BD	BD	758	3508	13.0	590000	BD	BD	BD	BD	6.2	BD	BD	0.5
B13-3c	BD	114	BD	NA	832	BD	BD	1760	6614	9.8	590000	BD	BD	BD	BD	4.7	BD	BD	0.4
B13-3c	BD	247	BD	NA	2404	BD	BD	1067	4570	8.2	590000	BD	BD	BD	BD	9.2	BD	BD	1.6
B13-3c	BD	165	BD	NA	2980	BD	BD	964	4304	9.5	590000	BD	BD	BD	BD	6.1	BD	BD	0.6
B-2	BD	241	BD	NA	8514	BD	BD	660	2577	12.3	590000	BD	BD	BD	BD	8.3	BD	BD	1.0
B-2	BD	224	BD	NA	6616	BD	BD	779	2985	15.8	590000	BD	BD	BD	BD	10.4	BD	BD	0.9
B-2	BD	256	BD	NA	3544	BD	BD	706	2496	14.7	590000	BD	BD	BD	BD	15.8	BD	BD	0.9
B-2	BD	162	BD	NA	1375	BD	BD	753	2835	19.6	590000	BD	BD	BD	BD	27.9	BD	BD	4.3
B-2	BD	138	BD	NA	BD	BD	BD	764	2927	17.9	590000	BD	BD	BD	BD	20.5	BD	BD	3.6

B30a	BD	BD	BD	NA	309	BD	BD	1067	4993	14.5	590000	BD	BD	BD	BD	24.1	BD	BD	4.0
B30a	BD	BD	BD	NA	405	BD	BD	703	3694	11.6	590000	BD	BD	BD	BD	16.7	BD	BD	2.0
B30a	BD	BD	BD	NA	83	BD	BD	937	19252	3.0	590000	BD	BD	BD	BD	8.7	BD	BD	0.5
B30a	BD	BD	BD	NA	240	BD	BD	1770	7217	12.4	590000	BD	BD	BD	BD	9.4	BD	BD	0.7
B30a	BD	BD	BD	NA	96	BD	BD	1755	7305	15.8	590000	BD	BD	BD	BD	9.5	BD	BD	0.8
B30a	BD	BD	BD	NA	366	BD	BD	1251	5389	14.8	590000	BD	BD	BD	BD	9.1	BD	BD	0.6
B30a	BD	BD	BD	NA	387	BD	BD	894	4038	12.2	590000	BD	BD	BD	BD	12.5	BD	BD	1.4
B30a	BD	BD	BD	NA	673	BD	BD	1351	5147	13.6	590000	BD	BD	BD	BD	8.2	BD	BD	1.1
B30b	BD	BD	BD	NA	652	BD	BD	662	3198	11.2	590000	BD	BD	BD	BD	12.0	BD	BD	1.3
B30b	BD	BD	BD	NA	995	BD	BD	660	3118	10.1	590000	BD	BD	BD	BD	10.5	BD	BD	1.1
B30b	BD	BD	BD	NA	1556	BD	BD	539	2606	9.9	590000	BD	BD	BD	BD	15.0	BD	BD	1.2
B30b	BD	BD	BD	NA	333	BD	BD	848	4065	12.4	590000	BD	BD	BD	BD	7.9	BD	BD	0.7
B30b	BD	BD	BD	NA	3988	BD	BD	565	2703	14.5	590000	BD	BD	BD	BD	7.8	BD	BD	0.9
B14-1	BD	BD	BD	NA	BD	BD	BD	1008	5026	17.7	590000	BD	BD	BD	BD	11.3	BD	BD	1.4
B14-1	BD	BD	BD	NA	BD	BD	BD	862	4155	15.0	590000	BD	BD	BD	BD	8.4	BD	BD	0.9
B14-1	BD	BD	BD	NA	BD	BD	BD	1585	6234	14.3	590000	BD	BD	BD	BD	21.9	BD	BD	5.9
B14-1	BD	BD	BD	NA	BD	BD	BD	961	3505	20.2	590000	BD	BD	BD	BD	13.5	BD	BD	1.8
B14-1	BD	BD	BD	NA	BD	BD	BD	1061	3644	11.9	590000	BD	BD	BD	BD	19.0	BD	BD	2.8
B14-1	BD	BD	BD	NA	BD	BD	BD	1027	3321	15.1	590000	BD	BD	BD	BD	18.0	BD	BD	1.9
B14-1	BD	BD	BD	NA	BD	BD	BD	969	2989	19.8	590000	BD	BD	BD	BD	16.1	BD	BD	1.0
B14-1	BD	BD	BD	NA	BD	BD	BD	919	3127	9.7	590000	BD	BD	BD	BD	20.0	BD	BD	3.2
B14-2	BD	BD	BD	NA	BD	BD	BD	996	2881	17.5	590000	BD	BD	BD	BD	28.1	BD	BD	3.1
B14-2	BD	BD	BD	NA	BD	BD	BD	1029	3154	13.5	590000	BD	BD	BD	BD	27.6	BD	BD	2.3
B14-2	BD	BD	BD	NA	BD	BD	BD	985	3205	14.9	590000	BD	BD	BD	BD	20.0	BD	BD	10.8
B14-2	BD	BD	BD	NA	BD	BD	BD	1052	3055	10.0	590000	BD	BD	BD	BD	17.4	BD	BD	2.6
B14-2	BD	BD	BD	NA	BD	BD	BD	1098	3873	15.9	590000	BD	BD	BD	BD	12.5	BD	BD	4.6
B14-2	BD	BD	BD	NA	BD	BD	BD	968	3015	10.9	590000	BD	BD	BD	BD	10.0	BD	BD	3.3
B14-2	BD	BD	BD	NA	BD	BD	BD	1493	3750	11.7	590000	BD	BD	BD	BD	12.1	BD	BD	0.8
B14-2	BD	BD	BD	NA	BD	BD	BD	1198	2973	10.2	590000	BD	BD	BD	BD	10.3	BD	BD	1.2

B14-2	BD	BD	BD	NA	BD	BD	BD	928	3122	19.5	590000	BD	BD	BD	BD	11.9	BD	BD	1.3
B14-2	BD	BD	BD	NA	BD	BD	BD	1394	3721	15.4	590000	BD	BD	BD	BD	14.8	BD	BD	3.6
B14-2	BD	BD	BD	NA	BD	BD	BD	939	3048	15.2	590000	BD	BD	BD	BD	15.0	BD	BD	2.0
B14-2	BD	BD	BD	NA	BD	BD	BD	1531	3726	9.0	590000	BD	BD	BD	BD	21.0	BD	BD	3.5
B14-2	BD	BD	BD	NA	BD	BD	BD	1333	6330	12.9	590000	BD	BD	BD	BD	13.0	BD	BD	0.3
B14-2	BD	BD	BD	NA	BD	BD	BD	1284	5940	8.6	590000	BD	BD	BD	BD	20.7	BD	BD	2.0
B14-2	BD	BD	BD	NA	BD	BD	BD	1596	7288	19.1	590000	BD	BD	BD	BD	13.3	BD	BD	0.9
B14-2	BD	BD	BD	NA	BD	BD	BD	1375	6537	13.2	590000	BD	BD	BD	BD	12.4	BD	BD	1.0
B14-2	BD	BD	BD	NA	BD	BD	BD	1345	6190	14.4	590000	BD	BD	BD	BD	10.8	BD	BD	0.7
B14-2	BD	BD	BD	NA	BD	BD	BD	1527	6660	13.2	590000	BD	BD	BD	BD	11.5	BD	BD	3.0
Syn-ore Calcite																			
B19a	BD	BD	BD	NA	326	BD	400000	NA	245	BD	BD	BD	BD	BD	96	BD	BD	0.13	1.5
B19a	BD	55	9	NA	20	BD	400000	NA	275	BD	BD	BD	BD	BD	105	BD	BD	0.14	1.7
B19a	BD	BD	9	NA	BD	BD	400000	NA	251	BD	BD	BD	BD	BD	100	BD	0.07	0.11	2.0
B19a	BD	BD	BD	NA	14	BD	400000	NA	242	BD	BD	BD	BD	BD	95	BD	0.07	0.08	1.1
B19a	BD	BD	BD	NA	139	BD	400000	NA	251	BD	BD	BD	BD	BD	100	BD	0.03	0.11	1.8
B19a	BD	88	BD	NA	BD	BD	400000	NA	240	BD	BD	BD	BD	BD	106	BD	0.04	0.18	0.8
B14-3	BD	458	BD	NA	BD	BD	400000	NA	246	BD	BD	BD	BD	BD	103	BD	0.08	0.47	1.6
B14-3	BD	BD	6	NA	BD	BD	400000	NA	242	BD	BD	BD	BD	BD	100	BD	0.03	0.07	1.2
B14-3	BD	BD	BD	NA	191	BD	400000	NA	259	BD	BD	BD	BD	BD	93	BD	0.03	BD	2.1
B14-3	BD	BD	BD	NA	63	BD	400000	NA	264	BD	BD	BD	BD	BD	105	BD	0.08	0.17	1.8
B14-3	BD	BD	9	NA	BD	BD	400000	NA	298	BD	BD	BD	BD	BD	110	BD	0.07	0.17	1.8
B14-3	BD	186	BD	NA	365	BD	400000	NA	176	BD	BD	BD	BD	BD	90	BD	0.05	BD	1.3
B14-3	BD	BD	BD	NA	286	BD	400000	NA	173	BD	BD	BD	BD	BD	94	BD	BD	0.22	1.4
B13-3e	BD	BD	28	NA	244	BD	400000	943	323	BD	BD	BD	BD	BD	79	BD	BD	0.13	1.5
B13-3e	BD	BD	6	NA	257	BD	400000	827	261	BD	BD	BD	BD	BD	92	BD	BD	0.16	1.4
B13-3e	BD	BD	9	NA	359	BD	400000	803	254	BD	BD	BD	BD	BD	85	BD	0.03	0.08	1.4
B13-3e	BD	73	7	NA	216	BD	400000	866	225	BD	BD	BD	BD	BD	88	BD	BD	0.09	1.5
B13-3e	BD	347	394	NA	BD	BD	400000	244	474	BD	BD	BD	BD	BD	96	BD	0.04	0.20	1.2

B13-3e	BD	150	16	NA	226	BD	400000	1072	478	BD	BD	BD	BD	BD	110	BD	0.06	0.92	1.1
B13-3e	BD	BD	BD	NA	BD	BD	400000	852	246	BD	BD	BD	BD	BD	86	BD	0.07	0.07	1.5
B19b	BD	BD	BD	NA	BD	BD	400000	981	320	BD	BD	BD	BD	BD	91	BD	0.04	0.25	1.4
B19b	BD	BD	BD	NA	BD	BD	400000	847	265	BD	BD	BD	BD	BD	87	BD	0.07	0.24	2.2
B19b	BD	BD	128	NA	BD	BD	400000	11802	2766	BD	BD	BD	BD	BD	149	BD	BD	0.25	1.8
B19b	BD	BD	95	NA	BD	BD	400000	9002	2012	BD	BD	BD	BD	BD	122	BD	BD	0.14	2.1
B19b	BD	284	BD	NA	BD	BD	400000	909	283	BD	BD	BD	BD	BD	86	BD	0.02	0.09	1.3
B19b	BD	BD	BD	NA	274	BD	400000	882	269	BD	BD	BD	BD	BD	97	BD	BD	0.09	1.5
B19b	BD	BD	BD	NA	BD	BD	400000	944	356	BD	BD	BD	BD	BD	88	BD	0.04	0.13	1.2
B19b	BD	BD	BD	NA	235	BD	400000	1293	304	BD	BD	BD	BD	BD	99	BD	0.12	0.13	1.3
B21	BD	317	8	NA	BD	BD	400000	1055	270	BD	BD	BD	BD	BD	83	BD	BD	0.05	1.2
B21	BD	BD	BD	NA	BD	BD	400000	897	252	BD	BD	BD	BD	BD	87	BD	0.10	BD	1.2
B21	BD	174	BD	NA	BD	BD	400000	918	310	BD	BD	BD	BD	BD	119	BD	0.06	BD	2.4
B21	BD	BD	BD	NA	BD	BD	400000	789	193	BD	BD	BD	BD	BD	130	BD	BD	0.07	1.4
B21	BD	204	11	NA	232	BD	400000	1048	282	BD	BD	BD	BD	BD	113	BD	BD	0.16	1.0
B21	BD	BD	BD	NA	BD	BD	400000	851	208	BD	BD	BD	BD	BD	142	BD	0.18	0.17	1.6
B21	BD	BD	BD	NA	BD	BD	400000	935	173	BD	BD	BD	BD	BD	107	BD	0.11	0.10	1.5
B21	BD	BD	BD	NA	BD	BD	400000	818	223	BD	BD	BD	BD	BD	94	BD	BD	BD	1.2
B21	BD	BD	8	NA	276	BD	400000	1078	240	BD	BD	BD	BD	BD	95	BD	BD	0.13	1.2
B21	BD	BD	BD	NA	BD	BD	400000	860	224	BD	BD	BD	BD	BD	97	BD	BD	0.12	1.7
Post-ore Calcite																			
B39a	BD	BD	BD	NA	BD	BD	400000	836	243	BD	BD	BD	BD	BD	93	BD	BD	0.11	1.4
B39a	BD	BD	9	NA	BD	BD	400000	836	247	BD	BD	BD	BD	BD	93	BD	BD	0.10	1.1
B39a	BD	BD	BD	NA	180	BD	400000	913	239	BD	BD	BD	BD	BD	89	BD	BD	0.13	1.4
B39a	BD	654	BD	NA	BD	BD	400000	1229	467	BD	BD	BD	BD	BD	97	BD	0.05	0.39	1.8
B39a	BD	BD	BD	NA	165	BD	400000	872	212	BD	BD	BD	BD	BD	92	BD	BD	0.09	1.4
B39b	BD	BD	8	NA	BD	BD	400000	880	280	BD	BD	BD	BD	BD	93	BD	0.10	0.09	1.3
B39b	BD	BD	9	NA	162	BD	400000	887	277	BD	BD	BD	BD	BD	101	BD	BD	0.09	1.3
B39b	BD	89	10	NA	196	BD	400000	866	241	BD	BD	BD	BD	BD	93	BD	0.04	0.10	1.2

B39b	BD	BD	BD	NA	171	BD	400000	917	261	BD	BD	BD	BD	BD	93	BD	0.02	0.07	1.3
B39b	BD	BD	BD	NA	BD	BD	400000	840	236	BD	BD	BD	BD	BD	92	BD	0.01	BD	1.4
B39b	BD	BD	BD	NA	BD	BD	400000	933	346	BD	BD	BD	BD	BD	93	BD	0.18	0.16	1.6
B39b	BD	102	305	NA	BD	BD	400000	149	458	BD	BD	BD	BD	BD	101	BD	BD	BD	1.4
B39b	BD	874	536	NA	BD	BD	400000	187	804	BD	BD	BD	BD	BD	112	BD	BD	0.32	1.7

Note: NA = Not Analyzed; BD = Below Detection.

Addendum to published chapters (Chapters 2, 3, 5)

Chapter 2

Page 33, Column 1, Line 2:

Excluding the two youngest ages of
Accuracy for most trace elements is better than 5%.
should be changed to:
Accuracy for most trace elements is better than 5%. Detailed analytical procedures have been described in Song et al. (2010).

Page 34, section 5.2, Line 9:

Excluding the two youngest ages of 126 ± 2 Ma (HSG03-08) and 128 ± 2 Ma (HSG03-12), the calculated weighted mean age accommodating the 23 remaining analyses is 137.6 ± 0.9 Ma (95% confidence) with an MSWD of 1.2 (Fig. 7).
should be changed to:
The two youngest ages of 126 ± 2 Ma (HSG03-08) and 128 ± 2 Ma (HSG03-12) are slightly discordant, and therefore have been excluded. The calculated weighted mean age accommodating the 23 remaining analyses is 137.6 ± 0.9 Ma (95% confidence) with an MSWD of 1.2 (Fig. 7).

Page 42, Column 1, Line 67:

A reference should be added:
Song, S., Su, L., Li, X.H., Zhang, G., Niu, Y., and Zhang, L., 2010, Tracing the 850-Ma continental flood basalts from a piece of subducted continental crust in the North Qaidam UHPM belt, NW China: Precambrian Research, v. 183, p. 805–816.

Chapter 3

Page 48, Column 1, Line 1:

Homogenization temperatures of fluid inclusion in vein quartz ranges from 225 to 510 °C, implying that the veins probably have undergone several rounds of cracking-sealing at various temperatures.
Should be deleted.

Page 48, Column 2, Line 2:

Microthermometric study shows that the homogenization temperatures of the fluid inclusions in the quartz veinlets associated with early potassic alteration can reach up to 480 °C. Quartz in sulfides-bearing veins contain coexisting high salinity brine and low-salinity vapor inclusions, with homogenization temperatures of ~340 °C, indicating the occurrence of fluid boiling.
Should be deleted.

Chapter 5

Page 100, Column 1, Line 45:

Measured Pb isotope ratios were corrected for instrumental mass fractionation of 0.11% per atomic mass unit by references to repeated analyses of NBS-981 Pb standard.

should be changed to:

Measured Pb isotope ratios were corrected for instrumental mass fractionation of 0.11% per atomic mass unit by references to repeated analyses of NBS-981 Pb standard, which gave average values of $^{208}Pb/^{204}Pb$ = 36.53069 ± 0.00755, $^{207}Pb/^{204}Pb$ = 15.44008 ± 0.00314, and $^{206}Pb/^{204}Pb$ = 16.90041 ± 0.00329, with uncertainties of <0.1 % at the 95 % confidence level.

Page 108, Column 1, Line 4:

As shown in Table 5 and Figure 11, the lead isotope compositions of three different types of sulfides are similar and homogeneous, and coincide well with that of the Yanshanian plutonic rocks ($^{206}Pb/^{204}Pb$ = 18.25–18.35, $^{207}Pb/^{204}Pb$ = 15.50–15.56, and $^{208}Pb/^{204}Pb$ = 38.14–38.32; n = 7) but are significantly different from that of the Permian marble ($^{206}Pb/^{204}Pb$ = 18.37 and 18.45, $^{207}Pb/^{204}Pb$ = 15.68 and 15.70, and $^{208}Pb/^{204}Pb$ = 38.47 and 38.47) and other rock types (i.e., the Hercynian intrusions, the Indosinian subvolcanic rocks, and the Jurassic volcanic rocks) exposed within the Baiyinnuo’er mining areas.

should be changed to:

As shown in Table 5 and Figure 11, the lead isotope compositions of three different types of sulfides coincide well with that of the Yanshanian plutonic rocks ($^{206}Pb/^{204}Pb$ = 18.25–18.35, $^{207}Pb/^{204}Pb$ = 15.50–15.56, and $^{208}Pb/^{204}Pb$ = 38.14–38.32; n = 7), and show a mixing trend between the Yanshanian plutons and the Permian marble ($^{206}Pb/^{204}Pb$ = 18.37 and 18.45, $^{207}Pb/^{204}Pb$ = 15.68 and 15.70, and $^{208}Pb/^{204}Pb$ = 38.47 and 38.47), but are significantly different from that of the other rock types (i.e., the Hercynian intrusions, the Indosinian subvolcanic rocks, and the Jurassic volcanic rocks) exposed within the Baiyinnuo’er mining areas.

Page 113, Column 2, Line 34:

Newly obtained Pb isotope data in this study, combined with previously reported results by Zeng et al. (2009), give two narrow ranges for sulfides in the lead isotope diagrams as shown in Figure 11, which coincide well with the ranges for the Yanshanian granite and granodiorite. It is also clear that the lead isotopes for other rocks present in the mining areas (e.g., Permian marble, Jurassic volcanic, Indosinian subvolcanic rocks, and Hercynian intrusions) are significantly different from that of the sulfides and Yanshanian plutonic rocks (Fig. 11). As such, we can draw the conclusion that ore-forming metals are closely related to the Yanshanian plutons while other rocks, including the Permian marble, have made little contribution to the mineralization.

should be changed to:

Newly obtained Pb isotope data in this study, combined with previously reported results by Zeng et al. (2009), give two ranges for sulfides in the lead isotope diagrams as shown in Figure 11, which coincide well with the ranges for the Yanshanian granite and granodiorite, and show a mixing trend between these Yanshanian plutons and the Permian marble. It is also clear that the lead isotopes for igneous rocks present in the mining areas (e.g., Jurassic volcanic, Indosinian subvolcanic rocks, and Hercynian intrusions) are significantly different from that of the sulfides (Fig. 11). As such, we can draw the conclusion that ore-forming metals are closely related to the Yanshanian plutons and the Permian marble, while other rocks igneous phases have made little contribution to the mineralization.